PHD PROGRAM IN TRANSLATIONAL AND MOLECULAR MEDICINE
DIMET

Molecular characterization of the sarcomeric Z-line proteins nebulette and palladin in the heart: roles in cardiac structure, function, and disease

- **Coordinator: Prof. Andrea Biondi**
- **Tutor: Prof. Marialuisa Lavitrano**
- **Co-Tutor Prof. Gianluigi Condorelli**
- **Supervisor: Dr. Marie-Louise Bang**

Dr. Giuseppina Mastrototaro

Matr. No. 774790

XXVIII CYCLE

ACADEMIC YEAR 2014-2015

Table of Contents

Chapter 1
General Introduction

1. The heart: basic anatomy

The heart is a muscular organ shaped like an inverted cone and located in the centre of the thoracic cavity where it occupies the space between the lungs. It is suspended by its attachments to great vessels within the *pericardium*, a thin fibrous sac that surrounds the heart. A small amount of fluid in the pericardium lubricates the outer wall of the heart and allows it to move freely during contraction and relaxation (Mohrman and Heller 2002). The thicker wall of the heart is called the *myocardium* and is composed of numerous layers of cardiac muscle fibers. The contraction of the myocardium allows the heart to continuously pump the blood throughout the body in order to transport oxygen and nutrients to the cells and remove carbon dioxide and metabolic waste products from the body. The innermost membrane of the heart, which lines the heart cavity, is the *endocardium*. It is made of endothelial cells and is continuous with the endothelium of the major blood vessels that attach to the heart.

The heart is composed of four chambers: *right atrium* (RA), *right ventricle* (RV), *left atrium* (LA), and *left ventricle* (LV) (figure1). The atria are the upper chambers of the heart and are smaller than the two ventricles. The left and the right ventricles are separated by a thick myocardial wall called the *intraventricular septum.* The walls of the left ventricle are thicker than those of the right ventricle since the left ventricle pumps the blood into systemic circulation, where the pressure is markedly higher compared to the

pulmonary circulation to which the blood is pumped by the right ventricle.

In the heart there are four valves: the *tricuspid valve* between the right atrium and the ventricle, the *mitral valve* between the left atrium and the ventricle, the *pulmonary valve* between the right ventricle and the pulmonary artery, and the *aortic valve* between the left ventricle and the aorta. Under normal conditions, the valves allow the blood to flow in only one direction in the heart. In particular, the deoxygenated blood coming from the body enters the right atrium from the superior and inferior vena cava. Here it is pumped into the right ventricle through the tricuspid valve from where the blood is pumped into the pulmonary artery through the pulmonary valve. The pulmonary artery transports blood to the lungs where it releases CO_2 and takes up oxygen whereafter the pulmonary veins carry oxygenated blood to the left atrium where it is pumped through the mitral valve into the left ventricle. The left ventricle contracts to pump oxygenated blood through the aortic valve into the aorta from where it enters into systemic circulation throughout the body until it returns to the heart via the vena cava and the cycle repeats (Mohrman and Heller 2002).

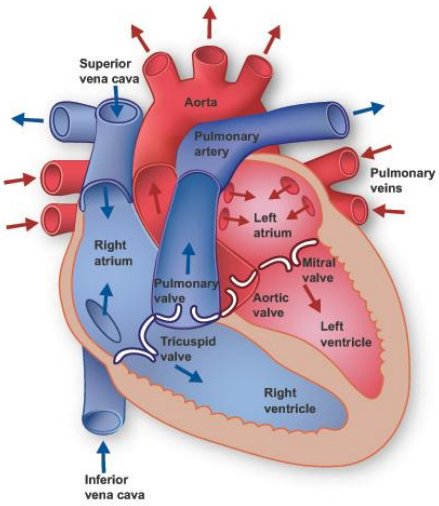

Figure 1: Heart anatomy. The heart wall is composed of three layers: the pericardium, a fibrous membrane that surrounds the heart like a sac, the myocardium, in the middle, which is the muscular part of the heart, and the epicardium, the inner serous layer that lines the interior of the heart. The heart has four chambers: the left and the right atria on the top and the left and the right ventricle on the bottom. The left and right ventricles are separated by the intraventicular septum. The tricuspid valve connects the right atrium and the ventricle, the mitral valve the left atrium and the ventricle, the pulmonary valve the right ventricle and the pulmonary artery, and the aortic valve the left ventricle and the aorta.

1.1 Structure of cardiac muscle cells

Cardiac muscle cells, also known as cardiomyocytes, make up the myocardial portion of the heart wall. They are cylindrical, generally short (about 100 µm) and branched fibers that contain one or two non-dense, slightly elongated nuclei in the center (Marian and Roberts, 2001). Cardiomyocytes are the contractile cells in the heart and need to contract in unison to provide an effective pump action that can allow adequate blood perfusion of all the organs and tissues. The concerted contractile activity of cardiomyocytes is due to the presence of intercalated discs, which connect them along the longitudinal axis and let the cardiomyocytes communicate between each other (Woodcock and Matkovich 2005).

The sarcolemma, with the exception of the intercalated disc, is called the *lateral sarcolemma* and is characterized by the presence of

costameres, specialized areas in which specific protein complexes permit the communication between the extracellular matrix, the sarcolemma, and the Z-disc of the sarcomere (Sarantitis et al., 2012). At the Z-disc level, the lateral sarcolemma invaginates to form the *transverse tubular system* or *T-system (Borg et al., 1983).* The deep invaginations of the sarcolemma into the cell and the presence of potassium channels allow the T-system to quickly and uniformly transmit the action potential from the sarcolemma to the cardiac muscle fiber (Russell et al., 2000).

The cytoskeleton provides mechanical support for cardiomyocytes and is important for the structural maintenance of cardiomyocytes. In particular, it is essential for the spatial arrangement of subcellular elements and organelles, intracellular transfer of vescicles, allocation of membrane receptors, intracellular comunication, and mechanical signal transduction (Schweitzer et al., 2001; Solaro and Van Eyk, 1996). The cytoskeleton is a highly complicated structure which can be functional divided into a *contractile* part, formed exclusively by the sarcomere, and a *non-contractile* part, which is essential for signal transduction, transmission of generated power, and the maintenance of the structural integrity of the cell (Gregorio and Antin, 2000).

2. The sarcomere

The sarcomere is the basic contractile unit of cardiac and skeletal muscle and is essentially a highly ordered array of *actin (thin)* and *myosin (thick) filaments*, which slide past each other during contraction and are stabilized by *titin filaments.* Sarcomeres, which

are between 1.5 and 2.2 µm in length, are consecutively connected in order to form the myofibril (Braunwald, 1971) and in the Z-disc *(Z-line or Z-band)* at the boundary between sarcomeres, actin and titin filaments from adjacent sarcomeres are cross-linked. Fascicles of myofibrils constitute the inner part of cardiomyocytes. Under the light microscope, myofibrils appear as an alternating pattern of light and dark bands, which gives them their typical striated appearance (figure 2).

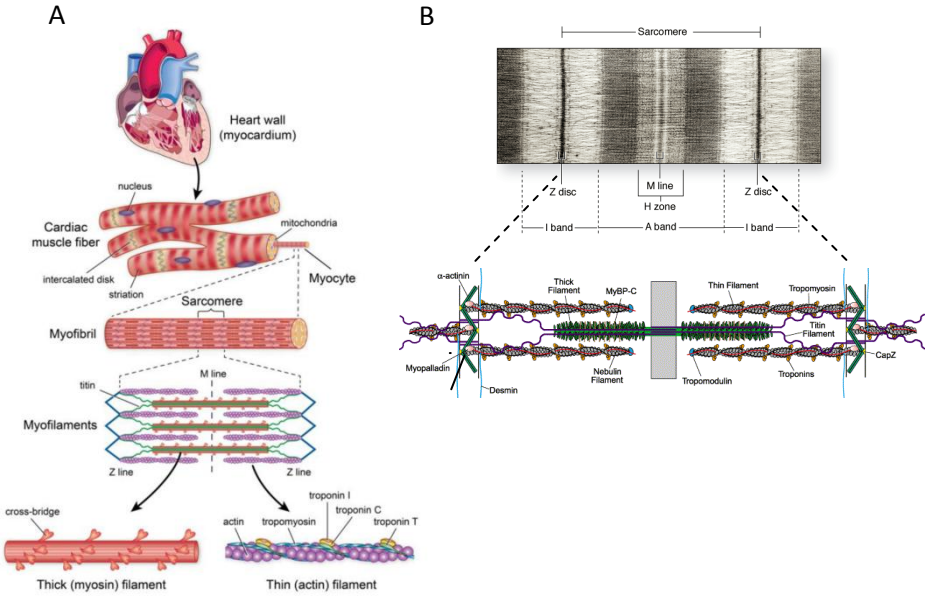

Figure 2: Sarcomere structure. A) The myocardium is the middle muscular layer of the heart wall and is predominantly composed of cardiac muscle fibers, whose contractions allow the heart to pump blood throughout the body. Each fiber is made up of adjacent sarcomeres, which are composed of thin and thick filaments arranged in repeating units. Thin filaments contain actin, tropomyosin, and troponin, while thick filaments are composed of myosin. The giant protein titin extends from the Z-disc to the M-line and acts as a spring during contraction and relaxation. Figure from (Golob et al., 2014). **B)** Electron micrograph of striated muscle in longitudinal section, showing one sarcomere. On each side of the Z disc are the lightly stained I-bands, composed of actin thin filaments. The H-zone which is made up exclusively of myosin thick filaments is in the center of the A-band that includes a zone of

overlap between the thick and thin filaments. Figure on top from (Junqueira and Carneiro, 2005); figure on the bottom adapted from (McElhinny et al., 2003).

The central dark band is composed of myosin thick filaments, while the light band corresponds to the actin thin filaments. These regions are termed the A- and I-bands, respectively, due to their anisotropic or isotropic appearance under polarized light. In the centre of the I-band, actin filaments of opposite orientation meet and form an electron dense structure called the Z-disc. The less dense region in the middle of the A-band is called the H-zone and in the centre of the H-zone there is a dense region known as the M-line. The thin filament extends into the A-band, thereby enhancing its intensity and leaving the paler H-zone in the non-overlapping region (Braunwald, 1971; Cooke, 1985; Huxley, 1973; Squire, 1981).

In the sarcomere, the thin and the thick filaments are constant in overall length, and during contraction the A-band remains unchanged, while the I-band decreases in length. This is explained by the "*sliding filament model*" (Huxley and Niedergerke, 1954; Huxley and Hanson, 1954) based on thin and thick filaments that slide over each other in an ATP-dependent manner to generate sarcomere shortening and consequently muscle contraction.

The thin filament is ~1.0 μm long and is composed of filamentous actin (F-actin), tropomyosin, and the troponin complex. F-actin is formed by two chains of spherical G-actin monomers twisted around each other to form a double helix. Each G-actin monomer has a binding site for myosin and polymerizes to create an actin filament with a distinctive polarity: the *barbed end* is anchored at the Z-disc by the cross-linking protein α-actinin and capped by

CapZ, whereas the *pointed end* reaches the A-band where is capped by tropomodulin, which is essential for the preservation of the proper length of thin filaments (reviewed in (Ono, 2010)). The barbed and pointed ends refer to the orientation of arrowheads generated by the myosin S1 fragment binding to actin filaments when observed under transmission electron microscopy and are the fast-growing and slow-growing end of the thin filaments, respectively.

The thick filament is ~1.6 μm long and consists mostly of myosin II and C-, H-, and X-myosin binding proteins, which have structural and regulatory roles. Myosin II is a large complex of ~500 kDa, composed of two heavy chains (MHC) and two pairs of different light chains (MLC1 and MLC2). Myosin heavy chains are thin and baculiform molecules with a length of 150 nm and a thickness of 2-3 nm and are made up of two chains twisted around each other. At one end of each chain there is a small ball-shaped domain, which creates the heads of myosin and contains binding site for both actin and ATP as well as has enzymatic capacity to hydrolyze ATP. The two pairs of light chains are connected to the head. Several hundred myosin molecules are required to form a thick filament and the heads of the myosin molecules project to the outside of the filaments and are responsible for moving the myosin molecules along adjacent actin filaments (Gregorio and Antin, 2000).

A third filament system in the sarcomere is formed by titin, the largest known protein in mammalian cells, which represents the third most abundant protein after actin and myosin in cardiac and skeletal muscle (Maruyama et al., 1977a; Maruyama et al., 1977b; Wang et al., 1979). Titin, also known as connectin, is a giant protein with a

molecular weight of 3.000 to 3.700 kDa extending over 1 μm from the Z-disc (N-terminus) to the M-line (C-terminus) of the sarcomere and is highly modular in structure. About 90% of titin's mass is made up of globular domains of immunoglobulin (Ig) and fibronection type III (FN3) repeats, while the remaining 10% is composed of non-repetitive sequences, including the PEVK region in the I-band region named after the predominant amino acids in the domain as well as the serine/threonine kinase domain in titin's C-terminal region at the M-line. The I-band region of titin is composed mainly of extensible Ig domains and the PEVK region, allowing titin to function as a molecular spring responsible for the passive elasticity of muscle. The A-band region of titin is comprised of Ig and FN3 modules arranged into super-repeats, providing binding sites for thick filament proteins such as MyBP-C, MyBP-H, myomesin-1 and -2, and the rod region of the myosin heavy chain (Baharvand et al., 2005; Camelliti et al., 2006; Kostin et al., 1998; Layland et al., 2005; McElhinny et al., 2005; Schweitzer et al., 2001; Solaro, 2005). (Baharvand et al., 2005). Thus, titin is essential for thick filament assembly and organization during myofibrillogenesis, and is responsible for keeping the thick filament centered during contraction. Within the Z-disc, titin contains a variable number of a specific 45-residue protein motif called the Z-repeat (Gautel et al., 1996). The number of the Z-repeats present in the central Z-disc region of titin is closely correlated with the width of the Z-disc (Gautel et al., 1996; Sorimachi et al., 1997). Moreover, titin interacts with thin filaments through its direct interaction with α-actinin and titin-cap (T-cap/telethonin) and permits force transmission at the Z-disc. Finally, it participates in mechanosignaling through

binding to proteins signaling to the nucleus, and functions as a sensory and signaling mediator though its kinase domain (Kostin, Scholz et al. 1998, Schweitzer, Klymkowsky et al. 2001,Baharvand, Azarnia et al. 2005, Solaro 2005, McElhinny, Schwach et al. 2005, Camelliti, Green et al. 2006, D'Angelo and Hetzer 2006). Titin is extensively spliced, especially in the extensible I-band region, resulting in N2BA and N2B (cardiac muscle) and N2A (skeletal muscle) isoforms, varying in length depending on muscle developmental stage and type, determining to the elastic properties of different muscle types.

2.1 Cardiac Muscle Contraction

Heart contraction is due to the coordinated contraction of cardiomyocytes occurring in response to a series of events that are initiated and coordinated by the cardiac action potential (AP). The AP is a transient depolarization of the membrane potential that allows the activation of voltage-gated L-type Ca^{2+} channels present on the sarcolemma. Ca^{2+} entering into the cell via these channels induce a further Ca^{2+} release from the sarcoplasmatic reticulum (SR) mediated by intracellular calcium receptors known as ryanodine receptors (RyR) (Woodcock and Matkovich, 2005).

Sarcolemmal Ca^{2+} channels are predominantly located in T-tubules (Brette and Orchard, 2003) and in the presence of AP, Ca^{2+} sparks occurs at the junction between the T-tubules and SR (Cheng et al., 1996; Parker et al., 1996). The free Ca^{2+}, released from SR, interacts with troponin C, inducing a subsequent enhancement of the interaction between actin and myosin, leading to cell shortening (Williams et al., 1992).

Troponin is a dimer composed of two α-helical coiled-coils and is associated with the actin filaments along its length. Each tropomyosin molecule spans 38.5 nm, corresponding to seven actin subunits, and is associated with one troponin complex. Thus, the stoichiometric ratio of troponin: tropomyosin: actin is 1:1:7. Troponin is composed of the three subunits T, I, and C, named after their **T**ropomyosin binding, **I**nhibitory, and **C**a^{2+}-binding activities. Troponin T is associated with tropomyosin, which is bound along the length of an actin filament, while troponin I binds to actin and inhibits the actomyosin interaction and troponin C binds to actin (Bagshaw, 1993; Squire, 1997). When, following the AP, troponin C binds to four molecules of Ca^{2+}, troponin I is released from actin causing a change in the position of tropomyosin on the actin filament. This conformational change exposes the myosin-binding region, allowing myosin S1 heads to bind to adjacent actin filaments. The myosin head has ATPase activity and hydrolyses ATP during the interaction with actin. After the hydrolysis of ATP to ADP and inorganic phosphate (Pi), the myosin head binds weakly to actin forming a cross-bridge, and Pi is released, causing the myosin head to bind tightly to the actin filament. Subsequently, the myosin head undergoes a conformational change that generates a "power stroke" that pulls the actin filaments towards the center of the sarcomere. Finally, ADP is released, allowing a new ATP molecule to bind to myosin inducing its detachment from the actin filament (Houdusse et al., 1999; Parry and Squire, 1973; Squire, 1997).

At the end of the AP, Ca^{2+} is removed from the cytosol by SR uptake via the SR Ca^{2+} transporter (SERCA) (Bers et al., 2003) and by

extrusion through the sarcolemma via the Na^{+}/ Ca^{2+} exchanger (Hilgemann, 2004). The regulation of the increase and decrease in Ca^{2+} levels regulates the contraction-relaxation cycle of the working myocytes.

2.2 Z-disc

Z-discs (Z-lines or Z-bands), which demarcate the lateral borders of sarcomeres, are composed of hundreds of different proteins and can be defined as the most complex macromolecular structures found in biology (Zou et al., 2006). The great number of proteins in the Z-disc makes it capable of functioning as a scaffold that links the sarcomeric contractile units in series by anchoring actin and titin from adjacent sarcomeres. The Z-band also anchors the ends of myofibrils at the intercalated disc, and links sarcomeres laterally to the sarcolemma through costameric proteins in both cardiac and skeletal muscle cells. Z-discs of flanking sarcomeres are aligned in parallel and connected via the intermediate filament protein desmin.

The backbone of the Z-disc is made up of layers of α-actinin aligned in an antiparallel fashion, each of them measuring ~19 nm. Thus, Z-disc width is determined by the number of α-actinin layers and, in cardiac and slow skeletal muscle is normally 100-140 nm, whereas in fast muscle fibers is 30-50 nm (Luther, 2009). In transverse view, in the light and electron microscopes, two different structural states of the Z-disc have been revealed: a predominant “basketweave” pattern and a “small square” pattern. Z-discs modify their lattice network in conjunction with changes in the actin-myosin

interaction supporting their role as mechanosensors (Goldstein et al., 1989; Goldstein et al., 1988; Luther et al., 2002).

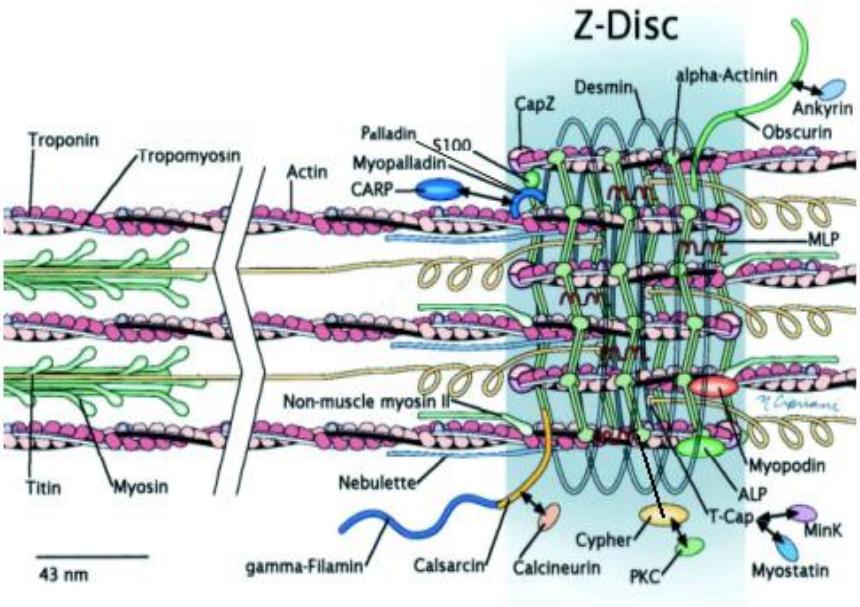

Figure 3: ***Z-disc structure.*** Schematic representation of the network of proteins making up the Z-disc. Stoichiometric relationships are not shown. Adapted from (Pyle and Solaro, 2004).

The basketweave conformation is likely to arise in part from patterns of distribution of a set of Z-disc proteins: actin, CapZ, α-actinin, the N-terminal region of titin, titin-cap (T-cap/telethonin), and the C-terminal region of nebulette, and obscurin (contains like titin, tandem Ig domains in an elastic region). Apart from these proteins, during the last decades, the detection of a multitude of novel Z-disc proteins and their interacting partners has led to the identification of new functions of the Z-disc. In fact these proteins are not only important for the structural and mechanical stability of the sarcomere, but also serve as docking site for transcription factors, Ca^{2+} signaling

proteins, phosphatases, and kinases, influencing function and gene expression. Moreover, many proteins move between the Z-disc and the nucleus and regulate transcription. Among the innumerable proteins anchored to the Z-disc giving its properties are: LIM proteins (muscle LIM protein, MLP and actin-associated LIM protein, ALP), myopalladin, palladin, myopodin, cypher (ZASP or oracle), calsarcins, CARP (cardiac ankyrin repeated protein), and S-100, a Ca^{2+} binding protein (figure 3) (reviewed in Knöll and Buyandelger, 2011). Thus, the Z-disc associated proteins are numerous and each of them has specific functions.

In this thesis, two of the Z-disc associate proteins, nebulette and palladin, will be further discussed since the understanding of their functional role in the heart has been the object of my PhD project.

2.3. Intercalated disks

Each cardiomyocyte is longitudinally connected to another through the intercalated disks (ICDs). ICDs are highly organized and specialized cell-cell junctions that ensure the electrochemical and mechanical coupling of cardiomyocytes during the contraction. They are formed by three different types of protein complexes: i) *desmosomes*, ii) *fascia adherens junctions*, iii) *gap junctions (Perriard et al., 2003; Sheikh et al., 2009; Woodcock and Matkovich, 2005).*

Desmosomes are essential for the mechanical stabilization of cardiomyocytes, anchoring the cell membrane to the intermediate filament network. Among the proteins composing the desmosomes, there are the desmosomal cadherins, desmogleins and desmocollins, which are transmembrane proteins that establish intercellular contacts,

and a cytoplasmatic protein complex formed by desmoplakin, plakopkilin, and plakoglobulin that mediates the anchorage to intermediate filaments such as desmin (Capetanaki, 2000; Jamora and Fuchs, 2002).

Fascia adherens junctions anchor cardiomyocytes tightly by connecting the cell membrane to the actin cytoskeleton. Components of adherens junctions are: i) N-cadherin, a transmembrane protein that establishes intercellular contacts; ii) α-, β-, and γ-catenin (plakoglobin), which bind to the cytoplasmatic tails of cadherin and allow, through interaction with α-catenin, the contact to the actin cytoskeleton; iii) vinculin and α-actinin, two catenin-related proteins, which connect the ICD to the actin cytoskeleton (Jamora and Fuchs, 2002; Yamada et al., 2005). In the last years, numerous proteins have been found to be associated with the adherens junctions such as ARVCF (Kaufmann et al., 2000), SPAL (Roy et al., 1999), ALP (Pashmforoush et al., 2001), N-RAP, and Mec3 (LIM)-domain (Zhang et al., 2001).

Gap junctions mediate intracellular communication, allowing small molecules (<1000 Da) to shuttle between adjacent cardiomyocytes. They are membrane-spanning channels (connexons) formed by six connexin molecules. In particular, the main connexin isoform present in the adult ventricular myocardium is connexin 43. These channels permit electrical and metabolic coupling between cardiomyocytes during beating (Noorman et al., 2009; Severs et al., 2008).

3. Nebulette

Nebulette is a modular protein of 109 kDa localized in the Z-disc. It is highly homologous to the C-terminal Z-disc region of the skeletal muscle protein nebulin (500 – 900 KDa) (Wang and Wright, 1988) as both proteins are made up of 35-residue nebulin-like repeats and a C-terminal SH3 domain preceded by a serine-rich linker region (Millevoi et al., 1998). However, while nebulin is composed of at least 185 repeats and extends from the Z-disc along the length of the thin filaments, nebulette contains only 23 nebulin-like repeats and, starting from the Z-disc, protrudes only a short distance along the actin filaments (Bang et al., 2006; Castillo et al., 2009; Pappas et al., 2008; Pappas et al., 2010). Nebulette binds to filamin C, an actin cross-linking protein through its N-terminus and the nebulin repeats (Holmes and Moncman, 2008), while it binds to actin, troponin, and tropomyosin through its central repeat domains (Esham et al., 2007). In the Z-disc, both nebulin and nebulette bind to α-actinin, through their SH3 domain and the nebulin repeats (Moncman and Wang, 1999). Moreover, their SH3 domain binds to proline-rich regions within different proteins, including: i) the PEVK and Z-disc regions of titin (Ma et al., 2006; Ma and Wang, 2002; Witt et al., 2006); ii) myopalladin, a striated muscle-specific protein associated with α-actinin in the Z-disc (Bang et al., 2001; Ma and Wang, 2002); iii) palladin, an ubiquitos protein, highly homologous to myopalladin, associated with α-actinin and F-actin, important for the organization of the actin cytoskeleton (Bang et al., 2001; Goicoechea et al., 2008); iv) zyxin, a protein involved in the organization of the cytoskeleton and associated with focal adhesions and other actin based structures

(Li et al., 2004); v) neuronal Wiscott-Aldrich syndrome protein (N-WASP), which regulates actin polymerization (Takano et al., 2010); vi) Xin and XIRP2, two members of the Xin actin-binding repeat-containing (XIRP) family with which nebulin and nebulette interact transiently during development (Eulitz et al., 2013).

In chick embryonic cardiomyocytes, overexpression of the nebulette serine-rich linker or SH3 domain, causing a reduction of endogenous nebulette levels, resulted in shorter thin filaments (Moncman and Wang, 2002), loss of tropomyosin and troponin T from the thin filament, and impaired beating of cardiomyocytes (Bonzo et al., 2008; Moncman and Wang, 2002), suggesting that nebulette is important for the stabilization of the thin filament. In the present project, we studied nebulette knockout mice, which surprisingly do not exhibit a functional phenotype, although Z-disc widening was observed, suggesting an important role of nebulette for the maintenance of Z-disc integrity (Mastrototaro et al., 2015). Recently, four nebulette variants (K60N, Q128R, G202R, A592E) have been found in patients with nonfamilial dilated cardiomyopathy (DCM). The K60N, Q128R, G202R, and A592E mutations have been identified in nebulin repeats 1, 3, 5, and 16, respectively (Purevjav, Varela et al. 2010). The pathological effects of these mutations have been functionally validated by the generation of cardiac transgenic mouse (Purevjav, Varela et al. 2010), which develop DCM of various degrees.

4. Palladin

Palladin (PALLD) is a recently discovered actin-associated phosphoprotein that has been shown to be essential for the maintenance of cell morphology and cytoskeleton organization (Parast and Otey, 2000a; Rachlin and Otey, 2006b) and to control many cellular functions, including myofibroblast (Rönty et al., 2006) and smooth muscle differentiation (Jin et al., 2010). However, its role in cardiac muscle has remained elusive. Palladin, myopalladin (MYPN), and myotilin (MYOT) make up a small protein family of immunoglobulin C2 (Ig)-containing proteins in the Z-disc, which are connected to α-actinin and associated with the actin cytoskeleton. Myopalladin and myotilin are expressed as single isoforms exclusively in striated muscle, while palladin is ubiquitously expressed and exists as multiple isoforms due to the presence of alternative promoters, alternative splicing and early termination (figure 4). The palladin isoforms contain from one to five Ig-domains, which are typically about 100 amino acids and made up of seven to nine β-strands that assume a sandwiched β-sheet fold (Beck et al., 2013). The three major expressed palladin isoforms are the 90-92, 140, and 200 kDa isoforms. The 90-92 kDa isoform is the major almost ubiquitously expressed isoform with highest levels in smooth muscle-rich tissues; the 140 kDa is present in mesenchymal tissues and represents the major isoform of the brain; and the 200 kDa is expressed only in striated muscle and testis (Wang and Moser, 2008a).

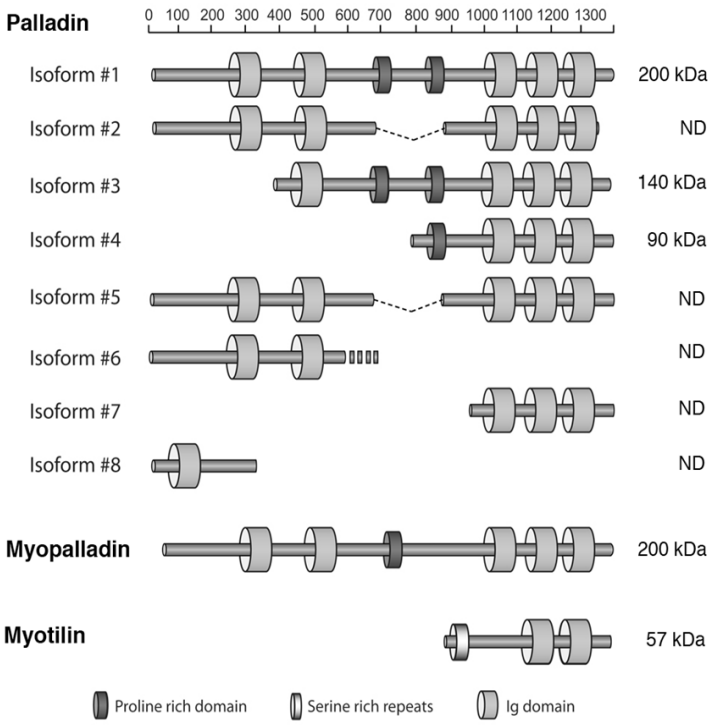

Figure 4: ***The myopalladin/palladin/myotilin family***. Adapted from Goicoechea et al., 2008.

Palladin's largest 200 kDa isoform is highly homologous in structure to myopalladin, containing five Ig-domains and a proline-rich region nearly identical to the one found in MYPN. In addition, it contains a second proline-rich region not present in MYPN. Within the sarcomeric Z-disc, both palladin and myopalladin bind to various proteins. In particular, they bind to α-actinin through a short sequence present in the region between Ig2 and Ig3 (Rönty et al., 2004) and to nebulette's C-terminal domain through the proline-rich region. The extreme C-terminal ends of palladin and myopalladin contain an ESDEL and ESEDEL motif, respectively, which binds in a phosphorylation dependent manner to class III PDZ domains present in PDZ-LIM proteins, such as cypher/ZASP, CLP36, ALP, and RIL

(von Nandelstadh et al., 2009). In the sarcomeric I-band, the N-terminal region of myopalladin binds to CARP, a negative regulator of gene expression in the nucleus induced by various forms of stress conditions, which, in turn, binds to the titin N2A region within its elastic I-band region (Bang et al., 2001; Miller et al., 2003), forming a complex, which may be involved in transduction of stress-induced signaling from the sarcomere to the nucleus. During my PhD, I found that also the N-terminal region of palladin's largest 200 kDa isoform can interact with CARP.

Recently, palladin's Ig3 was found to bind directly to F-actin as well as to bundle F-actin into multi-filament arrays, promoting actin polymerization (Beck et al., 2013; Boukhelifa et al., 2003a; Rachlin and Otey, 2006b). Like palladin, we found that also myopalladin is able to bind and bundle F-actin as well as to stimulate actin polymerization (unpublished data). Moreover, a second proline-rich region, present within palladin's most common isoforms (isoform 1, 3, 4 in Figure 4), bind to numerous actin-regulating proteins including VASP, Mena, EVL, profiling and Esp8 as well as to signaling proteins, such as ArgBP-2, SPIN-90, and src (Otey et al., 2009a). In addition, palladin binds to the actin-binding protein LASP1 through its first proline-rich region (Bang et al., 2001; Rachlin and Otey, 2006b).

The C-terminal region of palladin binds to ezrin, an actin-associated protein, as well as the myocardin related transcription factors (MRTFs) MRTF-A and MRTF-B (Jin et al., 2010). In particular, recent studies have shown that the C-terminus of palladin is targeted to the nucleus in podocytes and smooth muscle cells (SMCs),

where it binds to MRTFs and both directly and indirectly activates SMC gene expression through the serum response factor (SRF) pathway, thereby inducing SMC differentiation (Jin et al., 2010). Our findings demonstrate that also myopalladin can bind to MRTFs and that both palladin and myopalladin can activate MRTF-A-induced SRF signaling in myogenic cells (see below and unpublished data).

While mutations in the *mypn* gene have been identified in human dilated (DCM), hypertrophic (HCM), and restrictive (RCM) cardiomyopathy (Duboscq-Bidot et al., 2008; Meyer et al.; Purevjav et al.), a mutation in the *palld* gene has been identified in a family with a high incidence of pancreatic cancer and PALLD levels have been shown to correlate with increased invasiveness of cancer cells (reviewed in Otey et al., 2009b). However, it is currently unknown whether also mutations in PALLD can cause cardiomyopathies.

In vitro studies of PALLD's function by knockdown and overexpression experiments in various cellular systems have suggested its important role in the assembly, organization, and maintenance of the actin cytoskeleton. While knockdown of PALLD in cells inhibited the formation of stress fibers and resulted in abnormal cell morphology and loss of filamentous actin (Parast and Otey, 2000b), its overexpression caused an increase in the number and size of actin bundles (Boukhelifa et al., 2003b; Rachlin and Otey, 2006a). Furthermore, ablation of PALLD in mice resulted in embryonic lethality before E15.5 due to multiple defects, including failure of body walls to close, resulting in exencephaly (anterior neural tube closure defect) and herniation of abdominal organs (ventral body wall closure defect). In addition, analyses of PALLD

knockout (KO) embryos revealed a key role of PALLD in the induction of SMC differentiation in the developing vasculature (Jin et al.). Consistent with the *in vitro* knockdown studies, fibroblasts derived from KO embryos showed defects in stress fiber formation, cell adhesion, and motility (Luo et al., 2005b). The high expression levels of specific PALLD isoforms, especially the 200 kDa and 90-92 kDa isoforms, in cardiac muscle both during development and at adult stage suggest that it may play an important role also in heart (Wang and Moser, 2008b). For this reason, the aim of this thesis is to investigate the functional role of PALLD in the heart.

5. The MRTFs/SRF signaling pathway

The myocardin-related transcription factors (MRTFs) make up a family of highly homologous proteins, including myocardin, MRTF-A, and MRTF-B. They function as powerful transcriptional coactivators of serum response factor (SRF) and activate transcription of SRF-target genes that, among the other process, regulate cytoskeletal organization, actomyosin structure, and muscle cell differentiation. SRF is a ubiquitously expressed transcription factor containing a 57-amino acid MADS-box domain that allows its homodimerization (Wang et al., 2001; Wang et al., 2002). SRF, in fact, binds as a homodimer to a DNA motif ([CC(A/T)^{6}GG]) known as CArG box or serum response element, which was first found in the control regions of many growth- and serum-responsive genes such as c-fos and egr1(Norman et al., 1988; Treisman, 1995) and subsequently in transcriptionally regulatory elements of genes encoding myogenic contractile and cytoskeletal proteins, including cardiac muscle α-actin

(ACTC1), smooth muscle α-actin (α-SMA or ACTA2), α-skeletal actin (ACTA1), and smooth muscle 22-α (SM22α) (Blank et al., 1992; Chow and Schwartz, 1990; Kim et al., 1997; Li et al., 1997; Solway et al., 1995). Thus, the majority of the genes regulated by SRF are associated with cell growth and proliferation, organization of the cytoskeleton, cell migration, and muscle cell differentiation. In cardiac muscle, SRF is necessary for normal heart development and function, and has a crucial role in regulating cardiomyocyte differentiation and the morphogenetic program of cardiac development. Cardiac specific ablation of SRF in mice resulted in embryonic lethality due to cardiac insufficiency associated with reduced cardiomyocyte survival and increased apoptosis (Miano et al., 2004; Niu et al., 2005). Furthermore, SRF deficient cardiomyocytes exhibited disorganized sarcomeres, Z-discs, and stress fiber formation, (Balza and Misra, 2006; Miano et al., 2004). Conditional cardiac specific ablation of SRF in adult mice resulted in dilated cardiomyopathy, leading to heart failure (Parlakian et al., 2005). These studies demonstrate that SRF is necessary for cardiac morphogenesis and strongly suggest that SRF-target genes are important regulators of sarcomeric organization and cardiac contractility in the adult heart.

Myocardin and MRTFs evolved from an ancestral gene in Drosophila, known as DMRTF that is strictly related to MRTF-A (Han et al., 2004). The myocardin gene encodes two isoforms due to alternative splicing: the 935-amino acid isoform is expressed exclusively in cardiomyocytes, whereas the 856-amino acid isoform is expressed in SMCs. Both myocardin isoforms as well as MRTF-A, and MRTF-B contain conserved RPEL, basic and glutamine-rich domains (figure 5).

Moreover, they share a conserved 35-amino acid SAP domain (so called after the associated factors SAF-A/B, Acinus, and PIAS), a leucin zipper (LZ) domain, the B1 domain, situated between the basic and the glutamine-rich domains, and the B2 domain placed between RPEL motifs two end three (figure 5) (Posern and Treisman, 2006). In addition, the C-terminus of the myocardin-related transcription factors contains a transcriptional activation domain (TAD) that functions with heterologous promoters. However, the TAD domain of myocardin has a low level of sequence identity with the TADs of MRTF-A and MRTF-B (Wang et al., 2002).

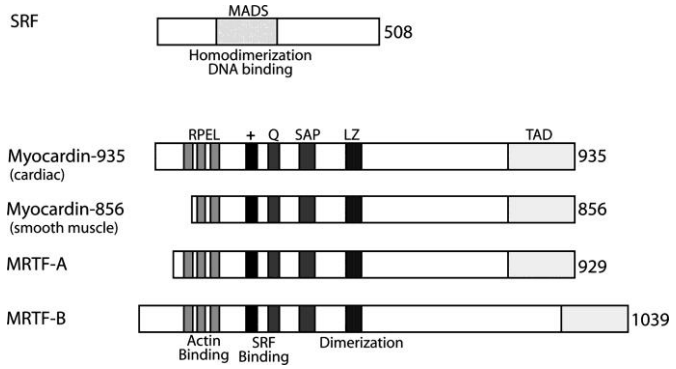

Figure 5: ***Schematic representation of SRF and myocardin-related transcription factors.*** The numbers to the right specify the number of amino acids (aa). **Top**. The SRF transcription factor contains a MADS box that regulates SRF homodimerization, cofactor-binding, and SRF-DNA binding. **Bottom**. Representation of the myocardin-related family of transcriptional coactivators. The grey and black rectangles show the localization of the RPEL, basic (+), glutamine-rich (Q), SAP, LZ, and TAD domains. Myocardin exists as 935 aa and 865 aa isoforms generated by alternative splicing. The 935 aa isoform is expressed mostly in the heart, whereas the 865 aa isoform is mainly expressed in SMCs. Figure from Parmacek, 2007.

MRTF-A is the major ubiquitously expressed isoform of the MRTFs and during embryonic development it is enriched in mesenchymal,

muscle, and epithelial cells (Pipes et al., 2006). MRTF-A is localized in the cytoplasm, where it is sequestered by its binding to G-actin through the RPEL motifs. In response to actin polymerization promoted by serum stimulation or other signals, it translocates to the nucleus where it binds to SRF, thereby inducing the activation of SRF-target genes (Miralles et al., 2003). In particular, actin polymerization influencing SRF-dependent transcription is regulated by Rho GTPases (Hill and Treisman, 1995; Sotiropoulos et al., 1999). The activation of Rho allows it to stabilize F-actin filaments and promote the assembly of monomeric G-actin into F-actin filaments via the ROCK/LIM kinase (LIMK)/cofilin pathway and mDia. The reduced concentration of free G-actin results in the translocation of MRTF-A from the cytoplasm to the nucleus (Du et al., 2004; Miralles et al., 2003; Posern et al., 2004). The B1 and the B2 domains play fundamental roles in the nuclear import of MRTF-A (Miralles et al., 2003). Striated muscle activator of Rho signaling (STARS) plays an important role in the nuclear import of MRTF-A binding to F-actin facilitating the translocation of MRTF-A to the nucleus (Kuwahara et al., 2005). Once in the nucleus, MRTF-A binds to SRF and activates the transcription of SRF-target genes, which include genes involved in cytoskeletal dynamic, and in particular, genes regulating cardiomyocyte differentiation and heart development, suggesting that the MRTF-A/SRF pathway is a critical regulator of heart development and homeostasis. Numerous mutations causing cardiomyopathy have been found in components of the nuclear matrix and sarcomere influencing actin dynamics, confirming that the MRTF-A/SRF

pathway plays critical roles in the development of heart failure (McNally and Dellefave, 2009; Morita et al., 2010).

6. Cardiomyopathies

Cardiomyopathy (CM) is a pathological abnormality of the myocardium. Cardiomyopathies are classified into four major forms: hypertrophic (HCM), dilated (DCM), restrictive (RCM) and arrhythmogenic right ventricular dysplasia (ARVD/C) cardiomyopathy (Richardson et al., 1996). HCM is characterized by ventricular wall thickening (hypertrophy), especially in the intraventricular septum, associated with a decrease in ventricular chamber volume and diastolic dysfunction (Maron, 2002). DCM results in a gradual prominent ventricular dilation generated by weakness of the ventricular chamber wall caused by damage to the myocardium, thus, resulting in systolic dysfunction (McNally et al., 2013). RCM is characterized by increased myocardial stiffness, resulting in diastolic dysfunction (McNally et al., 2013; Morimoto, 2008). ARVD/C is defined by reduced function and thinning of the right ventricle associated with fibrofatty infiltration (McNally et al., 2013; Morimoto, 2008).

HCM and DCM are the most common types of genetically inherited CMs with a respective incidence of 1/500 and 1/2500. Approximately 60% of HCM and 30-50% of DCM cases are familial, mostly with autosomal dominant inheritance, and often caused by mutations in genes expressing sarcomeric proteins (McNally et al., 2013). The first HCM-causing mutation was found in 1990 in the gene encoding β-myosin heavy chain (β-MHC) (Geisterfer-Lowrance et al.,

1990). Since then, more than 400 mutations have been found to be causative for HCM, DCM, RCM, and ARVD/C (reviewed in (McNally et al., 2013; Morimoto, 2008). In particular, the majority of cases of HCM are due to gene mutations in *β-mhc*, *mybp3*, and *tnnt2*, whereas causative mutations for DCM have been found in over 40 genes encoding proteins of the sarcomere, sarcolemma, cytoskeleton, nuclear lamina, and, in rare cases, mitochondria (McNally et al., 2013; Morimoto, 2008; Parvari and Levitas, 2012). In particular, a large number of cardiomyopathy mutations have been identified in genes encoding Z-disc proteins, including *nebulette* and *myopalladin*, the striated muscle specific homologue of palladin. More specifically, four missense mutations in the *nebulette* gene were reported to be causative for DCM (Purevjav et al., 2010) and an increasing number of missense and frame shift mutations in the *myopalladin* gene have been identified in patients with HCM, DCM, and RCM (Bagnall et al., 2010; Duboscq-Bidot et al., 2008; Meyer et al., 2013; Purevjav et al., 2012b). Based on the high homology of palladin to myopalladin, we hypothesized that also palladin may be involved in cardiac disease. The aim of my thesis project was to provide insights into the roles of the sarcomeric Z-disc proteins nebulette and palladin in cardiac structure, signaling, function, and disease. More insights into the mechanisms leading to cardiac disease are fundamental for the future development of novel therapeutic inventions.

7. Scope of the thesis

The heart is a muscular organ essentially composed of three layers: the *pericardium*, a fibrous membrane that surrounds the heart like a sac, the *myocardium*, in the middle, which is the muscular part of the heart, and the *epicardium*, the inner serous layer that lines the heart cavity (Mohrman and Heller, 2002). The contraction of the myocardium allows the heart to continuously pump the blood throughout the body. The myocardium is formed by numerous layers of cardiac muscle fibers and each fiber is made up of adjacent sarcomeres. The sarcomere is the basic contractile unit of muscle and is a highly ordered array of *actin (thin)* and *myosin (thick) filaments* that slide over each other during contraction and are stabilized by *titin filaments*, which acts as a spring during contraction and relaxation. At the Z-disc, a multiprotein complex at the boundary between sarcomeres, actin and titin filaments from adjacent sarcomeres are cross-linked, thereby connecting the contractile apparatus with the cytoskeleton and extracellular matrix. The Z-disc plays an essential role in efficient force generation and maintenance of striated muscle structure and function and is a focal point for mechanosensing and signal transduction. Consistent with the important role of the Z-disc, mutations in genes encoding Z-disc proteins have been identified in cardiomyopathy patients, including *nebulette* and *myopalladin*, the striated muscle specific homologue of palladin.

In vitro studies have suggested a role of nebulette in stabilizing the thin filament (Bonzo et al, 2008; Moncman and Wang, 2002) and missense mutations in the *nebulette* gene have been found to be

causative for dilated cardiomyopathy and endocardial fibroelastosis in human and mice (Maiellaro at al, 2013; Purevjav et al, 2010)

Palladin is an actin associated protein highly similar to the striated muscle specific protein myopalladin, which has been implicated in human cardiomyopathies. Palladin plays an important role in the organization of the actin cytoskeleton and has been studied in cell motility, breast cancer metastasis invasiveness, pancreatic cancer, and early SMC differentiation (Goicoechea et al., 2006; Goicoechea et al., 2009; Jin et al., 2010; Pogue-Geile et al., 2006). However, due to embryonic lethality of palladin knockout mice (Luo et al., 2005a) its role in the heart has remained elusive. Based on its strong expression in the heart and homology to myopalladin, we hypothesized that palladin plays an important role in the heart.

The scope of my PhD thesis is to shed light onto the still elusive function of nebulette and palladin in cardiac structure, signaling, function, and disease by taking advantage of knockout mice for the two proteins. A better understanding of the mechanisms underlying cardiac disease is of critical importance for the future development of novel therapeutic approaches.

References.

Bagnall, R.D., L. Yeates, and C. Semsarian. 2010. Analysis of the Z-disc genes PDLIM3 and MYPN in patients with hypertrophic cardiomyopathy. *Int J Cardiol*. 145:601-602.

Bagshaw, C.R. 1993. Muscle contraction. Springer Science & Business Media.

Baharvand, H., M. Azarnia, K. Parivar, and S.K. Ashtiani. 2005. The effect of extracellular matrix on embryonic stem cell-derived cardiomyocytes. *Journal of molecular and cellular cardiology*. 38:495-503.

Balza, R.O., Jr., and R.P. Misra. 2006. Role of the serum response factor in regulating contractile apparatus gene expression and sarcomeric integrity in cardiomyocytes. *The Journal of biological chemistry*. 281:6498-6510.

Bang, M.-L., X. Li, R. Littlefield, S. Bremner, A. Thor, K.U. Knowlton, R.L. Lieber, and J. Chen. 2006. Nebulin-deficient mice exhibit shorter thin filament lengths and reduced contractile function in skeletal muscle. *The Journal of cell biology*. 173:905-916.

Bang, M.-L., R.E. Mudry, A.S. McElhinny, K. Trombitás, A.J. Geach, R. Yamasaki, H. Sorimachi, H. Granzier, C.C. Gregorio, and S. Labeit. 2001. Myopalladin, a novel 145-kilodalton sarcomeric protein with multiple roles in Z-disc and I-band protein assemblies. *The Journal of cell biology*. 153:413-428.

Beck, M.R., R.D. Dixon, S.M. Goicoechea, G.S. Murphy, J.G. Brungardt, M.T. Beam, P. Srinath, J. Patel, J. Mohiuddin, and C.A. Otey. 2013. Structure and function of palladin's actin binding domain. *Journal of molecular biology*. 425:3325-3337.

Bers, D.M., D.A. Eisner, and H.H. Valdivia. 2003. Sarcoplasmic reticulum Ca2+ and heart failure roles of diastolic leak and Ca2+ transport. *Circulation Research*. 93:487-490.

Blank, R., T. McQuinn, K. Yin, M. Thompson, K. Takeyasu, R. Schwartz, and G. Owens. 1992. Elements of the smooth muscle alpha-actin promoter required in cis for transcriptional activation in smooth muscle. Evidence for cell type-specific regulation. *Journal of Biological Chemistry*. 267:984-989.

Bonzo, J.R., A.A. Norris, M. Esham, and C.L. Moncman. 2008. The nebulette repeat domain is necessary for proper maintenance of tropomyosin with the cardiac sarcomere. *Experimental cell research*. 314:3519-3530.

Borg, T.K., L.D. Johnson, and P.H. Lill. 1983. Specific attachment of collagen to cardiac myocytes: in vivo and in vitro. *Developmental biology*. 97:417-423.

Boukhelifa, M., S.J. Hwang, J.G. Valtschanoff, R.B. Meeker, A. Rustioni, and C.A. Otey. 2003a. A critical role for palladin in astrocyte morphology and response to injury. *Molecular and Cellular Neuroscience*. 23:661-668.

Boukhelifa, M., S.J. Hwang, J.G. Valtschanoff, R.B. Meeker, A. Rustioni, and C.A. Otey. 2003b. A critical role for palladin in astrocyte morphology and response to injury. *Mol Cell Neurosci*. 23:661-668.

Braunwald, E. 1971. Structure and function of the normal myocardium. *British heart journal*. 33:3.

Brette, F., and C. Orchard. 2003. T-tubule function in mammalian cardiac myocytes. *Circulation research*. 92:1182-1192.

Camelliti, P., C. Green, and P. Kohl. 2006. Structural and functional coupling of cardiac myocytes and fibroblasts. Karger Publishers.

Capetanaki, Y. 2000. Desmin cytoskeleton in healthy and failing heart. *Heart failure reviews*. 5:203-220.

Castillo, A., R. Nowak, K.P. Littlefield, V.M. Fowler, and R.S. Littlefield. 2009. A nebulin ruler does not dictate thin filament lengths. *Biophysical Journal*. 96:1856-1865.

Cheng, H., M.R. Lederer, W. Lederer, and M. Cannell. 1996. Calcium sparks and [Ca2+] i waves in cardiac myocytes. *American Journal of Physiology-Cell Physiology*. 270:C148-C159.

Chow, K., and R.J. Schwartz. 1990. A combination of closely associated positive and negative cis-acting promoter elements regulates transcription of the skeletal alpha-actin gene. *Molecular and cellular biology*. 10:528-538.

Cooke, P. 1985. A periodic cytoskeletal lattice in striated muscle. *In* Cell and muscle motility. Springer. 287-313.

Du, K.L., M. Chen, J. Li, J.J. Lepore, P. Mericko, and M.S. Parmacek. 2004. Megakaryoblastic leukemia factor-1 transduces cytoskeletal signals and induces smooth muscle cell differentiation from undifferentiated embryonic stem cells. *Journal of Biological Chemistry*. 279:17578-17586.

Duboscq-Bidot, L., P. Xu, P. Charron, N. Neyroud, G. Dilanian, A. Millaire, V. Bors, M. Komajda, and E. Villard. 2008. Mutations in the Z-band protein myopalladin gene and idiopathic dilated cardiomyopathy. *Cardiovasc Res*. 77:118-125.

Esham, M., K. Bryan, J. Milnes, W.B. Holmes, and C.L. Moncman. 2007. Expression of nebulette during early cardiac development. *Cell motility and the cytoskeleton*. 64:258-273.

Eulitz, S., F. Sauer, M.-C. Pelissier, P. Boisguerin, S. Molt, J. Schuld, Z. Orfanos, R.A. Kley, R. Volkmer, and M. Wilmanns. 2013. Identification of Xin-repeat proteins as novel ligands of the SH3 domains of nebulin and nebulette and analysis of their interaction during myofibril formation and remodeling. *Molecular biology of the cell*. 24:3215-3226.

Gautel, M., D. Goulding, B. Bullard, K. Weber, and D. Furst. 1996. The central Z-disk region of titin is assembled from a novel repeat in variable copy numbers. *Journal of Cell Science*. 109:2747-2754.

Geisterfer-Lowrance, A.A., S. Kass, G. Tanigawa, H.-P. Vosberg, W. McKenna, C.E. Seidman, and J. Seidman. 1990. A molecular basis for familial hypertrophic cardiomyopathy: a β cardiac myosin heavy chain gene missense mutation. *Cell*. 62:999-1006.

Goicoechea, S., D. Arneman, A. Disanza, R. Garcia-Mata, G. Scita, and C.A. Otey. 2006. Palladin binds to Eps8 and enhances the formation of dorsal ruffles and podosomes in vascular smooth muscle cells. *Journal of cell science*. 119:3316-3324.

Goicoechea, S., B. Bednarski, R. Garcia-Mata, H. Prentice-Dunn, H. Kim, and C. Otey. 2009. Palladin contributes to invasive motility in human breast cancer cells. *Oncogene*. 28:587-598.

Goicoechea, S.M., D. Arneman, and C.A. Otey. 2008. The role of palladin in actin organization and cell motility. *European journal of cell biology*. 87:517-525.

Goldstein, M., L. Michael, J. Schroeter, and R. Sass. 1989. Two structural states of Z-bands in cardiac muscle. *American Journal of Physiology-Heart and Circulatory Physiology*. 256:H552-H559.

Goldstein, M.A., L.H. Michael, J.P. Schroeter, and R.L. Sass. 1988. Structural states in the Z band of skeletal muscle correlate with states of active and passive tension. *The Journal of general physiology*. 92:113-119.

Golob, M., R.L. Moss, and N.C. Chesler. 2014. Cardiac tissue structure, properties, and performance: a materials science perspective. *Annals of biomedical engineering*. 42:2003-2013.

Gregorio, C.C., and P.B. Antin. 2000. To the heart of myofibril assembly. *Trends in cell biology*. 10:355-362.

Han, Z., X. Li, J. Wu, and E.N. Olson. 2004. A myocardin-related transcription factor regulates activity of serum response factor in Drosophila. *Proceedings of the National Academy of Sciences of the United States of America*. 101:12567-12572.

Hilgemann, D.W. 2004. New insights into the molecular and cellular workings of the cardiac Na+/Ca2+ exchanger. *American Journal of Physiology-Cell Physiology*. 287:C1167-C1172.

Hill, C.S., and R. Treisman. 1995. Transcriptional regulation by extracellular signals: mechanisms and specificity. *Cell*. 80:199-211.

Holmes, W.B., and C.L. Moncman. 2008. Nebulette interacts with filamin C. *Cell motility and the cytoskeleton*. 65:130-142.

Houdusse, A., V.N. Kalabokis, D. Himmel, A.G. Szent-Györgyi, and C. Cohen. 1999. Atomic structure of scallop myosin subfragment S1 complexed with MgADP: a novel conformation of the myosin head. *Cell*. 97:459-470.

Huxley, A.F., and R. Niedergerke. 1954. Structural changes in muscle during contraction. *Nature*. 173:971-973.

Huxley, H. 1973. Muscular contraction and cell motility.

Huxley, H., and J. Hanson. 1954. Changes in the cross-striations of muscle during contraction and stretch and their structural interpretation. *Nature*:973-976.

Jamora, C., and E. Fuchs. 2002. Intercellular adhesion, signalling and the cytoskeleton. *Nature cell biology*. 4:E101-E108.

Jin, L., Q. Gan, B.J. Zieba, S.M. Goicoechea, G.K. Owens, C.A. Otey, and A.V. Somlyo. The actin associated protein palladin is important for the early smooth muscle cell differentiation. *PLoS One*. 5:e12823.

Jin, L., Q. Gan, B.J. Zieba, S.M. Goicoechea, G.K. Owens, C.A. Otey, and A.V. Somlyo. 2010. The actin associated protein palladin is important for the early smooth muscle cell differentiation. *PloS one*. 5:e12823.

Junqueira, L.C., and J. Carneiro. 2005. Basic histology text and atlas. London: McGraw Hill, 2005.

Kaufmann, U., C. Zuppinger, Z. Waibler, M. Rudiger, C. Urbich, B. Martin, B.M. Jockusch, H. Eppenberger, and A. Starzinski-Powitz. 2000. The armadillo repeat region targets ARVCF to cadherin-based cellular junctions. *Journal of cell science*. 113:4121-4135.

Kim, S., H.S. Ip, M.M. Lu, C. Clendenin, and M.S. Parmacek. 1997. A serum response factor-dependent transcriptional regulatory program identifies distinct smooth muscle cell sublineages. *Molecular and Cellular Biology*. 17:2266-2278.

Knöll, R., and B. Buyandelger. 2011. The sarcomeric Z-disc and Z-discopathies. *BioMed Research International*. 2011.

Kostin, S., D. Scholz, T. Shimada, Y. Maeno, H. Mollnau, S. Hein, and J. Schaper. 1998. The internal and external protein scaffold of the T-tubular system in cardiomyocytes. *Cell and tissue research*. 294:449-460.

Kuwahara, K., T. Barrientos, G.T. Pipes, S. Li, and E.N. Olson. 2005. Muscle-specific signaling mechanism that links actin dynamics to serum response factor. *Molecular and cellular biology*. 25:3173-3181.

Layland, J., R.J. Solaro, and A.M. Shah. 2005. Regulation of cardiac contractile function by troponin I phosphorylation. *Cardiovascular research*. 66:12-21.

Li, B., L. Zhuang, and B. Trueb. 2004. Zyxin interacts with the SH3 domains of the cytoskeletal proteins LIM-nebulette and Lasp-1. *Journal of Biological Chemistry*. 279:20401-20410.

Li, L., Z.-c. Liu, B. Mercer, P. Overbeek, and E.N. Olson. 1997. Evidence for Serum Response Factor-Mediated Regulatory Networks GoverningSM22αTranscription in Smooth, Skeletal, and Cardiac Muscle Cells. *Developmental biology*. 187:311-321.

Luo, H., X. Liu, F. Wang, Q. Huang, S. Shen, L. Wang, G. Xu, X. Sun, H. Kong, and M. Gu. 2005a. Disruption of palladin results in neural tube closure defects in mice. *Molecular and Cellular Neuroscience*. 29:507-515.

Luo, H., X. Liu, F. Wang, Q. Huang, S. Shen, L. Wang, G. Xu, X. Sun, H. Kong, M. Gu, S. Chen, Z. Chen, and Z. Wang. 2005b. Disruption of palladin results in neural tube closure defects in mice. *Mol Cell Neurosci*. 29:507-515.

Luther, P.K. 2009. The vertebrate muscle Z-disc: sarcomere anchor for structure and signalling. *Journal of muscle research and cell motility*. 30:171-185.

Luther, P.K., J.S. Barry, and J.M. Squire. 2002. The three-dimensional structure of a vertebrate wide (slow muscle) Z-band: lessons on Z-band assembly. *Journal of molecular biology*. 315:9-20.

Ma, K., J.G. Forbes, G. Gutierrez-Cruz, and K. Wang. 2006. Titin as a Giant Scaffold for Integrating Stress and Src Homology Domain 3-mediated Signaling Pathways THE CLUSTERING OF NOVEL OVERLAP LIGAND MOTIFS IN THE ELASTIC PEVK SEGMENT. *Journal of Biological Chemistry*. 281:27539-27556.

Ma, K., and K. Wang. 2002. Interaction of nebulin SH3 domain with titin PEVK and myopalladin: implications for the signaling and assembly role of titin and nebulin. *FEBS letters*. 532:273-278.

Marian, A., and R. Roberts. 2001. The molecular genetic basis for hypertrophic cardiomyopathy. *Journal of molecular and cellular cardiology*. 33:655-670.

Maron, B.J. 2002. Hypertrophic cardiomyopathy: a systematic review. *Jama*. 287:1308-1320.

Maruyama, K., S. MATSUBARA, R. NATORI, Y. NONOMURA, S. KIMURA, K. OHASHI, F. MURAKAMI, S. HANDA, and G. EGUCHI. 1977a. Connectin, an elastic protein of muscle Characterization and Function. *Journal of biochemistry*. 82:317-337.

Maruyama, K., F. MURAKAMI, and K. OHASHI. 1977b. Connectin, an Elastic Protein of Muscle Comparative Biochemistry. *Journal of biochemistry*. 82:339-345.

Mastrototaro, G., X. Liang, X. Li, P. Carullo, N. Piroddi, C. Tesi, Y. Gu, N.D. Dalton, K.L. Peterson, and C. Poggesi. 2015. Nebulette knockout mice have normal cardiac function but show Z-line widening and upregulation of cardiac stress markers. *Cardiovascular research*:cvv156.

McElhinny, A.S., S.T. Kazmierski, S. Labeit, and C.C. Gregorio. 2003. Nebulin: the nebulous, multifunctional giant of striated muscle. *Trends in cardiovascular medicine*. 13:195-201.

McElhinny, A.S., C. Schwach, M. Valichnac, S. Mount-Patrick, and C.C. Gregorio. 2005. Nebulin regulates the assembly and lengths of the thin filaments in striated muscle. *The Journal of cell biology*. 170:947-957.

McNally, E., and L. Dellefave. 2009. Sarcomere mutations in cardiogenesis and ventricular noncompaction. *Trends in cardiovascular medicine*. 19:17-21.

McNally, E.M., J.R. Golbus, and M.J. Puckelwartz. 2013. Genetic mutations and mechanisms in dilated cardiomyopathy. *The Journal of clinical investigation*. 123:19-26.

Meyer, T., V. Ruppert, S. Ackermann, A. Richter, A. Perrot, S.R. Sperling, M.G. Posch, B. Maisch, and S. Pankuweit. Novel mutations in the sarcomeric protein myopalladin in patients with dilated cardiomyopathy. *Eur J Hum Genet*. 21:294-300.

Meyer, T., V. Ruppert, S. Ackermann, A. Richter, A. Perrot, S.R. Sperling, M.G. Posch, B. Maisch, and S. Pankuweit. 2013. Novel mutations in the sarcomeric protein myopalladin in patients with dilated cardiomyopathy. *Eur J Hum Genet*. 21:294-300.

Miano, J.M., N. Ramanan, M.A. Georger, K.L. de Mesy Bentley, R.L. Emerson, R.O. Balza, Jr., Q. Xiao, H. Weiler, D.D. Ginty, and R.P. Misra. 2004. Restricted inactivation of serum response factor to the cardiovascular system. *Proceedings of the National Academy of Sciences of the United States of America*. 101:17132-17137.

Miller, M.K., M.-L. Bang, C.C. Witt, D. Labeit, C. Trombitas, K. Watanabe, H. Granzier, A.S. McElhinny, C.C. Gregorio, and S. Labeit. 2003. The muscle ankyrin repeat proteins: CARP, ankrd2/Arpp and DARP as a family of titin filament-based stress response molecules. *Journal of molecular biology*. 333:951-964.

Millevoi, S., K. Trombitas, B. Kolmerer, S. Kostin, J. Schaper, K. Pelin, H. Granzier, and S. Labeit. 1998. Characterization of nebulette and nebulin and emerging concepts of their roles for vertebrate Z-discs. *Journal of molecular biology*. 282:111-123.

Miralles, F., G. Posern, A.-I. Zaromytidou, and R. Treisman. 2003. Actin dynamics control SRF activity by regulation of its coactivator MAL. *Cell*. 113:329-342.

Mohrman, D.E., and L.J. Heller. 2002. Cardiovascular physiology.

Moncman, C.L., and K. Wang. 1999. Functional dissection of nebulette demonstrates actin binding of nebulin-like repeats and Z-line targeting of SH3 and linker domains. *Cell motility and the cytoskeleton*. 44:1-22.

Moncman, C.L., and K. Wang. 2002. Targeted disruption of nebulette protein expression alters cardiac myofibril assembly and function. *Experimental cell research*. 273:204-218.

Morimoto, S. 2008. Sarcomeric proteins and inherited cardiomyopathies. *Cardiovascular research*. 77:659-666.

Morita, H., R. Nagai, J. Seidman, and C.E. Seidman. 2010. Sarcomere gene mutations in hypertrophy and heart failure. *Journal of cardiovascular translational research*. 3:297-303.

Niu, Z., W. Yu, S.X. Zhang, M. Barron, N.S. Belaguli, M.D. Schneider, M. Parmacek, A. Nordheim, and R.J. Schwartz. 2005. Conditional mutagenesis of the murine serum response factor gene blocks cardiogenesis and the transcription of downstream gene targets. *The Journal of biological chemistry*. 280:32531-32538.

Noorman, M., M.A. van der Heyden, T.A. van Veen, M.G. Cox, R.N. Hauer, J.M. de Bakker, and H.V. van Rijen. 2009. Cardiac cell–cell junctions in health and disease: electrical versus mechanical coupling. *Journal of molecular and cellular cardiology*. 47:23-31.

Norman, C., M. Runswick, R. Pollock, and R. Treisman. 1988. Isolation and properties of cDNA clones encoding SRF, a transcription factor that binds to the c-fos serum response element. *Cell*. 55:989-1003.

Ono, S. 2010. Dynamic regulation of sarcomeric actin filaments in striated muscle. *Cytoskeleton*. 67:677-692.

Otey, C.A., R. Dixon, C. Stack, and S.M. Goicoechea. 2009a. Cytoplasmic Ig-domain proteins: cytoskeletal regulators with a role in human disease. *Cell motility and the cytoskeleton*. 66:618.

Otey, C.A., R. Dixon, C. Stack, and S.M. Goicoechea. 2009b. Cytoplasmic Ig-domain proteins: cytoskeletal regulators with a role in human disease. *Cell Motil Cytoskeleton*. 66:618-634.

Pappas, C.T., N. Bhattacharya, J.A. Cooper, and C.C. Gregorio. 2008. Nebulin interacts with CapZ and regulates thin filament architecture within the Z-disc. *Molecular biology of the cell*. 19:1837-1847.

Pappas, C.T., P.A. Krieg, and C.C. Gregorio. 2010. Nebulin regulates actin filament lengths by a stabilization mechanism. *The Journal of cell biology*. 189:859-870.

Parast, M.M., and C.A. Otey. 2000a. Characterization of palladin, a novel protein localized to stress fibers and cell adhesions. *The Journal of cell biology*. 150:643-656.

Parast, M.M., and C.A. Otey. 2000b. Characterization of palladin, a novel protein localized to stress fibers and cell adhesions. *J Cell Biol*. 150:643-656.

Parker, I., W. Zang, and W. Wier. 1996. Ca2+ sparks involving multiple Ca2+ release sites along Z-lines in rat heart cells. *The Journal of Physiology*. 497:31-38.

Parlakian, A., C. Charvet, B. Escoubet, M. Mericskay, J.D. Molkentin, G. Gary-Bobo, L.J. De Windt, M.-A. Ludosky, D. Paulin, and D. Daegelen. 2005. Temporally controlled onset of dilated cardiomyopathy through disruption of the SRF gene in adult heart. *Circulation*. 112:2930-2939.

Parmacek, M.S. 2007. Myocardin-Related Transcription Factors Critical Coactivators Regulating Cardiovascular Development and Adaptation. *Circulation research*. 100:633-644.

Parry, D., and J. Squire. 1973. Structural role of tropomyosin in muscle regulation: analysis of the x-ray diffraction patterns from relaxed and contracting muscles. *Journal of molecular biology*. 75:33-55.

Parvari, R., and A. Levitas. 2012. The mutations associated with dilated cardiomyopathy. *Biochemistry research international*. 2012.

Pashmforoush, M., P. Pomiès, K.L. Peterson, S. Kubalak, J. Ross, A. Hefti, U. Aebi, M.C. Beckerle, and K.R. Chien. 2001. Adult mice deficient in actinin–associated LIM-domain protein reveal a developmental pathway for right ventricular cardiomyopathy. *Nature medicine*. 7:591-597.

Perriard, J.-C., A. Hirschy, and E. Ehler. 2003. Dilated cardiomyopathy: a disease of the intercalated disc? *Trends in cardiovascular medicine*. 13:30-38.

Pipes, G.T., E.E. Creemers, and E.N. Olson. 2006. The myocardin family of transcriptional coactivators: versatile regulators of cell growth, migration, and myogenesis. *Genes & development*. 20:1545-1556.

Pogue-Geile, K.L., R. Chen, M.P. Bronner, T. Crnogorac-Jurcevic, K.W. Moyes, S. Dowen, C.A. Otey, D.A. Crispin, R.D. George, and D.C. Whitcomb. 2006. Palladin mutation causes familial pancreatic cancer and suggests a new cancer mechanism. *PLoS Med*. 3:e516.

Posern, G., F. Miralles, S. Guettler, and R. Treisman. 2004. Mutant actins that stabilise F-actin use distinct mechanisms to activate the SRF coactivator MAL. *The EMBO journal*. 23:3973-3983.

Posern, G., and R. Treisman. 2006. Actin'together: serum response factor, its cofactors and the link to signal transduction. *Trends in cell biology*. 16:588-596.

Purevjav, E., T. Arimura, S. Augustin, A.C. Huby, K. Takagi, S. Nunoda, D.L. Kearney, M.D. Taylor, F. Terasaki, J.M. Bos, S.R. Ommen, H. Shibata, M. Takahashi, M. Itoh-Satoh, W.J. McKenna, R.T. Murphy, S. Labeit, Y. Yamanaka, N. Machida, J.E. Park, P.M. Alexander, R.G. Weintraub, Y. Kitaura, M.J. Ackerman, A. Kimura, and J.A. Towbin. 2012a. Molecular Basis for Clinical Heterogeneity in Inherited Cardiomyopathies Due to Myopalladin Mutations. *Hum Mol Genet*.

Purevjav, E., T. Arimura, S. Augustin, A.C. Huby, K. Takagi, S. Nunoda, D.L. Kearney, M.D. Taylor, F. Terasaki, J.M. Bos, S.R. Ommen, H. Shibata, M. Takahashi, M. Itoh-Satoh, W.J. McKenna, R.T. Murphy, S. Labeit, Y. Yamanaka, N. Machida, J.E. Park, P.M. Alexander, R.G. Weintraub, Y. Kitaura, M.J. Ackerman, A. Kimura, and J.A. Towbin. 2012b. Molecular Basis for Clinical Heterogeneity in Inherited Cardiomyopathies Due to Myopalladin Mutations. *Hum Mol Genet*. 21:2039-2053.

Purevjav, E., J. Varela, M. Morgado, D.L. Kearney, H. Li, M.D. Taylor, T. Arimura, C.L. Moncman, W. McKenna, and R.T. Murphy. 2010. Nebulette mutations are associated with dilated cardiomyopathy and endocardial fibroelastosis. *Journal of the American College of Cardiology*. 56:1493-1502.

Pyle, W.G., and R.J. Solaro. 2004. At the crossroads of myocardial signaling the role of Z-discs in intracellular signaling and cardiac function. *Circulation Research*. 94:296-305.

Rachlin, A.S., and C.A. Otey. 2006a. Identification of palladin isoforms and characterization of an isoform-specific interaction between Lasp-1 and palladin. *J Cell Sci*. 119:995-1004.

Rachlin, A.S., and C.A. Otey. 2006b. Identification of palladin isoforms and characterization of an isoform-specific interaction between Lasp-1 and palladin. *Journal of cell science*. 119:995-1004.

Richardson, P., R. McKenna, M. Bristow, B. Maisch, B. Mautner, J. O'connell, E. Olsen, G. Thiene, J. Goodwin, and I. Gyarfas. 1996. Report of the 1995 World Health Organization/International Society and Federation of Cardiology Task Force on the definition and classification of car diomyopathies. *Circulation*. 93:841-842.

Rönty, M., A. Taivainen, M. Moza, C.A. Otey, and O. Carpén. 2004. Molecular analysis of the interaction between palladin and α-actinin. *FEBS letters*. 566:30-34.

Rönty, M.J., S.-K. Leivonen, B. Hinz, A. Rachlin, C.A. Otey, V.-M. Kähäri, and O.M. Carpén. 2006. Isoform-specific regulation of the actin-organizing protein palladin during TGF-β1-induced myofibroblast differentiation. *Journal of investigative dermatology*. 126:2387-2396.

Roy, B.C., T. Kuroda, S. Mori, K. Kohu, T. Akiyama, and T. Senda. 1999. Localization of a novel GAP family protein SPAL in the rat esophagus and heart. *Medical Electron Microscopy*. 32:20-24.

Russell, B., D. Motlagh, and W.W. Ashley. 2000. Form follows function: how muscle shape is regulated by work. *Journal of Applied Physiology*. 88:1127-1132.

Sarantitis, I., P. Papanastasopoulos, M. Manousi, N.G. Baikoussis, and E. Apostolakis. 2012. The cytoskeleton of the cardiac muscle cell. *Hellenic journal of cardiology: HJC= Hellēnikē kardiologikē epitheōrēsē*. 53:367-379.

Schweitzer, S.C., M.W. Klymkowsky, R.M. Bellin, R.M. Robson, Y. Capetanaki, and R.M. Evans. 2001. Paranemin and the organization of desmin filament networks. *Journal of cell science*. 114:1079-1089.

Severs, N.J., A.F. Bruce, E. Dupont, and S. Rothery. 2008. Remodelling of gap junctions and connexin expression in diseased myocardium. *Cardiovascular research*. 80:9-19.

Sheikh, F., R.S. Ross, and J. Chen. 2009. Cell-cell connection to cardiac disease. *Trends in cardiovascular medicine*. 19:182-190.

Solaro, J.R., and J. Van Eyk. 1996. Altered interactions among thin filament proteins modulate cardiac function. *Journal of molecular and cellular cardiology*. 28:217-230.

Solaro, R.J. 2005. Remote control of A-band cardiac thin filaments by the IZI protein network of cardiac sarcomeres. *Trends in cardiovascular medicine*. 15:148-152.

Solway, J., J. Seltzer, F.F. Samaha, S. Kim, L.E. Alger, Q. Niu, E.E. Morrisey, H.S. Ip, and M.S. Parmacek. 1995. Structure and expression of a smooth muscle cell-specific gene, SM22α. *Journal of Biological Chemistry*. 270:13460-13469.

Sorimachi, H., A. Freiburg, B. Kolmerer, S. Ishiura, G. Stier, C. Gregorio, D. Labeit, W.A. Linke, K. Suzuki, and S. Labeit. 1997. Tissue-specific expression and α-actinin binding properties of the Z-disc titin: implications for the nature of vertebrate Z-discs. *Journal of molecular biology*. 270:688-695.

Sotiropoulos, A., D. Gineitis, J. Copeland, and R. Treisman. 1999. Signal-regulated activation of serum response factor is mediated by changes in actin dynamics. *Cell*. 98:159-169.

Squire, J. 1981. Introduction. *In* The Structural Basis of Muscular Contraction. Springer. 1-38.

Squire, J.M. 1997. Architecture and function in the muscle sarcomere. *Current opinion in structural biology*. 7:247-257.

Takano, K., H. Watanabe-Takano, S. Suetsugu, S. Kurita, K. Tsujita, S. Kimura, T. Karatsu, T. Takenawa, and T. Endo. 2010. Nebulin and N-WASP Cooperate to Cause IGF-1–Induced Sarcomeric Actin Filament Formation. *Science*. 330:1536-1540.

Treisman, R. 1995. Journey to the surface of the cell: Fos regulation and the SRE. *The EMBO Journal*. 14:4905.

von Nandelstadh, P., M. Ismail, C. Gardin, H. Suila, I. Zara, A. Belgrano, G. Valle, O. Carpen, and G. Faulkner. 2009. A class III PDZ binding motif in the myotilin and FATZ families binds enigma family proteins: a common link for Z-disc myopathies. *Molecular and cellular biology*. 29:822-834.

Wang, D.-Z., P.S. Chang, Z. Wang, L. Sutherland, J.A. Richardson, E. Small, P.A. Krieg, and E.N. Olson. 2001. Activation of cardiac gene expression by myocardin, a transcriptional cofactor for serum response factor. *Cell*. 105:851-862.

Wang, D.-Z., S. Li, D. Hockemeyer, L. Sutherland, Z. Wang, G. Schratt, J.A. Richardson, A. Nordheim, and E.N. Olson. 2002. Potentiation of serum response factor activity by a family of myocardin-related transcription factors. *Proceedings of the National Academy of Sciences*. 99:14855-14860.

Wang, H.V., and M. Moser. 2008a. Comparative expression analysis of the murine palladin isoforms. *Developmental Dynamics*. 237:3342-3351.

Wang, H.V., and M. Moser. 2008b. Comparative expression analysis of the murine palladin isoforms. *Dev Dyn*. 237:3342-3351.

Wang, K., J. McClure, and A. Tu. 1979. Titin: major myofibrillar components of striated muscle. *Proceedings of the National Academy of Sciences*. 76:3698-3702.

Wang, K., and J. Wright. 1988. Architecture of the sarcomere matrix of skeletal muscle: immunoelectron microscopic evidence that suggests a set of parallel inextensible nebulin filaments anchored at the Z line. *The Journal of cell biology*. 107:2199-2212.

Williams, D.A., L.M. Delbridge, S.H. Cody, P. Harris, and T. Morgan. 1992. Spontaneous and propagated calcium release in isolated cardiac myocytes viewed by confocal microscopy. *American Journal of Physiology-Cell Physiology*. 262:C731-C742.

Witt, C.C., C. Burkart, D. Labeit, M. McNabb, Y. Wu, H. Granzier, and S. Labeit. 2006. Nebulin regulates thin filament length, contractility, and Z-disk structure in vivo. *The EMBO Journal*. 25:3843-3855.

Woodcock, E.A., and S.J. Matkovich. 2005. Cardiomyocytes structure, function and associated pathologies. *The international journal of biochemistry & cell biology*. 37:1746-1751.

Yamada, S., S. Pokutta, F. Drees, W.I. Weis, and W.J. Nelson. 2005. Deconstructing the cadherin-catenin-actin complex. *Cell*. 123:889-901.

Zhang, J.Q., B. Elzey, G. Williams, S. Lu, D.J. Law, and R. Horowits. 2001. Ultrastructural and biochemical localization of N-RAP at the interface between myofibrils and intercalated disks in the mouse heart. *Biochemistry*. 40:14898-14906.

Zou, P., N. Pinotsis, S. Lange, Y.-H. Song, A. Popov, I. Mavridis, O.M. Mayans, M. Gautel, and M. Wilmanns. 2006. Palindromic assembly of the giant muscle protein titin in the sarcomeric Z-disk. *Nature*. 439:229-233.

Chapter 2

Nebulette knockout mice have normal cardiac function but show Z-line widening and upregulation of cardiac stress markers

Giuseppina Mastrototaro[1,2,*], Xingqun Liang[3,6,*], Xiaodong Li[3,7], Pierluigi Carullo[1,4], Nicoletta Piroddi[5], Chiara Tesi[5], Yusu Gu[3], Nancy D. Dalton[3], Kirk L. Peterson[3], Corrado Poggesi[5], Farah Sheikh[3], Ju Chen[3,§], and Marie-Louise Bang[1,4,§]

[1]Humanitas Clinical and Research Center, Rozzano, Milan, Italy; [2]University of Milano-Bicocca, Milan, Italy; [3]Department of Medicine, University of California San Diego, La Jolla, California, USA; [4]Institute of Genetic and Biomedical Research, UOS Milan, National Research Council, Milan, Italy; [5]Department of Experimental and Clinical Medicine, University of Florence, Florence, Italy; [6]Current address: Key Laboratory of Arrhythmia, Ministry of Education, East Hospital, Tongji University School of Medicine, Shanghai 200120, China; [7]Current address: Department of Pathology, Keck Medical School, University of Southern California, Los Angeles, USA.

Short title: Nebulette knockout mice have normal heart function

*The two authors equally contributed to the work
§Corresponding authors

Published : *Cardiovasc Res.* 2015 Jul 15;107(2):216-25.

Abstract

Aims Nebulette is a 109 kDa modular protein localized in the sarcomeric Z-line of the heart. In vitro studies have suggested a role of nebulette in stabilizing the thin filament, and missense mutations in the nebulette gene were recently shown to be causative for dilated cardiomyopathy and endocardial fibroelastosis in human and mice. However, the role of nebulette in vivo has remained elusive. To rovide insights into the function of nebulette in vivo, we generated and studied nebulette-deficient (*nebl* $^{-/-}$) mice.

Methods and results *Nebl* $^{-/-}$ mice were generated by replacement of exon 1 by Cre under the control of the endogenous nebulette promoter, allowing for lineage analysis using the ROSA26 Cre reporter strain. This revealed specific expression of nebulette in the heart, consistent with in situ hybridization results. *Nebl* $^{-/-}$ mice exhibited normal cardiac function both under basal conditions and in response to transaortic constriction as assessed by echocardiography and haemodynamic analyses. Furthermore, histological, IF, and western blot analysis showed no cardiac abnormalities in *nebl* $^{-/-}$ mice up to 8 months of age. In contrast, transmission electron microscopy showed Z-line widening starting from 5 months of age, suggesting that nebulette is important for the integrity of the Z-line. Furthermore, up-regulation of cardiac stress responsive genes suggests the presence of chronic cardiac stress in *nebl* $^{-/-}$ mice.

Conclusion Nebulette is dispensable for normal cardiac function, although Z-line widening and up-regulation of cardiac stress markers were found in n*ebl* $^{-/-}$ heart. These results suggest that the nebulette disease causing mutations have dominant gain-of-function effects.

1. Introduction

Nebulette is a 109 kDa cardiac-specific sarcomeric protein, highly homologous to the C-terminal Z-disc region of the larger protein nebulin (~500-900 kDa), which is predominantly expressed in skeletal muscle.(Wang and Wright 1988) Like nebulin, nebulette is composed of 35-residue nebulin-like repeats, a serine-rich region, and a C-terminal SH3 domain.(Millevoi, Trombitas et al. 1998) However, while nebulin contains up to 185 nebulin-like repeats and extends from the Z-line along the length of the thin filament, nebulette contains only up to 23 repeats and is localized at the Z-line from which it protrudes only a short distance along the thin filament.(Millevoi, Trombitas et al. 1998) The nebulin-like repeats of both nebulin and nebulette bind to the thin filament components actin,(Jin and Wang 1991, Pfuhl, Winder et al. 1994, Moncman and Wang 1999, Ogut, Hossain et al. 2003) tropomyosin 1,(Labeit and Kolmerer 1995, Moncman and Wang 1999, Ogut, Hossain et al. 2003, Bonzo, Norris et al. 2008, Holmes and Moncman 2008, Marttila, Hanif et al. 2014) and troponin T(Labeit and Kolmerer 1995, Ogut, Hossain et al. 2003), while their C-terminal SH3 domains have been reported to interact with myopalladin,(Bang, Mudry et al. 2001) palladin,(Bang, Mudry et al. 2001) α-actinin,(Moncman and Wang 1999) zyxin,(Li, Zhuang et al. 2004) N-WASP,(Takano, Watanabe-Takano et al. 2010) and titin's Zis1 and PEVK regions,(Ma and Wang 2002, Ma, Forbes et al. 2006, Witt, Burkart et al. 2006) in the Z-disc. Additionally, nebulette binds to filamin C(Holmes and Moncman 2008) and possibly Cypher/ZASP,(Holmes and Moncman 2008) while nebulin C-terminal repeats M160-164 were reported to interact with

CapZ(Pappas, Bhattacharya et al. 2008) and desmin.(Bang, Gregorio et al. 2002, Conover, Henderson et al. 2009) It remains to be determined whether nebulette can also interact with CapZ and desmin. Based on its interaction with thin filament components and close connection to the actin filament along its length, nebulin was long thought to be a ruler regulating thin filament length.(Wang and Wright 1988, Labeit, Gibson et al. 1991) However, recent findings by us and others has revealed that it does not directly regulate thin filament length, but rather stabilizes the thin filament, allowing it reach its final length.(Bang, Li et al. 2006, Pappas, Bhattacharya et al. 2008, Castillo, Nowak et al. 2009, Pappas, Krieg et al. 2010) Although nebulette is localized in the Z-line and does not extend the length of the thin filament, loss of endogenous nebulette in chicken embryonic cardiomyocytes as a result of overexpression of the nebulette serine-rich region and/or SH3 domain, resulted in shorter thin filaments,(Moncman and Wang 2002) similar to observations in skeletal muscle of nebulin knockout mice.(Bang, Li et al. 2006, Witt, Burkart et al. 2006) Thus, despite of its localization in the Z-line, also nebulette appears to play a role in stabilizing the thin filament. Furthermore, consistent with the finding that nebulette repeats increase the affinity of the tropomyosin-troponin T complex for F-actin,(Ogut, Hossain et al. 2003) loss of nebulette was reported to cause a reduction in tropomyosin and troponin T staining along the thin filament without affecting the organization of the Z-line or the thick filament.(Moncman and Wang 2002, Bonzo, Norris et al. 2008) The role of nebulette in the Z-line remains elusive but based on its high homology with the C-terminal Z-line region of nebulin, the two

proteins are thought to play similar roles in the Z-line. Nebulin knockout mice exhibit widened and misaligned Z-lines,(Bang, Li et al. 2006, Witt, Burkart et al. 2006, Tonino, Pappas et al. 2010) suggesting a role for nebulin in the maintenance of Z-line width and the lateral registration of Z-lines, likely through its binding to desmin.(Bang, Li et al. 2006, Tonino, Pappas et al. 2010) Furthermore, we recently showed that mice deficient for the nebulin SH3 domain are more susceptible to eccentric contraction induced injury,(Yamamoto, Vitiello et al. 2013) consistent with a role for nebulin in maintaining Z-line structure during load, protecting the muscle from injury. The recent identification of *nebulette* variants in patients with dilated cardiomyopathy (DCM) and endocardial fibroelastosis(Purevjav, Varela et al. 2010) suggests that nebulette may play a similar important role in the heart. The identified variants include four heterozygous missense mutations localized within different regions of the *nebulette* gene, associated with DCM of different severity and age of disease onset. The K60N, Q128R, and G202R variants reside in the nebulin-like repeat region in the I-band region, while the A592E variant is localized in the Z-line region. The patients carrying the Q128R and A592 variants (the patient carrying the A582 variant also carried a mutation in α-actinin 2) were affected from birth, while the patients carrying the K60N and G202R variants developed adult-onset DCM. The cardiomyopathy phenotype was recapitulated in transgenic mouse models overexpressing nebulette mutations, resulting in various phenotypes ranging from embryonic lethality (K60N, Q128R) to adult-onset progressive DCM (G202R, A592E) associated with disruption of I-band and Z-line proteins.(Purevjav, Varela et al. 2010,

Maiellaro-Rafferty, Wansapura et al. 2013) To provide new insights into the function of nebulette in the heart *in vivo*, we generated and studied nebulette deficient (*nebl*$^{-/-}$) mice. Surprisingly, *nebl*$^{-/-}$ mice exhibited normal cardiac function, although Z-line widening and upregulation of markers associated with cardiac stress were observed.

2. Methods

2.1 Generation of nebulette knockout mice

Nebulette genomic DNA was isolated from a 129SVJ mouse genomic library (Stratagene, La Jolla, CA) and used to generate a nebulette-targeting construct for the replacement of nebulette exon 1 by a cre-FRT-neo-FRT cassette under the control of the endogenous *nebulette* promoter essentially as described previously (*Figure 1A*) (Bang, Li et al. 2006). The targeting construct was verified by sequencing and linearized with NotI before electroporation into R1 ES cells at the Transgenic Core Facility at the University of California, San Diego. G418-resistant ES clones were screened for homologous recombination by BamHI digestion of ES cell DNA and Southern blot analysis with the probe shown in *Figure 1B*. G418-resistant ES clones were screened for homologous recombination by Southern blot analysis with the probe shown in *Figure 1B*. The wildtype (WT) allele is represented by the band of 8.5 kb, whereas the 5.4 kb band represents the correctly targeted mutant allele. Cells from two independent homologous recombinant ES clones were microinjected into C57BL/6 blastocysts and transferred into pseudopregnant mice. Male chimeras resulting from the microinjections were bred with

female Black Swiss mice to generate germ line transmitted heterozygous nebulette knockout mice (*nebl*$^{+/-}$), which were subsequently intercrossed to generate homozygous knockout mice (*nebl*$^{-/-}$). Offspring from intercrosses were genotyped by PCR analysis using mouse tail DNA and WT (sense: GTGCCCCAGAGACTTGGTAG; reverse: AGAGGGAGGGAGAAGGTCTG), and mutant allele-specific primers (sense: GTTCGCAAGAACCTGATGCACA; reverse: CTAGAGCCTGTTTTGCACGTTC). Successful ablation of the nebulette gene was confirmed by Western blot analysis using polyclonal antibodies against nebulette (kindly provided by Dr. Siegfried Labeit, Medical Faculty Mannheim, University of Heidelberg, Germany). All animal studies were approved by the University of California San Diego Animal Care and Use Committee and the Italian Ministry of Health. Animal procedures were performed in full compliance with the guidelines for the Guide for the Care and Use of Laboratory Animals, eighth edition (2011) published by the US National Institutes of Health (NIH) and the Directive 2010/63/EU of the European Parliament on the protection of animals use for scientific purposes. Mice for experiments were sacrificed by cervical dislocation following anesthesia by intraperitoneal injection of a mixture of ketamine (100 mg/kg) and xylazine (5 mg/kg).

2.2 β-galactosidase staining

To perform fate mapping of nebulette-expressing cells, *nebl*$^{+/-}$ mice were crossed with the ROSA26 reporter line to generate double heterozygous *nebl*$^{+/-}$/R26R mice in which lacZ is expressed from the ROSA26 promoter after Cre-mediated recombination.(Soriano 1999) E9.5 and E11.5 *nebl*$^{+/-}$/R26R embryos were fixed in 4% PFA and β-galactosidase staining of whole mount and transverse sections were performed as previously described.(Bang, Li et al. 2006) Imaging was performed on a dissecting microscope (SV-6; Carl Zeiss MicroImaging, Inc.) with a 35-mm camera (C-mount; Nikon).

2.3 *In situ* hybridization

Whole-mount in situ hybridization of paraffin sections at different stages of mouse development was carried out using digoxigenin-labeled RNA probes as previously described.(Wilkinson 1992, Liang, Zhou et al. 2005) A 718 bp RNA probe spanning bp 646 to 1363 of mouse nebulette XM_006497555 was utilized.

2.4 Histology, immunohistochemistry, and transmission electron microscopy (TEM)

For histology and immunostaining, mouse hearts were harvested and relaxed in 50 mM KCl in PBS before overnight fixation in 4% paraformaldehyde in PBS. For histology, hearts were dehydrated and embedded in paraffin, whereafter 10 μm sections were cut and analyzed by staining with hematoxylin and eosin, or Picro Sirius red. For immunostainings, fixed hearts were saturated in 10 and 30% sucrose in PBS and subsequently frozen in OCT, whereafter 10 μm

cryosections were cut. Permeabilization and blocking was performed for 1 hour in blocking solution containing 3% normal goat serum, 0.3% Triton X-100, 50 mM glycine, and 1% cold water fish gelatin (Sigma Aldrich) in PBS after which sections were incubated with primary antibodies in wash buffer (blocking buffer diluted 10 times in PBS) overnight at 4°C. The following primary antibodies were used: nebulette (1:50; kindly provided by Dr. Siegfried Labeit), myopalladin(Yamamoto, Vitiello et al. 2013) (1:50), palladin 621 (1:100; kindly provided by Dr. Carol Otey, University of North Carolina, Chapel Hill, NC, USA), N-WASP (1:25; Santa Cruz D15, #sc-10122), cypher (1:100; (Zhou, Chu et al. 2001), CapZ β1 (5 μg/ml; Developmental Studies Hybridoma Bank, University of Iowa, USA (DSHB), #1E5.25.4), sarcomeric α-actinin (1:500; Sigma Aldrich #A7811), desmin (1:80; Abcam #ab8592), filamin C (1:1000; kindly provided by Dr. Dieter Fürst, University of Bonn, Germany), tropomyosin CH1 (5 μg/ml; DSHB, CH1), troponin T (5 μg/ml; DSHB, CT3), and tropomodulin (1:500; kindly provided by Dr. Mark Sussman, San Diego State University, San Diego, CA, USA). After washing, sections were incubated at room temperature for 4 hours with rhodamine-labeled phalloidin (1:100, Sigma-Aldrich) or Alexa-Fluor-488 or -568-conjugated IgG secondary antibodies (1:500, Life Technologies). Confocal microscopy was performed using an Olympus Fluoview FV1000 laser scanning confocal microscope with a 60X oil immersion lens (N. A. 1.3; Olympus). Individual images (1024 x 1024) were converted to tiff format and merged as pseudocolor RGB images using ImageJ. For TEM, the heart was excised and fixed in 2% paraformaldehyde and 2% glutaraldehyde in

0.15 M sodium cacodylate buffer, pH 7.4 as previously described.(Zhang, Bang et al. 2008) Briefly, the left ventricle was cut into small pieces (~1 mm cubes) and stained overnight in 1% osmium tetroxide, 0.8% potassium ferrocyanide. The following day, tissue was stained for 2 hours in 2% uranyl acetate and subsequently dehydrated in a series of ethanol and acetone washes. The tissue was embedded in Durcupan resin (EMD, Gibbstown, NJ, USA) and ultra thin sections (60-70 nm) were stained with lead citrate. Electron micrographs were recorded by using a JEOL 1200EX electron microscope operated at 80 kV. Z-line width was measured using ImageJ 2.0.0 software based on the analysis of >100 Z-lines per heart from 2-3 mice per genotype and time point. Z-line values were binned in 10 nm binds and plotted in histograms fitted with the Gaussian distribution using PRISM 6 software (*Figure 4B*).

2.5 Western blot analysis

Total left ventricular tissue was homogenized in lysis buffer (50 mM Tris pH 7.5, 150 mM NaCl, 10 mM MgCl2, 0.5 mM DTT, 1 mM EDTA, 10% glycerol, 2% SDS, 1% Triton X-100, Roche Complete Protease Inhibitor Cocktail, 1 mM PMSF, 1 mM NaVO3, 5 mM NaF) using a TissueLyser II (Qiagen), whereafter Western blot analysis was performed using primary antibodies against the following proteins: nebulette (1:200), myopalladin (1:1000), palladin 621 (1:500), N-WASP (1:50), CapZ β1 (0.4 μg/ml), zyxin (1:50, Transduction lab no. Z45420), α-actinin (1:300.000), desmin (1:30.000), cypher (1:500), filamin C (1:10.000), tropomyosin (1:10.000), troponin I (0.2 ng/ml; DSHB TI-4), troponin T (2.3 ng/ml), tropomodulin (1:1000), CARP

(1:50), MYL2/MLC2v(Kubalak, Miller-Hance et al. 1994) (1:5000), MYL7/MLC2a(Kubalak, Miller-Hance et al. 1994) (1:10.000), and myomesin (1 μg/ml; DSHB mMaC myomesin B4). α-Tubulin antibodies (Abcam; 1:4000) were used for normalization.

2.6 *In vivo* cardiac physiology

For transthoracic echocardiography, mice were anesthetized with 1% isoflurane and imaged as previously described.(Tanaka, Dalton et al. 1996) For surgical procedures, mice were anesthetized by intraperitoneal injection of a mixture of ketamine (100 mg/kg) and xylazine (5 mg/kg) and the depth of anesthesia was monitored by toe pinch. Cardiac hemodynamic parameters were evaluated by insertion of a 1.4 French Millar catheter-tip micromanometer catheter through the right carotid artery into the left ventricle. Pressure was recorded at baseline and following stimulation with graded doses of the β-adrenergic agonist dobutamine (0.75, 2, and 4 μg/kg/min) as previously described.(Arber, Hunter et al. 1997) Transortic constriction (TAC) was performed with a 27-gauge needle as previously described.(Tanaka, Dalton et al. 1996) Echocardiography was performed 14 days after TAC and the pressure gradient was measured by Doppler echocardiography. Only mice showing an adequate pressure gradient (>70 mmHg) were included in the analysis. SHAM operated mice were used as controls.

2.7 RNA analyses

Total RNA was isolated from left ventricles of mice 3 weeks after SHAM or TAC-surgery using TRIzol reagent (Life Technologies) according to the manufacturer's instructions. For quantitative RT-PCR (qRT-PCR), first-strand cDNA synthesis was performed using the High Capacity cDNA Reverse Transcription kit from Applied Biosystems (Life Technologies), whereafter qRT-PCR was performed in triplicate with custom designed oligos (see Supplementary material online, *Table SI*) using the SYBR Select Master Mix (Life Technologies). Relative expression analysis was performed using the ΔΔCt method.

2.8 Mechanical experiments in isolated myofibrils

Mechanical experiments were performed at 15°C in single myofibrils and small bundles of a few myofibrils from frozen ventricular strips of *nebl*$^{-/-}$ and WT mice as previously described.(Kreutziger, Piroddi et al. 2011) Myofibrils (30-80 µm long, 1-4 µm wide, initial sarcomere length around 2.2 µm) were mounted between a length control motor and an opto-electronic force transducer and were maximally Ca^{2+}-activated (pCa 4.5) and fully relaxed (pCa 8.0) by fast (<5 ms) solution switching. Activating and relaxing solutions were as previously described (EGTA 10mM, MgATP 5 mM, free Mg^{2+}1 mM, inorganic Pi <5 µM).(Kreutziger, Piroddi et al. 2011) Maximal tension and the kinetics of force activation following rapid Ca^{2+}-activation, force redevelopment following release-restretch protocols, and force relaxation following rapid Ca^{2+} removal were measured (see Supplementary material online, *Figure S3*). Quasi-steady-state

sarcomere length - resting tension relations were determined in relaxing solution (pCa 8.0) for both myofibril groups. Ramp elongations of different extent (10–40% of the slack myofibril length) were applied to the preparations. Sarcomere length and resting tension were measured several seconds after each length change, when most of stress relaxation was over.

2.9 Statistical analysis

Data are presented as mean ± standard deviation (SD) or standard error of the mean (SEM) as indicated. Statistical comparisons between WT and *nebl*$^{-/-}$ mice were done using the unpaired Student's t-test. $P < 0.05$ was considered significant.

3. Results

3.1 Generation of Nebulette knockout (*nebl*$^{-/-}$) mice To study the role of nebulette *in vivo*, nebulette knockout mice (*nebl*$^{-/-}$) were generated by replacement of exon 1 by Cre under the control of the endogenous *nebl* promoter (*Figure 1A*). Targeted ES cells clones were identified by Southern blot analysis (*Figure 1B*) and the successful ablation of nebulette was confirmed by PCR and Western blot analysis (*Figure 1C*). Unexpectedly, we also found a 23 fold downregulation in mRNA levels of *lasp2* (encoding LIM and SH3 Protein-2/LIM-Nebulette), a splice variant of nebulette transcribed from a distinct promoter(Katoh 2003) (*Figure 5* and Supplementary material online, *Table SII*). While the *nebl* gene consists of 28 exons, *lasp2* is composed of only 7 exons, and encodes a protein with a domain structure significantly different from that of *nebl,* i.e. LASP2 contains

a LIM domain, three central nebulin repeats, and an SH3 domain. *Lasp2* exons 5, 6, 7 correspond to *nebl* exons 24, 27, 28, while *lasp2* exons 1-4 are 5' of *nebl* exon 1. It is possible that the replacement of *nebl* exon 1 and part of intron 1 with Cre cDNA may have affected *lasp2* splicing, leading to the dramatically decreased transcript levels of *lasp2*. *Nebl*$^{-/-}$ mice were born at Mendelian ratios, were indistinguishable from their wildtype (WT) littermates, and had a normal life span.

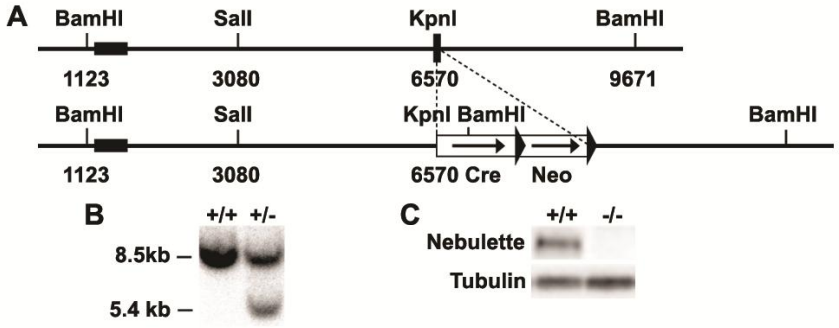

Figure 6: Targeting of the *nebulette* gene. (*A*) Targeting strategy for generation of nebulette knockout (*nebl*$^{-/-}$) mice. A restriction map of the relevant genomic region of *nebulette* is shown on top and the mutated locus after recombination is shown at the bottom. The black box indicates exon 1 and arrows indicate frt sites. Neo, neomycin resistance gene. **(*B*)** Detection of WT and targeted alleles by Southern blot analysis after digestion with BamHI using the probe shown in A. **(*C*)** Detection of nebulette protein by Western blot analysis. α-Tubulin antibody was used as loading control.

3.2 Lineage analysis shows specific expression of nebulette in the heart.

The insertion of Cre under the control of the endogenous *nebulette* promoter allowed us to perform lineage tracing by crossing heterozygous nebulette knockout (*nebl*$^{+/-}$) mice with the ROSA26 Cre

reporter strain, (Soriano 1999) which upon Cre-mediated recombination of the R26R locus expresses lacZ, thus resulting in selective lacZ expression in nebulette expressing cells or precursors. E9.5 and E11.5 *nebl*$^{+/-}$/*R26R* mouse embryos were stained for β-galactosidase activity, which revealed specific and homogeneous expression of nebulette in the heart in agreement with its reported localization (*Figure 2*). Consistent with these findings, whole mount *in situ* hybridization analysis of WT embryos at E8.5, E9.5, and E11.5 revealed specific expression of nebulette in the heart (see Supplementary material online, *Figure S1*).

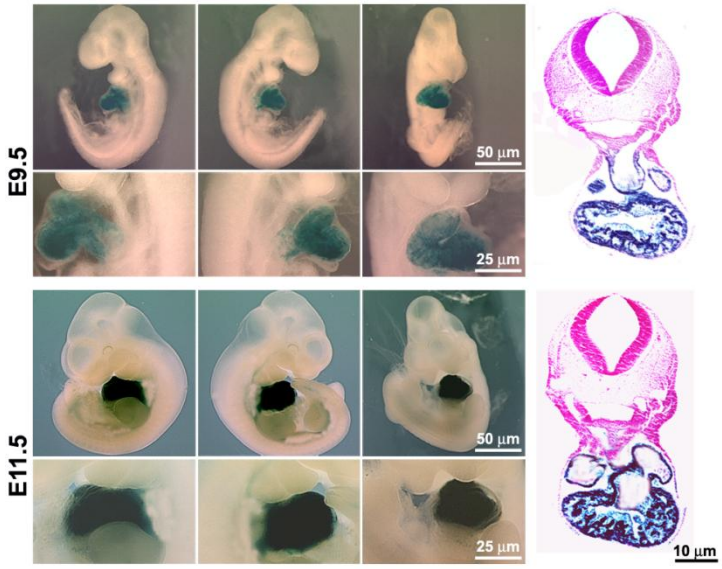

Figure 2: Lineage tracing shows specific expression of nebulette in the heart. X-galalactosidase staining of whole mount (left, right, and center view) and transverse sections of *nebl*$^{+/-}$/*R26R* embryos at E9.5 and E11.5.

3.3 *Nebl*$^{-/-}$ mouse hearts have normal cytoskeletal organization but show progressive Z-line widening

Nebl$^{-/-}$ mice had normal heart weight to body weight ratios and histological analyses by hematoxylin and eosin and Picro Sirius red stainings showed no cardiac abnormalities up till 8 months of age (Supplementary material online, *Figure S2A* and data now shown). In addition, immunostainings for nebulette-associated and sarcomeric proteins showed normal cytoskeletal organization and no effects on the localization of any of the tested proteins (Supplementary material online, *Figure S2A*). Likewise, Western blot analyses on left ventricular lysate showed no changes in protein levels of various sarcomeric proteins, many of which associated with nebulette (*Figure 3*).

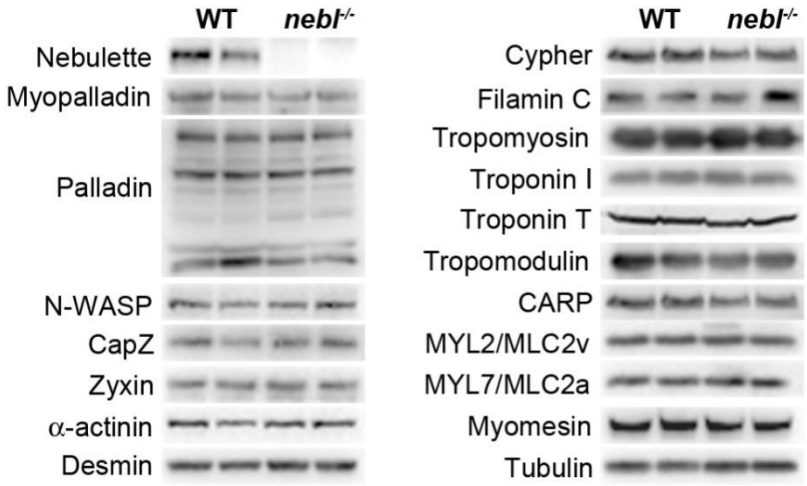

Figure 3: Western blot analysis on left ventricular lysate from WT and *nebl*$^{-/-}$ mice for various nebulette-associated and sarcomeric proteins. α-Tubulin antibody was used as loading control. The blots are representative of at least three different experiments.

On the other hand, transmission electron microscopy analysis revealed progressive Z-line abnormalities, including regions with severe Z-line widening and irregularities, in the left ventricle of *nebl*$^{-/-}$ mice compared to WT controls starting from around 5 months of age (*Figure 4A*). As evident from the histograms in *Figure 4B,* moderately increased Z-line width was observed in the left ventricle of *nebl*$^{-/-}$ mice both at 5 and 9 months of age, while regions with severely widened Z-lines (> 250 nm) were observed at 9 months of age (about 5% of Z-lines). Furthermore, localized areas with irregular Z-line were observed as shown in *Figure 4A* (top center). The average Z-line width in WT and *nebl*$^{-/-}$ mice was 79±11 nm and 119±28 nm at 5 months of age and 85±14 nm and 122±67 nm at 9 months of age. No abnormalities in mitochondria or other organelles were observed.

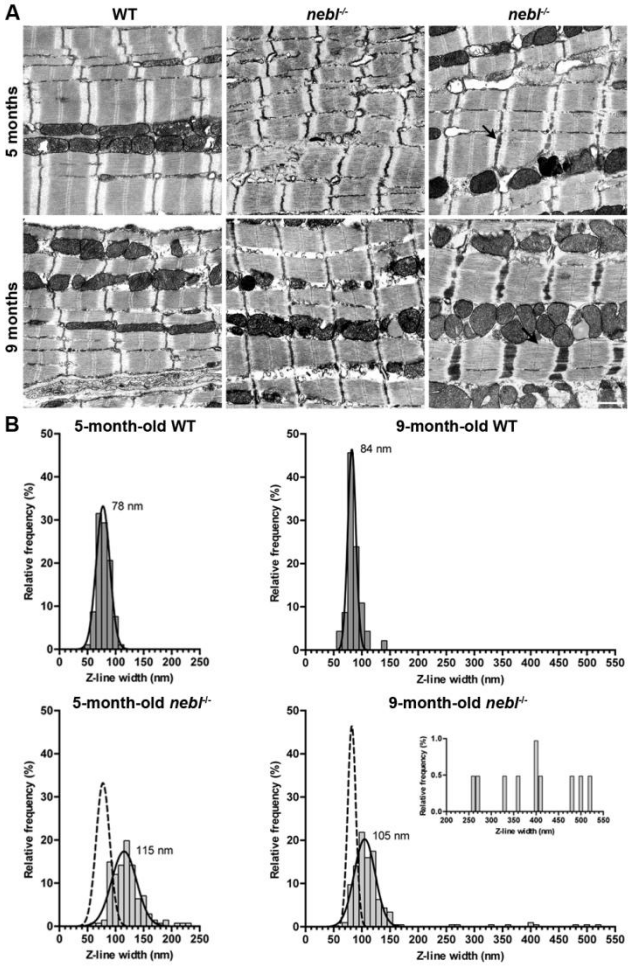

Figure 4: Transmission electron microscopy (TEM) analysis show Z-disc widening and irregularities in left ventricle from *nebl*$^{-/-}$ mice. (*A*) Representative electron micrographs of left ventricle from 5- and 9-month-old WT and *nebl*$^{-/-}$ mice. Moderate Z-line widening was observed in *nebl*$^{-/-}$ mice and at 9 months of age, areas with severely widened Z-discs were observed. Arrows show examples of wide Z-discs. Scale bar: 1 μm. **(*B*)** Analysis of Z-line widths (n = >100 per heart, n = 2-3 per genotype and time point). Histograms fitted with the Gaussian distribution are shown. The Gaussian fits of Z-line width in WT fibers are superimposed on the histograms from the analysis of *nebl*$^{-/-}$ fibers. The insert is a zoom-in of the Z-line measurements over 200 nm in 9-month-old *nebl*$^{-/-}$ mice.

3.4 *Nebl*$^{-/-}$ mice exhibit normal cardiac morphology and function both under basal conditions and in response to mechanical pressure overload

To determine the effect of nebulette KO on cardiac morphology and function, echocardiography was performed on 8-week- and 9-month-old *nebl*$^{-/-}$ mice compared to WT control mice. As shown in *Table I* and *II*, no significant differences were found between *nebl*$^{-/-}$ and WT mice in any of the parameters.

Table I Echocardiographic analysis of 9-month-old male *nebl*$^{-/-}$ mice compared to WT mice under basal conditions.

	WT (n = 6)	***nebl*$^{-/-}$ (n = 6)**
Body weight (g)	35.5 ± 2.6	33.2 ± 2.6
Heart rate (bpm)	574 ± 44	568 ± 72
LVIDd (mm)	4.03 ± 0.58	3.86 ± 0.43
LVIDs (mm)	2.54 ± 0.50	2.29 ± 0.47
IVSd (mm)	0.64 ± 0.05	0.61 ± 0.03
LVPWd (mm)	0.63 ± 0.05	0.62 ± 0.04
LV %FS	37.3 ± 3.5	41.1 ± 6.2
LVM (mg)	87.7 ± 17.2	77.9 ± 15.2
LVM/BW (mg/g)	2.47 ± 0.05	2.34 ± 0.04

All data are presented as mean ± standard deviation.
BW, body weight; LVIDd, left ventricular internal diameter in diastole; LVIDs, left ventricular internal diameter in systole; LVSd, interventricular septal thickness in diastole; LVPWd, left ventricular posterior wall thickness in diastole; LV %FS, left ventricular fractional shortening; LVM, left ventricular mass; bpm, beats per minute.

Likewise, hemodynamic function, as assessed by cardiac catherization of 12-week-old *nebl*$^{-/-}$ mice and WT in the absence and presence of graded doses of dobutamine, was comparable in *nebl*$^{-/-}$ and WT mice (*Table III*). To determine the response to mechanical pressure overload, 8-week-old *nebl*$^{-/-}$ and WT mice were subjected to transaortic constriction (TAC). Pressure gradients were measured by Doppler echocardiography and cardiac morphology and function was

evaluated by echocardiography 2 weeks after the procedure. As shown in *Table II*, *nebl*$^{-/-}$ and WT mice showed a similar cardiac hypertrophic response with a consequent reduction in fractional shortening. Thus, we conclude that ablation of nebulette has no effect on cardiac morphology and function, either at basal conditions or in response to mechanical pressure overload for up to 2 weeks.

Table II Echocardiographic analysis of 8-week-old male *nebl*$^{-/-}$ mice compared to WT mice before and 14 days after mechanical pressure overload induced by transaortic constriction.

	Before TAC		**14 days after TAC**	
	WT (n = 6)	***nebl*$^{-/-}$ (n = 7)**	**WT (n = 6)**	***nebl*$^{-/-}$ (n = 7)**
Age (weeks)	13.3 ± 0.0	13.3 ± 0.0	15.3 ± 0.0***	15.3 ± 0.0§§§
Body weight (g)	26.7 ± 1.1	26.1 ± 1.6	27.5 ± 0.6	26.6 ± 1.7
Heart rate (bpm)	517 ± 19	497 ± 23	461 ± 29	506 ± 12
LVIDd (mm)	3.16 ± 0.08	3.10 ± 0.17	3.07 ± 0.07	3.08 ± 0.03
LVIDs (mm)	1.63 ± 0.11	1.69 ± 0.36	1.99 ± 0.04***	2.00 ± 0.03§
IVSd (mm)	0.86 ± 0.05	0.86 ± 0.06	1.08 ± 0.03***	1.09 ± 0.02§§§
LVPWd (mm)	0.92 ± 0.02	0.88 ± 0.09	1.09 ± 0.01***	1.07 ± 0.03§§§
LV %FS	48.3 ± 3.7	49.1 ± 12.8	35.3 ± 1.2***	34.8 ± 1.4§§
LVMd (mg)	110.4 ± 18.1	101.0 ± 15.7	148.9 ± 1.8	128.1 ± 18.8
LVM/BW (mg/g)	4.14 ± 0.65	3.88 ± 0.57	5.32 ± 0.07	4.83 ± 0.70
HW/BW (mg/g)			6.01 ± 0.19	6.12 ± 0.59

See the Table I legend for details and description of abbreviations. TAC, transverse aortic constriction. Data comparison was carried out before and after TAC. ***P < 0.001 for WT TAC vs. WT baseline; §P < 0.05, §§P < 0.01, §§§P < 0.001 for *nebl*$^{-/-}$ TAC vs. *nebl*$^{-/-}$ baseline.

Table III Cardiac hemodynamic properties of 12-week-old male *nebl*$^{-/-}$ mice compared to WT mice at baseline and following dobutamine stimulation.

	DOB	WT (n = 8)	*nebl*$^{-/-}$ (n = 8)
Heart rate (bpm)	basal	392 ± 44	408 ± 13
	0.75u	422 ± 33	430 ± 35
	2u	468 ± 35	462 ± 32
	4u	522 ± 47	510 ± 16
LVP_{max} (mmHg)	basal	133 ± 17	122 ± 16
	0.75u	145 ± 14	132 ± 16
	2u	158 ± 14	143 ± 13
	4u	158 ± 21	147 ± 11
dP/dt_{max} (mmHg/s)	basal	10003 ± 1166	11834 ±2576
	0.75u	11829 ± 1532	13363 ± 2599
	2u	16126 ± 1858	16743 ± 3087
	4u	20464 ± 1796	20528 ± 2145
dP/dt_{min} (mmHg/s)	basal	-8164 ± 1368	-7997 ± 1306
	0.75u	-9559 ± 1826	-9105 ± 1317
	2u	-12017 ± 2415	-10925 ± 1358**
	4u	-14080 ± 2671	-13542 ± 1314
EDP (mmHg)	basal	0.58 ± 2.31	-1.00 ± 1.02
	0.75u	0.12 ± 1.61	-0.93 ± 1.40
	2u	-0.34 ± 1.77	-1.00 ± 1.50
	4u	0.02 ± 1.96	-0.50 ± 1.53
Exp. Tau (ms)	basal	10.7 ± 1.26	11.5 ± 2.2
	0.75u	9.6 ± 1.0	10.7 ± 1.5
	2u	7.9 ± 0.7	9.3 ± 1.2*
	4u	6.7 ± 0.6	7.3 ± 1.0
HW/BW (mg/g)		4.3 ± 0.5	4.0 ± 0.3

Values are mean ± standard deviation. LVP_{max}, maximum end-systolic left ventricular pressure; dP/dt_{max}, maximum positive first derivative of LVP (contractility); dP/dt_{min}, maximum negative first derivative of LVP (relaxation); EDP, end-diastolic pressure; Exp. Tau, experimental Tau; DOB: dobutamine; u: units. *P < 0.05; **P < 0.01.

3.5 Modulation of markers of cardiac remodeling in *nebl*$^{-/-}$ mice

To determine the potential effect of nebulette KO on cardiac gene expression under basal conditions and following mechanical stress, we performed qRT-PCR on left ventricular tissue from *nebl*$^{-/-}$ and WT mice following TAC or SHAM surgery (*Figure 5* and Supplementary material online, *Table SII*). This revealed upregulation of several markers of pathological cardiac remodeling in *nebl*$^{-/-}$ left ventricle, including *skeletal muscle alpha-actin* (*acta1*), *natriuretic peptide A* (*nppa*/*ANF*), *natriuretic peptide B* (*nppb*/*BNP*), *beta-cardiac myosin heavy chain* (*myh7*), and *cardiac ankyrin repeat protein*/*ankyrin repeat domain 1* (*ankrd1*). The highest levels of upregulation were found under basal conditions where in particular *acta1* (22.5 fold) and *nppa* (8.5 fold), and *nppb* (3.9 fold) were highly upregulated. In

addition, *nppa* (2.7 fold), *acta1* (2.2 fold) and *ankrd1* (1.9 fold) were upregulated after TAC. *Collagen type III, alpha 1* (*col3a1)* was slightly upregulated under basal conditions (1.4 fold), while other markers of fibrosis, such as *transforming growth factor, beta 1* (*tgfb1)* and *connective tissue growth factor* (*ctgf)*, were unchanged. No changes in apoptosis-related genes (*caspase 3* (*casp3*), *B-cell CLL/Lymphoma 2* (*bcl2*), *bcl2-associated X-protein* (*bax*), *tumor protein p53* (*tp53*)) were found. To determine whether the absence of a cardiac functional phenotype in *nebl*$^{-/-}$ mice may be due to compensation by nebulin, we performed qRT-PCR for *nebulin* (*neb)* and found a 3.4 fold upregulation in *nebl*$^{-/-}$ mice subjected to SHAM, while no changes were found in TAC-operated mice. On the other hand, Western blot analysis on left ventricular tissue lysate showed barely detectable levels of nebulin in both WT and *nebl*$^{-/-}$ mice, and immunofluorescence staining showed no specific staining for nebulin in *nebl*$^{-/-}$ hearts (data not shown). This is consistent with the previously reported very low level of nebulin in the heart where it is expressed in only a small fraction of cardiomyocytes.(Bang, Li et al. 2006) Thus, the slight increase in *nebulin* transcript levels in *nebl*$^{-/-}$ hearts under basal conditions is unlikely to compensate for the absence of nebulette.

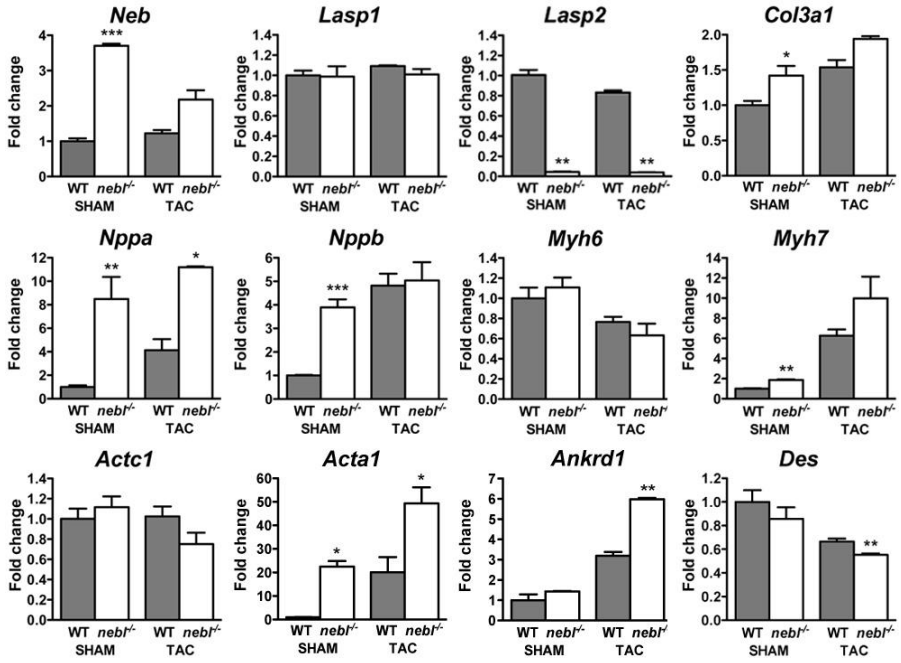

Figure 5: Upregulation of transcript levels of *nebulin* and markers of cardiac pathological remodeling in *nebl*$^{-/-}$ heart. qRT-PCR analysis for *nebulin* and cardiac markers on left ventricular tissue from WT and *nebl*$^{-/-}$ mice 3 weeks after SHAM- or TAC-surgery (n = 3 mice per group performed in triplicate). *P ≤ 0.05; **P ≤ 0.01. ***P ≤ 0.001.

3.6 Sarcomere mechanics and cross bridge kinetics are unaffected in *nebl*$^{-/-}$ hearts

To determine whether the absence of nebulette may affect sarcomere mechanics at rest and/or during contraction we compared biomechanical properties of myofibril preparations from 1-year-old *nebl*$^{-/-}$ and WT mice. As shown in *Figure 6*, no significant differences in mean sarcomere slack length and resting sarcomere length-tension relationships were found in WT and *nebl*$^{-/-}$ myofibrils.

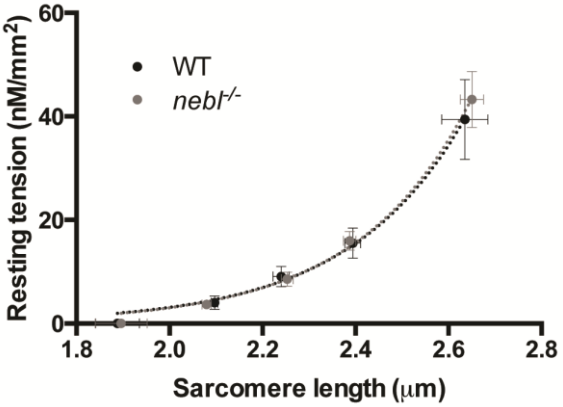

Figure 6: Average sarcomere-length resting tension relationship in myofibrils from WT and *nebl*$^{-/-}$ left ventricle. Each data point is mean ± SEM from 5 to 15 myofibrils. Logarithmic curves are fitted to the data points.

In WT myofibrils, Ca^{2+}-activated contraction and kinetic parameters were essentially the same as those previously reported in mouse ventricular myofibrils(Kreutziger, Piroddi et al. 2011) (*Table IV*). Neither maximal active tension, nor the kinetics of force generation and relaxation following rapid Ca^{2+} increase and removal were significantly different in WT and *nebl*$^{-/-}$ myofibrils. The results demonstrate that cardiac sarcomere mechanics and cross bridge kinetics are not affected by the absence of nebulette.

Table IV Tension generation and relaxation in ventricular myofibrils from 1-year-old *nebl*$^{-/-}$ mice and WT mice at 15°C.

MYOFIBRIL BATCHES	TENSION GENERATION			RELAXATION		
				Slow Phase		Fast Phase
	P_0 (mN mm^{-2})	k_{ACT} (s^{-1})	k_{TR} (s^{-1})	Duration (ms)	k_{REL} (s^{-1})	k_{REL} (s^{-1})
WT	82 ± 12 (12)	8.9 ± 0.4 (14)	8.6 ± 0.5 (14)	65 ± 6 (14)	1.79 ± 0.20 (14)	25.3 ± 3.1 (14)
***nebl*$^{-/-}$**	83 ± 9 (14)	8.4 ± 0.6 (14)	8.4 ± 0.8 (14)	79 ± 6 (14)	1.51 ± 0.11 (15)	23.4 ± 1.9 (13)

All values are presented as mean ± standard error of mean (SEM). Numbers in parentheses are number of myofibrils. P_0, maximum isometric tension; k_{ACT}, rate constant of tension rise following step-wise pCa decrease (8.0→3.5) by fast solution switching; k_{TR}, rate constant of tension redevelopment following release-restretch of maximally activated myofibrils. Full tension relaxation kinetics were characterized by the duration and rate constant of tension decay of the isometric slow relaxation phase (slow k_{REL}) and the rate constant of the fast relaxation phase (fast k_{REL}) (see Supplementary material online, *Figure S3*).

4. Discussion

Although nebulette has been extensively studied *in vitro* and *nebulette* gene mutations have been associated with DCM with or without associated endocardial fibroelastosis,(Purevjav, Varela et al. 2010) the functional role of nebulette in the heart has remained elusive. Therefore, to provide insights into the role of nebulette *in vivo*, we generated and studied *nebl*$^{-/-}$ mice.

4.1. *Nebl*$^{-/-}$ mice exhibit no cardiac functional phenotype but develop progressive Z-line widening and upregulation of cardiac stress markers

Surprisingly, *nebl*$^{-/-}$ mice exhibited no functional cardiac phenotype or changes in myofilament function. *Nebl*$^{-/-}$ mice had a normal life span, even though ultrastructural analyses of the left ventricle revealed moderate Z-line widening, including areas with severely increased Z-line width, similar to observations in skeletal muscle of nebulin deficient mice.(Bang, Li et al. 2006) This suggests that nebulette, like nebulin,(Bang, Li et al. 2006, Witt, Burkart et al. 2006, Yamamoto, Vitiello et al. 2013) is important for the maintenance of Z-line structure and integrity in cardiac muscle, although the Z-line abnormalities in *nebl*$^{-/-}$ mice were not sufficient to affect cardiac function. Furthermore, the presence of cardiac stress in *nebl*$^{-/-}$ mice is indicated by the increased expression of stress responsive genes in the left ventricle of *nebl*$^{-/-}$ mice both under basal conditions (*nppa*, *nppb*, *acta1*, *myh7*) and following TAC (*nppa*, *acta1*, and *ankrd1*).

4.2. No changes in the expression and location of sarcomeric proteins in *nebl*$^{-/-}$ mouse hearts

Knockdown of nebulette in chicken embryonic cardiomyocytes has previously been associated with decreased thin filament length and reduced tropomyosin and troponin T along the thin filament.(Moncman and Wang 2002, Bonzo, Norris et al. 2008) In contrast, we found no changes in the expression levels and localization of tropomyosin and troponin T or any other known nebulette-interaction partners in *nebl*$^{-/-}$ hearts. In particular, although N-WASP has been shown to be targeted to the Z-line through interaction with the SH3 domain of nebulin and nebulette in a GSK3β-dependent manner,(Takano, Watanabe-Takano et al. 2010) its localization in the Z-line was unaffected by the absence of nebulette, consistent with our recent findings in mice deficient for the nebulin SH3 domain.(Yamamoto, Vitiello et al. 2013) The absent effect of nebulette knockout on the expression and localization of nebulette interaction partners is in contract to observations in transgenic mice overexpressing different DCM-associated *nebulette* mutations.(Purevjav, Varela et al. 2010) In these studies, depending on the overexpressed mutation, various sarcomeric proteins were found to be downregulated (troponin T, troponin I, tropomyosin, ALP, Cypher/ZASP, α-actinin 2, myopalladin), cleaved (filamin C, myopalladin), smeared (myopalladin, α-actinin 2), or lost from the Z-line (desmin).(Purevjav, Varela et al. 2010) It is unclear whether these changes are direct consequences of the mutations or indirect secondary changes as a consequence of the resulting cardiomyopathy. Also, it is possible that the non-physiological overexpression of

mutant nebulette in transgenic mice may cause non-specific effects and a better model system would be to generate knock-in mice for the mutations, ensuring expression at physiological levels. Nevertheless, the absence of a cardiac functional phenotype in *nebl*$^{-/-}$ mice, despite the fact that *nebulette* missense mutations have been found to result in severe DCM and endocardial fibroelastosis in both human and transgenic mouse models,(Purevjav, Varela et al. 2010, Maiellaro-Rafferty, Wansapura et al. 2013) suggests that the identified *nebulette* gene mutations have dominant gain-of-function effects and could explain why no *nebulette* loss-of function mutations leading to complete absence of nebulette have been found in DCM patients. A similar example has been observed with the myotilin knockout mouse model,(Moza, Mologni et al. 2007) which exhibits no phenotype, although myotilin gene mutations are causative for limb girdle muscular dystrophy 1A, myofibrillar myopathy, and spheroid body myopathy, and transgenic mice overexpressing myotilin mutations develop a myopathy phenotype.(Garvey, Miller et al. 2006) Similarly, while *ankrd1* gene mutations have been described in patients with human dilated and hypertrophic cardiomyopathy,(Arimura, Bos et al. 2009, Duboscq-Bidot, Charron et al. 2009, Meyer, Ruppert et al. 2013) CARP/Ankrd1 knockout mice exhibit no cardiac phenotype either under basal conditions or following TAC.(Bang, Gu et al. 2014) It should also be pointed out that it is well known that differences in genetic background can influence the phenotype.(Barnabei, Palpant et al. 2010) The *nebl*$^{-/-}$ mice were generated and analyzed in a mixed sv129/Black Swiss background in our study. It is possible that *nebl*$^{-/-}$

mice may display cardiac phenotypes in a different genetic background.(Bang, Gu et al. 2014).

5. Conclusions

Although nebulette has been implicated in DCM, our results demonstrate that *nebl*$^{-/-}$ mice exhibit normal cardiac function, suggesting that nebulette is dispensable for normal cardiac function. This is in contrast to findings in nebulin knockout mice, which recapitulate many of the features of nemaline myopathy.(Bang, Li et al. 2006, Ottenheijm, Witt et al. 2009) Nevertheless, Z-line widening in *nebl*$^{-/-}$ hearts and the presence of localized areas with severe Z-line widening suggests a role of nebulette for the maintenance of Z-line integrity, similar to nebulin in skeletal muscle.[6, 21, 26] The absence of a functional phenotype in *nebl*$^{-/-}$ mice under basal conditions up to 9 months of age and following 2 weeks of TAC does not exclude that the *nebl*$^{-/-}$ mice may display impaired cardiac function in old age, after long-term TAC, or in response to other types of stress conditions, such as cardiac ischemia, in particular since the upregulation of cardiac stress responsive genes indicates the presence of chronic cardiac stress in *nebl*$^{-/-}$ mice. The fact that ablation of nebulette has no functional consequence in our study suggests that *nebulette* missense mutations, which are associated with DCM and endocardiac fibroelastosis, are not loss-of-function mutations. Further studies are needed to determine the exact mechanisms by which the missense mutations are associated with human cardiomyopathy.

Acknowledgements

The authors thank Alessandra Rodanò for the maintenance and genotyping of mice. TEM was carried out at the National Center for Microscopy and Imaging Research, University of California San Diego, La Jolla, CA, USA.

Conflict of interest: none declared

Funding

This work was supported by grants from the National Institutes of Health, National Heart, Lung, and Blood Institute [R01-HL66100, R01-HL123626, and R01-HL106968 to J.C.]; the Telethon Foundation, Italy [GGP12282 to M.L.B.]; the Italian Ministry of Education, Universities and Research [PRIN 2010-2011 number 2010R8JK2X_006 to M.L.B.]; and a Transatlantic Network of Excellence grant from the Fondation Leducq [to J.C]. J.C. is the American Heart Association (AHA) Endowed Chair in Cardiovascular Research.

Supplementary material

Nebulette knockout mice have normal cardiac function but show Z-line widening and upregulation of cardiac stress markers

Giuseppina Mastrototaro*, Xingqun Liang*, Xiaodong Li, Pierluigi Carullo, Nicoletta Piroddi, Chiara Tesi, Yusu Gu, Nancy D. Dalton, Kirk L. Peterson, Corrado Poggesi, Farah Sheikh, Ju Chen[§], and Marie-Louise Bang[§]

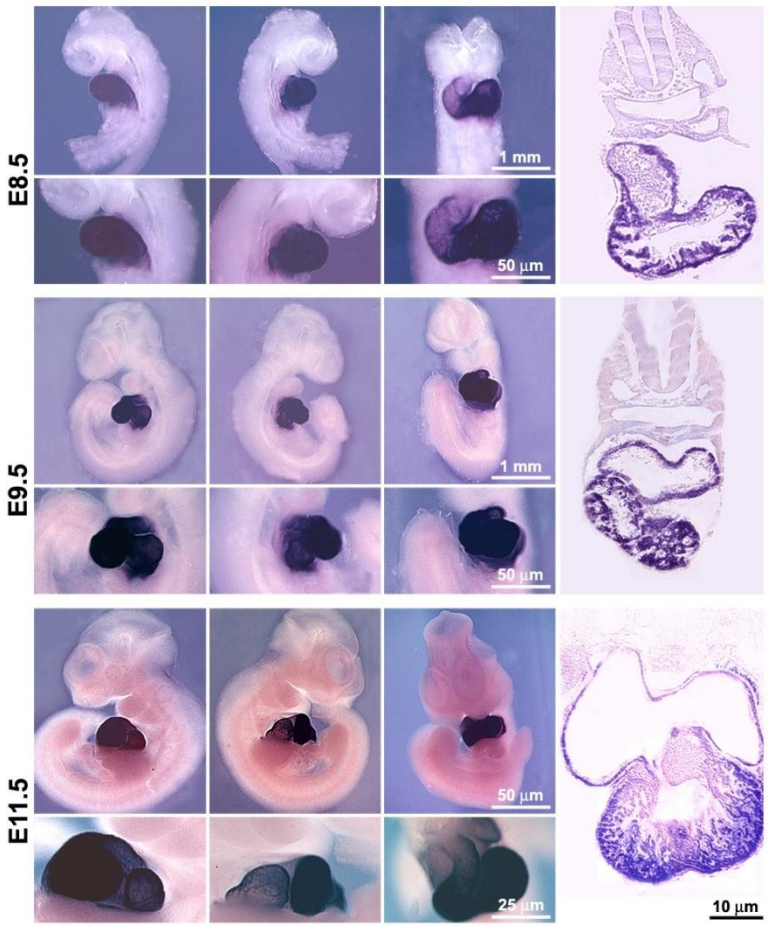

Figure S1 Nebulette is specifically expressed in heart from E8.5. *In situ* hybridization analysis of whole mount (left, right, and center view) and transverse sections of mouse embryos at E8.5, E9.5, and E11.5, revealing specific expression of nebulette in the heart.

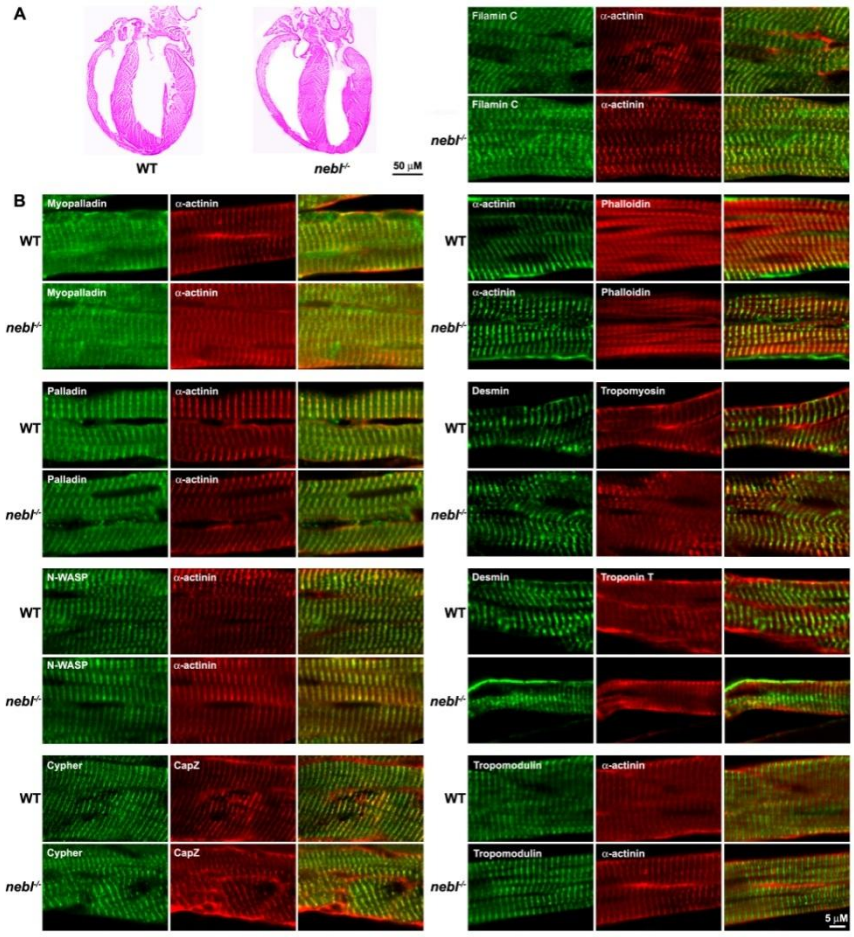

Figure S2 Histological and immunofluorescence analyses show normal morphological and cytoskeletal organization in *nebl*$^{-/-}$ mice. (*A*) Hematoxylin and eosin staining of heart sections from 8-month-old WT and *nebl*$^{-/-}$ mice. (*B*) Immunostainings of heart sections from WT and *nebl*$^{-/-}$ mice.

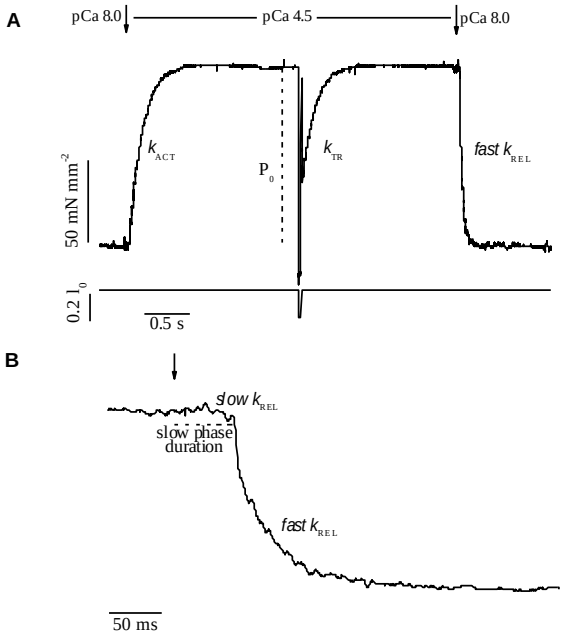

Figure S3 Representative recording of full force activation and relaxation by fast solution switching in mouse ventricular myofibril preparation and measured parameters. (*A*) The myofibril was fully activated and relaxed by rapid translation between two continuous streams of relaxing (pCa 8) and activating (pCa 4.5) solution flowing by gravity from a double-barrelled glass pipette placed at a right angle to, and within 1 mm of the preparation.(Colomo, Nencini et al. 1998) pCa changes at arrows as indicated; the solution change was completed within 5 ms. Experiments were performed at 15 °C in a thermostatically controlled myofibril observation chamber and microscope enclosure. P_o is the tension developed by the preparation at maximal Ca^{2+}-activation; k_{ACT} is the rate constant of tension generation after fast Ca^{2+} activation estimated from the monoexponential fit. Release-restretch protocols are used to measure k_{TR} , the rate of force redevelopment at steady-state activation.(Brenner 1988) (*B*) Full tension relaxation following fast Ca^{2+} removal; same trace as in A on a faster time base. The arrow marks the start of the solution change in the preparation. Full tension relaxation is biphasic. The rate constant of the early slow force decline (*slow* k_{REL}) is estimated from the slope of the regression line fitted to the tension trace normalized to the entire amplitude of the tension relaxation transient. The duration of the slow relaxation phase is estimated from the start of the solution change. The rate constant for the final fast phase of tension decline (*fast* k_{REL}) is estimated from the monoexponential fit.

Supplementary Table I: Mouse specific qRT-PCR primers**.**

Gene	Sense primer	Reverse primer
Neb	CTTCATGCAGACCGAAACAC	GTCTGCTTTTCCTTTATTCTTTTCA
Lasp1	TCGTCCTATGGTGGGTACAAG	GGCAGCGCTGTAGTCATACAC
Lasp2	GCGGATACACCTGAAAACCT	CCTGCCTTTGCTTTCTTCAA
Mypn	CATGCTTTGCTTCCAACATT	GGCTTCTGGATTCGATTCAT
Ankrd1	GCTGGAGCCCAGATTGAA	CTCCACGACATGCCCAGT
Tnnc1	GAAGGACGACAGCAAAGGGA	CGGAAGAGATCCGACAGCTC
Tnnt2	TCAATGTGCTCTACAACCGCATCAG	CAGGTCATGTCCTGGCAGTCTCACT
Des	GTGACTGAAGCTTGTCGCTGTC	CCCAGCTAGGAAGCAAGGTACA
Nppa	CACAGATCTGATGGATTTCAAGA	CCTCATCTTCTACCGGCATC
Nppb	GTCAGTCGTTTGGGCTGTAAC	AGACCCAGGCAGAGTCAGAA
Myh6	CGCATCAAGGAGCTCACC	CCTGCAGCCGCATTAAGT
Myh7	CGCATCAAGGAGCTCACC	CTGCAGCCGCAGTAGGTT
Actc1	GCTTCCGCTGTCCAGAGA	ATGCCAGCAGATTCCATACC
Acta1	AATGAGCGTTTCCGTTGC	ATCCCCGCAGACTCCATAC
Myl2	CGACAAGAATGACCTAAGGGACAC	GCCAAGACTTCCTGTTTATTTGCG
Atp2a2	TCGACCAGTCAATTCTTACAGG	CAGGGACAGGGTCAGTATGC
Col3a1	CCTGGCTCAAATGGCTCAC	CAGGACTGCCGTTATTCCCG
Ctgf	TGACCTGGAGGAAAACATTAAGA	AGCCCTGTATGTCTTCACACTG
Casp3	ATGGCTTGCCAGAAGATACC	CCCGTCCTTTGAATTTCTCC
Bcl2	GTACCTGAACCGGCATCT	GGGGCCATATAGTTCCACAA
Bax	GTCAGCGGCTGCTTGTCT	GGTCCCGAAGTAGGAGAGGA
Tp53	AGACTGGCCCTTCTTGGTCT	ATGCCCATGCTACAGAGGAG
Tgfb1	TGGAGCAACATGTGGAACTC	CAGCAGCCGGTTACCAAG
Ckn	CCAGCCAGCCAGGGTCCCAA	ACTCCTCATCGCCGGCCACA

Supplementary Table II: qRT-PCR analysis of transcript levels in left ventricle from WT and *nebl*-/- mice 3 weeks after TAC or SHAM surgery.

Gene	SHAM			3 weeks TAC		
	WT (n = 3)	*nebl*$^{-/-}$ (n = 3)	P value	WT (n = 3)	*nebl*$^{-/-}$ (n = 3)	P value
Neb	1.00 ± 0.08	3.70 ± 0.06	< **0.0001*****	1.23 ± 0.09	2.18 ± 0.26	0.0708
Lasp1	1.00 ± 0.05	0.99 ± 0.10	0.9160	1.09 ± 0.01	1.01 ± 0.05	0.2629
Lasp2	1.00 ± 0.05	0.04 ± 0.00	**0.0002*****	0.83 ± 0.02	0.04 ± 0.00	< **0.0001*****
Mypn	1.00 ± 0.16	1.07 ± 0.17	0.7833	0.80 ± 0.06	0.73 ± 0.07	0.5403
Ankrd1	1.00 ± 0.29	1.44 ± 0.02	0.3296	3.19 ± 0.19	5.98 ± 0.07	**0.0053****
Tnnc1	1.00 ± 0.06	1.13 ± 0.14	0.4269	0.88 ± 0.03	0.75 ± 0.10	0.3687
Tnnt2	1.00 ± 0.10	0.95 ± 0.14	0.7812	0.77 ± 0.05	0.70 ± 0.12	0.5730
Des	1.00 ± 0.10	0.86 ± 0.10	0.3548	0.66 ± 0.03	0.55 ± 0.01	**0.0027***
Nppa	1.00 ± 0.15	8.49 ± 1.89	**0.0031****	4.13 ± 0.94	11.19 ± 0.08	**0.0174***
Nppb	1.00 ± 0.02	3.89 ± 0.34	< **0.0001*****	4.82 ± 0.51	5.04 ± 0.78	0.8315
Actc1	1.00 ± 0.10	1.12 ± 0.11	0.5115	1.03 ± 0.10	0.75 ± 0.11	0.2077
Acta1	1.00 ± 0.04	22.47 ± 2.39	**0.0122***	20.10 ± 6.46	49.35 ± 6.82	**0.0357***
Myh6	1.00 ± 0.11	1.11 ± 0.10	0.5365	0.76 ± 0.05	0.63 ± 0.12	0.4054
Myh7	1.00 ± 0.04	1.86 ± 0.07	**0.0075****	6.27 ± 0.63	9.98 ± 2.16	0.2814
Ankrd1	1.00 ± 0.29	1.44 ± 0.02	0.3296	3.19 ± 0.19	5.98 ± 0.07	**0.0053****
Myl2	1.00 ± 0.09	0.93 ± 0.17	0.7326	0.51 ± 0.05	0.25 ± 0.09	0.0750
Atp2a2	1.00 ± 0.01	0.88 ± 0.14	0.5569	0.54 ± 0.02	0.41 ± 0.09	0.1888
Col3a1	1.00 ± 0.06	1.42 ± 0.14	**0.027***	1.54 ± 0.10	1.94 ± 0.04	0.0676
Ctgf	1.00 ± 0.08	0.94 ± 0.07	0.6190	1.65 ± 0.37	1.95 ± 0.36	0.6201
Casp3	1.00 ± 0.34	0.92 ± 0.13	0.8550	1.67 ± 0.17	1.45 ± 0.27	0.5556
Bcl2	1.00 ± 0.07	1.20 ± 0.04	0.0669	1.02 ± 0.17	1.18 ± 0.07	0.4278
Bax	1.00 ± 0.03	1.01 ± 0.11	0.9542	1.06 ± 0.14	0.85 ± 0.04	0.2343
Tp53	1.00 ± 0.10	0.95 ± 0.07	0.7050	0.91 ± 0.07	0.85 ± 0.06	0.5348
Tgfb1	1.00 ± 0.05	1.10 ± 0.08	0.3829	0.81 ± 0.06	0.70 ± 0.05	0.2236
Ckn	1.00 ± 0.09	0.71 ± 0.11	0.0857	0.93 ± 0.17	0.63 ± 0.06	0.1687

References

Arber, S., et al. (1997). "MLP-deficient mice exhibit a disruption of cardiac cytoarchitectural organization, dilated cardiomyopathy, and heart failure." Cell **88**(3): 393-403.

Arimura, T., et al. (2009). "Cardiac ankyrin repeat protein gene (ANKRD1) mutations in hypertrophic cardiomyopathy." J Am Coll Cardiol **54**(4): 334-342.

Bang, M. L., et al. (2002). "Molecular dissection of the interaction of desmin with the C-terminal region of nebulin." J Struct Biol **137**(1-2): 119-127.

Bang, M. L., et al. (2014). "The muscle ankyrin repeat proteins CARP, Ankrd2, and DARP are not essential for normal cardiac development and function at basal conditions and in response to pressure overload." PLoS One **9**(4): e93638.

Bang, M. L., et al. (2006). "Nebulin-deficient mice exhibit shorter thin filament lengths and reduced contractile function in skeletal muscle." J Cell Biol **173**(6): 905-916.

Bang, M. L., et al. (2001). "Myopalladin, a novel 145-kilodalton sarcomeric protein with multiple roles in Z-disc and I-band protein assemblies." J Cell Biol **153**(2): 413-427.

Barnabei, M. S., et al. (2010). "Influence of genetic background on ex vivo and in vivo cardiac function in several commonly used inbred mouse strains." Physiol Genomics **42A**(2): 103-113.

Bonzo, J. R., et al. (2008). "The nebulette repeat domain is necessary for proper maintenance of tropomyosin with the cardiac sarcomere." Exp Cell Res **314**(19): 3519-3530.

Brenner, B. (1988). "Effect of Ca2+ on cross-bridge turnover kinetics in skinned single rabbit psoas fibers: implications for regulation of muscle contraction." Proc Natl Acad Sci U S A **85**(9): 3265-3269.

Castillo, A., et al. (2009). "A nebulin ruler does not dictate thin filament lengths." Biophys J **96**(5): 1856-1865.

Colomo, F., et al. (1998). "Calcium dependence of the apparent rate of force generation in single striated muscle myofibrils activated by rapid solution changes." Adv Exp Med Biol **453**: 373-381; discussion 381-372.

Conover, G. M., et al. (2009). "A myopathy-linked desmin mutation perturbs striated muscle actin filament architecture." Mol Biol Cell **20**(3): 834-845.

Duboscq-Bidot, L., et al. (2009). "Mutations in the ANKRD1 gene encoding CARP are responsible for human dilated cardiomyopathy." Eur Heart J **30**(17): 2128-2136.

Garvey, S. M., et al. (2006). "Transgenic mice expressing the myotilin T57I mutation unite the pathology associated with LGMD1A and MFM." Hum Mol Genet **15**(15): 2348-2362.

Holmes, W. B. and C. L. Moncman (2008). "Nebulette interacts with filamin C." Cell Motil Cytoskeleton **65**(2): 130-142.

Jin, J. P. and K. Wang (1991). "Nebulin as a giant actin-binding template protein in skeletal muscle sarcomere. Interaction of actin and cloned human nebulin fragments." FEBS Lett **281**(1-2): 93-96.

Katoh, M. (2003). "Identification and characterization of LASP2 gene in silico." Int J Mol Med **12**(3): 405-410.

Kreutziger, K. L., et al. (2011). "Calcium binding kinetics of troponin C strongly modulate cooperative activation and tension kinetics in cardiac muscle." J Mol Cell Cardiol **50**(1): 165-174.

Kubalak, S. W., et al. (1994). "Chamber specification of atrial myosin light chain-2 expression precedes septation during murine cardiogenesis." J Biol Chem **269**(24): 16961-16970.

Labeit, S., et al. (1991). "Evidence that nebulin is a protein-ruler in muscle thin filaments." FEBS Lett **282**(2): 313-316.

Labeit, S. and B. Kolmerer (1995). "The complete primary structure of human nebulin and its correlation to muscle structure." J Mol Biol **248**(2): 308-315.

Li, B., et al. (2004). "Zyxin interacts with the SH3 domains of the cytoskeletal proteins LIM-nebulette and Lasp-1." J Biol Chem **279**(19): 20401-20410.

Liang, X., et al. (2005). "PINCH1 plays an essential role in early murine embryonic development but is dispensable in ventricular cardiomyocytes." Mol Cell Biol **25**(8): 3056-3062.

Ma, K., et al. (2006). "Titin as a giant scaffold for integrating stress and Src homology domain 3-mediated signaling pathways: the clustering of novel overlap ligand motifs in the elastic PEVK segment." J Biol Chem **281**(37): 27539-27556.

Ma, K. and K. Wang (2002). "Interaction of nebulin SH3 domain with titin PEVK and myopalladin: implications for the signaling and assembly role of titin and nebulin." FEBS Lett **532**(3): 273-278.

Maiellaro-Rafferty, K., et al. (2013). "Altered regional cardiac wall mechanics are associated with differential cardiomyocyte calcium handling due to nebulette mutations in preclinical inherited dilated cardiomyopathy." J Mol Cell Cardiol **60**: 151-160.

Marttila, M., et al. (2014). "Nebulin interactions with actin and tropomyosin are altered by disease-causing mutations." Skelet Muscle **4**: 15.

Meyer, T., et al. (2013). "Novel mutations in the sarcomeric protein myopalladin in patients with dilated cardiomyopathy." Eur J Hum Genet **21**(3): 294-300.

Millevoi, S., et al. (1998). "Characterization of nebulette and nebulin and emerging concepts of their roles for vertebrate Z-discs." J Mol Biol **282**(1): 111-123.

Moncman, C. L. and K. Wang (1999). "Functional dissection of nebulette demonstrates actin binding of nebulin-like repeats and Z-line targeting of SH3 and linker domains." Cell Motil Cytoskeleton **44**(1): 1-22.

Moncman, C. L. and K. Wang (2002). "Targeted disruption of nebulette protein expression alters cardiac myofibril assembly and function." Exp Cell Res **273**(2): 204-218.

Moza, M., et al. (2007). "Targeted deletion of the muscular dystrophy gene myotilin does not perturb muscle structure or function in mice." Mol Cell Biol **27**(1): 244-252.

Ogut, O., et al. (2003). "Interactions between nebulin-like motifs and thin filament regulatory proteins." J Biol Chem **278**(5): 3089-3097.

Ottenheijm, C. A., et al. (2009). "Thin filament length dysregulation contributes to muscle weakness in nemaline myopathy patients with nebulin deficiency." Hum Mol Genet **18**(13): 2359-2369.

Pappas, C. T., et al. (2008). "Nebulin Interacts with CapZ and Regulates Thin Filament Architecture within the Z-disc." Mol Biol Cell **19** 1837-1847.

Pappas, C. T., et al. (2010). "Nebulin regulates actin filament lengths by a stabilization mechanism." J Cell Biol **189**(5): 859-870.

Pfuhl, M., et al. (1994). "Nebulin, a helical actin binding protein." Embo J **13**(8): 1782-1789.

Purevjav, E., et al. (2010). "Nebulette mutations are associated with dilated cardiomyopathy and endocardial fibroelastosis." J Am Coll Cardiol **56**(18): 1493-1502.

Soriano, P. (1999). "Generalized lacZ expression with the ROSA26 Cre reporter strain." Nat Genet **21**(1): 70-71.

Takano, K., et al. (2010). "Nebulin and N-WASP cooperate to cause IGF-1-induced sarcomeric actin filament formation." Science **330**(6010): 1536-1540.

Tanaka, N., et al. (1996). "Transthoracic echocardiography in models of cardiac disease in the mouse." Circulation **94**(5): 1109-1117.

Tonino, P., et al. (2010). "Reduced myofibrillar connectivity and increased Z-disk width in nebulin-deficient skeletal muscle." J Cell Sci **123**(Pt 3): 384-391.

Wang, K. and J. Wright (1988). "Architecture of the sarcomere matrix of skeletal muscle: immunoelectron microscopic evidence that suggests a set of parallel inextensible nebulin filaments anchored at the Z line." J Cell Biol **107**(6 Pt 1): 2199-2212.

Wilkinson, D. G. (1992). "In situ hybridization: a practical approach." Oxford University Press, New Year, N.Y.

Witt, C. C., et al. (2006). "Nebulin regulates thin filament length, contractility, and Z-disk structure in vivo." Embo J **25**(16): 3843-3855.

Yamamoto, D. L., et al. (2013). "The nebulin SH3 domain is dispensable for normal skeletal muscle structure but is required for effective active load bearing in mouse." J Cell Sci **126**(Pt 23): 5477-5489.

Zhang, J., et al. (2008). "Syncoilin is required for generating maximum isometric stress in skeletal muscle but dispensable for muscle cytoarchitecture." Am J Physiol Cell Physiol **294**(5): C1175-1182.

Zhou, Q., et al. (2001). "Ablation of Cypher, a PDZ-LIM domain Z-line protein, causes a severe form of congenital myopathy." J Cell Biol **155**(4): 605-612.

Chapter 3

Ablation of palladin in adult cardiac muscle causes dilated cardiomyopathy

Mastrototaro G[1,2], Carullo P[2,3], Zhang J[4], Boncompagni S[5], Chen J[4], Bang ML[2,3]

[1] University of Milan-Bicocca, Milan, Italy

[2] Humanitas Research Hospital, Rozzano, Milan, Italy

[3]Institute of Genetic and Biomedical Research, Milan Unit, National Research Council, Milan, Italy

[4]University of California, San Diego School of Medicine, La Jolla, CA, USA

[5]CeSI - Center for Research on Aging & DNICS, Department of Neuroscience, Imaging and Clinical Sciences, University G. d'Annunzio, Chieti, Italy.

In preparation

Abstract

Rationale: Palladin (PALLD), myopalladin (MYPN), and myotilin (MYOT) make up a small protein family of immunoglobulin-containing proteins in the sarcomeric Z-line associated with the actin cytoskeleton. While MYPN and MYOT are expressed in striated muscle, PALLD is ubiquitously expressed in several isoforms. The longest 200 kDa PALLD isoform is expressed predominantly in striated muscle and is highly homologous in structure to MYPN, suggesting that they play similar roles in striated muscle.

Objective: Mutations in the *mypn* gene have been identified in patients with cardiomyopathies, while the role of PALLD in the heart remains unknown. The aim of this study was to investigate the function of PALLD in cardiac muscle.

Methods and Results: Due to embryonic lethality of PALLD KO mice, we generated constitutive (cPKO) and inducible (cPKOi) cardiac specific PALLD knockout mice. Detailed analyses of cPKO mice revealed no cardiac phenotype either under basal conditions or following pressure overload. In contrast, inducible knockout of PALLD in adult cPKOi mice resulted in progressive cardiac dilation and systolic dysfunction associated with fibrosis, upregulation of markers of pathological remodeling, and ERK activation. Furthermore, PALLD was found to activate serum response factor (SRF) signaling, likely through its direct interaction with MRTF-A and its role in modulating actin dynamics.

Conclusions: The development of DCM in cPKOi mice induced at adult stage demonstrates that PALLD is essential for normal cardiac

function, suggesting that *palld* gene mutations may be causative for cardiomyopathy. In contrast, cPKO mice exhibited no cardiac phenotype, possibly due to compensatory mechanisms.

Key Words: Heart • Sarcomere • Z-line • dilated cardiomyopathy• SRF signaling

---

Palladin (PALLD) is an actin associated protein, which together with myopalladin (MYPN) and myotilin (MYOT) belong to a small protein family of immunoglobulin C2 (IgC2)-containing proteins in the Z-line (Otey et al., 2009a; Otey et al., 2005b). While MYPN and MYOT are specifically expressed in striated and skeletal muscle, respectively, PALLD is ubiquitously expressed in various tissues, but is expressed at high levels in the heart (Wang and Moser, 2008). Mutations in the *mypn* gene have been associated with dilated (DCM), hypertrophic (HCM), and restrictive (RCM) cardiomyopathy (Bagnall et al., 2010; Duboscq-Bidot et al., 2008; Meyer et al., 2013; Purevjav et al., 2012), while *myot* gene mutations can cause various skeletal muscle disorders (reviewed in Otey et al., 2009b; Otey et al., 2005a). A mutation in the *palld* gene has been linked to pancreatic cancer (Goicoechea et al., 2010; Pogue-Geile et al., 2006) and PALLD levels have been shown to correlate with increased invasiveness of cancer cells (Goicoechea et al., 2009; Pogue-Geile et al., 2006). However, the role of *palld* in the heart remains unknown. While MYPN and MYOT exist as single isoforms, PALLD exists in 8 different isoforms due to the presence of four alternative promoters, alternative splicing and

early terminations (Goicoechea et al., 2010; Wang and Moser, 2008). The longest 200 kDa isoform of PALLD, is predominantly expressed in striated muscle and highly homologous in structure to MYPN, sharing 5 IgC2 domain and a central proline rich region (Otey et al., 2005b). Furthermore, also the 140 kDa and 90-92 kDa isoforms containing 4 and 3 IgC1 domains, respectively, are expressed in the heart (Wang and Moser, 2008). Additional isoforms exist but their expression profiles have not been determined in detail (Goicoechea et al., 2010; Wang and Moser, 2008). The structural similarity between MYPN and the PALLD 200 kDa isoform suggests their similar role in the heart. Within the Z-line, they both bind to α-actinin through a short sequence present in the unique region between Ig2 and Ig3, while their central proline-rich region binds to the C-terminal SH3 domain of nebulette (Bang et al. JCB 2001). A second proline-rich region in the major PALLD isoforms binds to various actin-regulating proteins in non muscle cells, including VASP, Mena, EVL, profilin, and Eps8 as well as the signaling proteins ArgBP-2, SPIN-90, and src (reviewed in Otey et al., 2009a). Moreover, a short motif in the extreme C-terminal end of PALLD and MYPN binds in a phosphorylation dependent manner to members of the PDZ-LIM protein family (cypher/ZASP, ALP; CLP36, RIL), known to be involved in regulation of actin dynamics (von Nandelstadh et al., 2009). In addition, PALLD has been shown to bind directly to filamentous actin (F-actin) through its Ig3 domain and function as an actin cross-linking protein promoting actin polymerization (Beck et al., 2013; Dixon et al., 2008). Furthermore, PALLD's C-terminal region binds to the actin-associated protein ezrin as well as myocardin

related transcription factors (MRTFs) (Jin et al., 2010). Consistent with the interaction of PALLD with F-actin and various actin binding proteins, PALLD is associated with various actin-based structures, including focal adhesions, stress fibers, cell-cell junctions, and Z-lines and important for the assembly, organization, and maintenance of the actin cytoskeleton (Goicoechea et al., 2006; Goicoechea et al., 2008; Mykkänen et al., 2001; Otey et al., 2009a; Otey et al., 2005b; Parast and Otey, 2000).

From the literature PALLD is known for its involvement in cell motility and smooth muscle cell differentiation, implicating it in cancer (reviewed in Jin, 2011), while its role in the heart has remained elusive, in part due to embryonic lethality of PALLD KO mice (Luo et al., 2005). Thus, to provide insights into the function of PALLD in cardiac muscle, we generated constitutive (cPKO) and inducible (cPKOi) cardiac specific knockout mice for the most common PALLD isoforms. While constitutive knockout of PALLD in the heart did not result in any cardiac phenotype, PALLD knockdown at adult stage resulted in cardiac dilation and systolic dysfunction associated with fibrosis as well as Z-disc and intercalated disc abnormalities. This was accompanied by ERK activation and upregulation of markers of cardiac remodelling. Furthermore, we demonstrated that PALLD strongly activates serum factor (SRF) signaling in myoblasts, suggesting that PALLD ablation may be associated with altered SRF signaling.

Methods

Cell culture

The myogenic C2C12 mouse cell line was cultured in Dulbecco's modified Eagle's medium (DMEM) containing 4.5 g/L glucose supplemented with 20% heat inactivated Fetal Bovine Serum (FBS), 1 mM Ultraglutamine, and 1% penicillin/streptomycin. The cells were grown at 37°C in a humidified atmosphere with 5% of CO2 in air. C2C12 cells were differentiated when they were at 95% confluence by reducing serum levels to 2% horse serum.

SRF-luciferase reporter assay

C2C12 cells were plated on 12-well dishes coated with 0.1% gelatin from porcine skin and transiently transfected with expression vectors encoding PALLD isoform 4 (Pxj40-HA-PALLD isoform 4) and/or MRTF-A (Pxj40-FLAG-MRTF-A) (quantity as indicated in figure 1) with a luciferase reporter gene controlled by the smooth muscle 22 (SM22) promoter (5 ng), activated by SRF. The transfection efficiency was normalized by cotransfecting cells with Renilla standardization reporter plasmid (5 ng) in which Renilla luciferase is under the control of the thymidine kinase promoter (pRLTK). 1 μg of total plasmid DNA was used and the total amount of each plasmid DNA was kept constant by adding empty expression vector. 24 hours after transfection, C2C12 myoblasts were induced to differentiate and after 48 hours of differentiation cells were lysed. Luciferase and Renilla activities were measured on a SinergyH4 (Biotek) system using the Dual-Luciferase Reporter Assay System (Promega)

according to the manufacturer's instructions. Luciferase activity was normalized to Renilla activity to account for variations in transfection efficiency. All experiments were performed in triplicates and repeated at least three times.

Generation of constitutive (cPKO) and inducible (cPKOi) cardiac muscle specific PALLD KO mice

Palld genomic DNA was obtained from a 129SVJ mouse genomic library (Stratagene, La Jolla, CA) and used for the generation of a targeting construct containing loxP sites flanking exon 15 as well as a neomycin (neo) cassette flanked by Flpase Recognition Target (FRT) sites. Exon 15 was floxed, since it is present in the most common PALLD isoforms and contains a number of nucleotides not evenly dividable by 3. The construct was generated in the pBluescript II KS+ vector, and the 5′ arm of homology consisted of a 3,983 bp *Not*I–*EcoR*V fragment (5' forward: gctccaccgcggtggcggccgc/AGAGCAGTTATCCTAAG; 5' reverse: gttatattaagggttccggatcgatgatatc/AACATGAAATG) fused with a loxP site upstream of *Palld* exon 15. The 3′ arm of homology was a 3,062 kb *Sal*I–*Sal*I fragment (3' forward: ccaagctgatcctctagagtcgac/TCCATGAGGCTCTGTC, and 3' reverse: cgggccccccctcgaggtcgac/GGAAAGGAAAACACAG) located downstream of exon 15 followed by a FRT-neo-FRT cassette and a second loxP site (Figure 2A). The Diphteria toxin A fragment (DTA) gene was inserted for negative selection. The final targeting construct was verified by sequencing and linearized with *Not*I before electroporation into R1 embryonic stem (ES) cells at the Transgenic

Core Facility at the University of California, San Diego. G418-resistant ES clones were screened for homologous recombination by Southern blot analysis of *EcoR*V digested ES cell DNA with a 471 bp probe generated by PCR on mouse genomic DNA with *palld* specific primers (sense: ATTCTTGAATGTATGGTGCCCTTGA; reverse: CTCAAAGCAGACCTCATCACAAAAC) (see Figure 2A and 2B). The wildtype (WT) allele is represented by the band of 19,607 kb, whereas the 10,130 kb band represents the correctly targeted mutant allele. One clone out of 480 G418-resistant ES clones that had undergone homologous recombination was identified. The homologous recombinant ES clone was microinjected into C57BL/6J blastocysts and transferred into pseudopregnant mice. Male chimeras were bred with female C57BL/6J mice to generate germ line transmitted heterozygous PALLD floxed ($palld^{fl/+}$) mice, which were crossed with FLPe deleter mice mice (KANKI et al., 2006) to remove the neo gene and subsequently backcrossed for 6 generations with C57BL/6J mice. To generate constitutive (cPKO) and inducible (cPKOi) cardiac specific KO mice, homozygous PALLD floxed ($palld^{fl/fl}$) mice were interbreed with α-myosin heavy chain (MHC)-nuclear cre (Abel et al., 1999) and α-MHC MerCreMer transgenic mice (Sohal et al., 2001), respectively. The resulting $palld^{fl/+}$;$Cre^{+/-}$, mice were crossed with $palld^{fl/+}$;$Cre^{-/-}$ mice to generate $palld^{fl/fl}$; $Cre^{+/-}$ as cPKO mice and $palld^{fl/fl}$;$Cre^{-/-}$ mice as control littermates. Furthermore, WT; $Cre^{+/-}$ mice derived from the same crossings were used as additional controls. Knockout of *palld* in PKOi male mice was induced at 7 weeks of age by intraperitoneal injection of tamoxifen dissolved in sesame oil (25 mg/kg/day) for 5 days, a dose that does not

produce toxicity in mice. Tamoxifen-treated *palld*$^{fl/fl}$;*Cre*$^{+/-}$ and WT;*Cre*$^{+/-}$ mice as well as *palld*$^{fl/fl}$;*Cre*$^{+/-}$ not receiving tamoxifen served as controls. Genotyping was performed on mouse tail DNA using PALLD specific primers (sense: GCTTCGCTTCAAGGAGGACCTTCTG; reverse: TGTATATCATGTTGTGGTGTCAGCC), giving rise to a 348 band for the WT allele and a 418 band for the targeted allele. The presence of cre was verified using cre specific primers (sense: ACGTTCACCGGCATCAACGT, reverse: CTGCATTACCGGTCGATGCA), giving rise to a 356 bp band. Effective knockout in the heart of cPKOi mice was confirmed by qRT-PCR analysis for PALLD isoform 1, which is not present in fibroblasts and SMCs (Figure 2C; see Online Table I for primers). Furthermore, Western blot analysis using an antibody against all PALLD isoforms (622; kindly provided by Prof. Carol Otey; Figure 1D) confirmed the ablation of PALLD. All animal studies were approved by the Italian Ministry of Health and the University of California San Diego Animal Care and Use Committee. Animal procedures were performed in full compliance with the guidelines for the Guide for the Care and Use of Laboratory Animals, eighth edition (2011) published by the US National Institutes of Health (NIH) and the Directive 2010/63/EU of the European Parliament on the protection of animals use for scientific purposes. Mice for experiments were sacrificed by cervical dislocation following anesthesia by intraperitoneal injection of a mixture of ketamine (100 mg/kg) and xylazine (5 mg/kg).

In vivo cardiac physiology

Mice anaesthetized with 1% isofluorane were subjected to transthoracic echocardiography using a Vevo 2100 System (VisualSonics) and a 30 MHz probe as previously described (Tanaka et al., 1996). Transverse Aortic Constriction (TAC) was executed with a 27-gauge needle on 8-week-old cPKO and control mice anaesthetized by intraperitoneal injection of a mixture of ketamine (100 mg/kg) and xylazine (5 mg/kg) as described (Tanaka et al., 1996). Cardiac morphology and function was assessed by echocardiography and the gradient for the arterial blood pressure within the constriction was evaluated by Echo Doppler analysis. Only mice with a pressure gradient >70 mmHg were included in the analysis. Sham-operated mice were used as controls.

Quantitative RT-PCR

RNA from the left ventricle of tamoxifen-induced cPKOi and control mice was extracted using PureZOL (Bio-Rad) according to the manufacturer's instructions. For quantitative RT-PCR (qRT-PCR), cDNA synthesis was generated using the High Capacity cDNA Reverse Transcription kit from Applied Biosystems (Life Technologies), whereafter qRT-PCR was performed in triplicate with custom designed oligos (see Online Table I) using the SYBR Select Master Mix (Life Technologies). Relative expression analysis was performed using the ΔΔCt method.

Isolation of adult ventricular cardiomyocytes (CMCs)

For isolation of ventricular CMCs, hearts were cannulated and

mounted on a Langendorff perfusion apparatus and perfused with Hank's Balanced Salt Solution (HBSS w/o $CaCl_2$ and $MgCl_2$) supplemented with 1.2 mM MgSO4, 15 mM glucose, 30 mM Taurine, and 1 mM $MgCl_2$ hexahydrate for 10 min at 37°C. Liberase blendzyme (Roche) (50 μg/ml) was then added to the solution and perfusion was continued for about 10 min until the heart became flaccid. Subsequently, the heart was removed and cells were dissociated and filtered through a 70 μm filter after which bovine serum albumin (fraction V; Sigma) was added to a final concentration of 4% to inactivate the enzyme. The cells were then allowed to settle and resuspended in fresh solution.

Cardiomyocyte contractility and intracellular Ca^{2+} transient measurements

Isolated adult ventricular cardiomyocytes (CMCs) from cPKOi and controls mice 3 months after tamoxifen induction were resuspended in Hank's Balanced Salt Solution (HBSS w/o $CaCl_2$ and $MgCl_2$) supplemented with 1.2 mM MgSO4, 15 mM glucose, 30 mM Taurine, 1 mM $MgCl_2$ hexahydrate, and 1.2 mM $CaCl_2$, which was added stepwise. CMCs were loaded with the calcium indicator Fura-2/AM (0.5 μM) for 20 minutes and subsequently placed in a chamber mounted on the stage of an inverted microscope (Nikon Eclipse TE2000-S, Tokyo, Japan) and imaged through a Nikon Fluor 40x oil objective. CMCs were continuously perfused at a constant flow rate of 1 ml/min at 37°C and electrically stimulated (25 V) via two electrodes at frequencies of 0.5, 1, and 2 Hz in the presence and absence of 1 μM forskolin. Mechanical properties of CMCs (sarcomere shortening and

relengthening) were evaluated using a MyoCam-S system (IonOptix) and fluorescence intensity was simultaneously recorded using a dual-excitation fluorescence photomultiplier system (IonOptix) and taken as an index of intracellular calcium concentration as described (Ren and Wold, 2001). Contractile parameters and intracellular Ca^{2+} concentration of CMCs were analyzed using IonWizard analysis software.

Histology

For histology, mouse hearts were harvested, relaxed in 50 mM KCl in PBS and fixed overnight in 4% paraformaldehyde in PBS. Subsequently, hearts were dehydrated, embedded in paraffin, and cut in 10 μm sections. The heart sections were stained with hematoxylin and eosin, or Picro Sirius red and imaged using a DotSlide Digital Virtual Microscopy System (Olympus).

Transmission Electron Microscopy (TEM)

For TEM, hearts from cPKOi mice and controls mice 6 months after tamoxifen induction were excised and fixed in 3.5% glutaraldehyde in 0.15 M sodium cacodylate buffer, pH 7.4 as described (Boncompagni et al., 2009a; Boncompagni et al., 2009b). Small bundles of cells teased from the papillary muscles were then post-fixed in 2% OsO4 in NaCaCo buffer for 2 hr and block-stained in saturated uranyl acetate. After dehydration, specimens were embedded in an epoxy resin (Epon 812). Ultrathin sections (~50 nm) were cut using a Leica Ultracut R microtome (Leica Microsystem, Austria) with a Diatome diamond knife (DiatomeLtd., CH-2501 Biel, Switzerland) and double-stained

with uranyl acetate and lead citrate. Sections were viewed in a FP 505 Morgagni Series 268D electron microscope (FEI Company, Brno, Czech Republic), equipped with Megaview III digital camera and Soft Imaging System (Munster, Germany) at 60 kV.

Western Blot analysis

Total left ventricle from cPKOi and control mice 2 months after tamoxifen induction was homogenized in RIPA buffer (50 mM Tris pH 7.5, 150 mM NaCl, 0.5 mM DTT, 1 mM EDTA, 1% SDS, 1% Triton X-100, Roche Complete Protease Inhibitor Cocktail, Pierce Phosphatase Inhibitor, 1 mM PMSF) using TissueLyser II (Qiagen) and Western blot analysis was performed using primary antibodies against the following proteins: PALLD 622 (1:500; kindly provided by Dr Carol Otey, University of North Carolina, Chapel Hill, NC, USA), nebulette (1:200; kindly provided by Dr. Siegfried Labeit, Medical Faculty Mannheim, University of Heidelberg, Germany), myopalladin (1:1.000, (Yamamoto et al., 2013)), α-actinin (1:50.000; Sigma), desmin (1:30.000; Abcam), cypher (1:500, (Zhou et al., 2001), calpain 3 (1:500), CARP (1:1.000; (Miller et al., 2003), connexin 43 (1:8.000; Sigma), troponin I (0.2 ng/ml; DSHB TI-4), troponin I S23/24 (1:1.000; Cell Signaling), TGFβ (1:600), SMAD 1/5-S463/465/SMAD 8-S426/428 (1:1.000; Cell Signaling), PDK-S241 (1:1.000), AKT-T308 (1:1.000; Cell Signaling), AKT-S473 (1:1.000; Cell Signaling), GSK3β-S9 (1:500; Cell Signaling), GSK3β (1:500; Cell Signaling), p70S6K-T421/S424 (1:1.000; Cell Signaling), p70S6K (1:1.000; Cell Signaling), MEK 1/2-S217/221 (1:1.000; Cell Signaling), ERK 1/2-T202/Y204 (1:1.000; Cell Signaling), ERK 1/2

(1:500; Cell Signaling), p38-Thr180/Tyr182 (1:200; Cell Signaling), p38 MAPK (1:1.000; Cell Signaling), PKCα (1:1.000; Cell signaling). GAPDH antibody (1:15.000; Proteintech Europe) was used for normalization.

Results

PALLD activates the MRTF/SRF signaling pathway

The C-terminal region of PALLD was recently shown to target to the nucleus in podocytes (Endlich et al., 2009) and smooth muscle cells (SMCs) (Jin et al., 2010), where it binds to MRTFs and both directly and indirectly activates SMC promoter activity through the serum response factor (SRF) pathway, thereby inducing SMC differentiation. To determine whether PALLD can activate the SRF signaling pathway also in striated muscle, we performed SRF-luciferase reporter assays by cotransfecting myogenic C2C12 cells with increasing amounts of HA-PALLD expression vector in the presence or absence of FLAG-MRTF-A as well as SM22 luciferase reporter and *Renilla* standardization reporter plasmid. After transfection, C2C12 myoblasts were induced to differentiate and the reporter assay was performed after 2 days of differentiation, showing that PALLD promotes SRF-activity and increases MRTF-A-mediated activation of SRF activity in a dose dependent manner (Figure 1A and 1B). An additional SRF-luciferase reporter assay was performed by cotransfection of C2C12 cells with HA-PALLD, FLAG-MRTF-A, and MYC-actin. This revealed that while cotransfection of MRTF-A with actin inhibited MRTF-A-induced SRF activation, likely through sequestration of

MRTF-A in the cytoplasm through its binding to G-actin, the activation of SRF promoted by PALLD was unaffected by the presence of actin (Figure 1C). This is consistent with a strong role of PALLD in promoting actin polymerization, resulting in the release of MRTF-A from actin and its translocation to the nucleus.

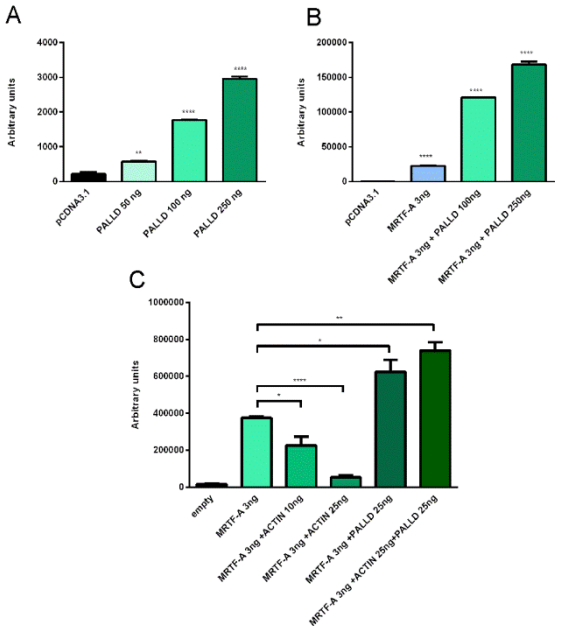

Figure 1: PALLD activates MRTF-A induced SRF signaling. A and **B**, Myogenic C2C12 cells were transfected with increasing amounts of HA-PALLD in the presence or absence of FLAG-MRTF-A together with a SM22 luciferase vector and Renilla standardization reporter plasmid. The SRF-luciferase reporter assay showed that PALLD increase MRTF-A activation of SRF activity in a dose dependent manner. **C**, C2C12 cells cotransfected with FLAG-MRTF-A, MYC-ACTIN, and HA-PALLD, suggesting that PALLD enhance SRF activity through promotion of actin polymerization.

Constitutive (cPKO) cardiac specific PALLD knockout mice exhibit a normal cardiac phenotype

To overcome the embryonic lethality of PALLD deficient mice (Luo et al., 2005), which has previously precluded the analysis of PALLD's role in the heart, we generated PALLD floxed mice for exon 15, which is present in the most common PALLD isoforms (90-92 kDa, 140 kDa, 100 kDa, Figure 2) and contains a number of nucleotides not evenly dividable by 3, so that cre-mediated recombination would result in an early stop codon and consequent mRNA degradation.

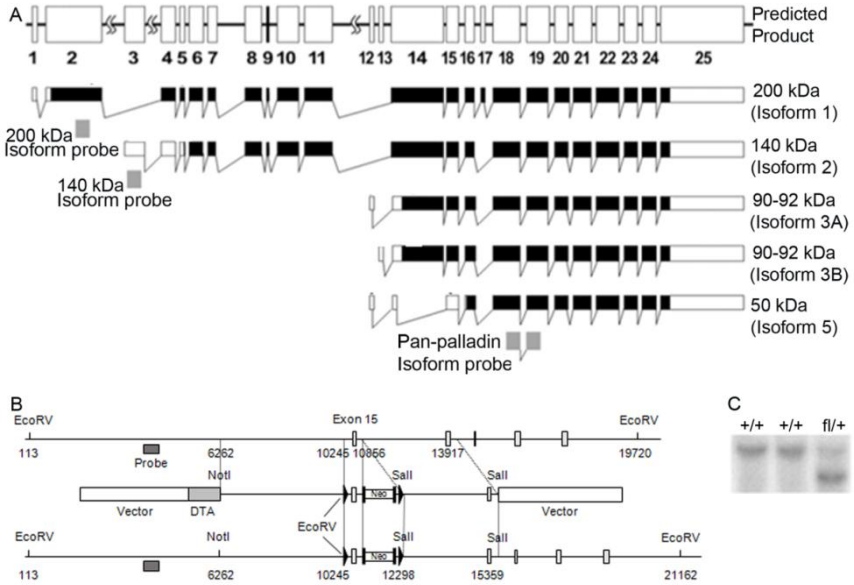

Figure 2: Generation of PALLD exon 15 floxed mice. A, Exon 15 is part of the most common PALLD isoforms. **B**, Targeting strategy for the generation of PALLD exon 15 floxed mice. **C**, Detection of WT and targeted alleles by Southern blot analysis after following digestion with EcoRV using the probe showed in B.

Following removal of the neo cassette and backcrossing into the C57BL/6J background for 7 generations, PALLD floxed mice were interbred with α-MHC-nuclear-cre (Abel et al., 1999) to generate cardiac specific PALLD knockout mice (cPKO) mice. As shown in

Figure 3, an about 70% reduction in PALLD mRNA levels was observed in cPKO mice compared to control mice. Similarly, Western blot analysis using a polyclonal antibody recognizing all PALLD isoforms (PALLD 622 kindly provided by Prof. Carol Otey, University of North Carolina at Chapel Hill, NC, USA) showed a similar 70% knockdown of PALLD at the protein level.

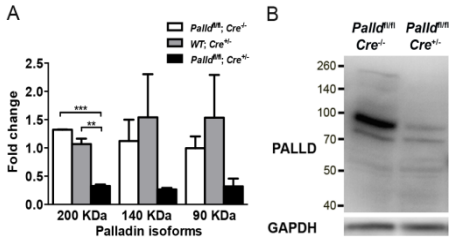

Figure 3: Generation of cardiac specific PALLD knockout (cPKO) mice. qRT-PCR (**A**) and Western blot (WB) analysis (**B**) on left ventricle (LV) from 8-week-old cPKO mice compared to WT mice, showing an about 70% knockdown of the most common PALLD isoforms in the heart. n=3

The effect of PALLD knockout on cardiac morphology and function was analyzed by echocardiography on 3- and 6-month-old cPKO male mice compared to control mice. As shown in Table I, no significant differences were found between cPKO and control mice in any of the parameters analyzed.

Table I: Echocardiographic analysis of 3- and 6-moth-old male cPKO mice compared to controls under basal conditions.

	3-month-old mice			6-month-old mice		
	Palld$^{fl/fl}$; *Cre*$^{-/-}$ (n = 9)	*WT*; *Cre*$^{+/-}$ (n = 10)	*Palld*$^{fl/fl}$; *Cre*$^{+/-}$ (n = 10)	*Palld*$^{fl/fl}$; *Cre*$^{-/-}$ (n = 6)	*WT*; *Cre*$^{+/-}$ (n = 6)	*Palld*$^{fl/fl}$; *Cre*$^{+/-}$ (n = 6)
Body weight (g)	30.0 ± 2.7	29.8 ± 3.1	26.5 ± 3.2	33.6 ± 4.9	32.8 ± 3.6	36.0 ± 3.2
Heart rate (bpm)	592.9 ± 28.7	597.4 ± 53.1	566.1 ± 49.4	569.4 ± 52.5	594.5 ± 31.6	608.2 ± 41.1
LVIDd (mm)	3.7 ± 0.3	3.6 ± 0.2	3.8 ± 0.2	3.5 ± 0.2	3.5 ± 0.2	3.5 ± 0.4
LVIDs (mm)	2.3 ± 0.3	2.5 ± 0.2	2.7 ± 0.2	2.2 ± 0.2	2.2 ± 0.1	2.3 ± 0.3
IVSd (mm)	0.9 ± 0.1	0.9 ± 0.1	0.9 ± 0.1	0.8 ± 0.1	0.9 ± 0.1	0.8 ± 0.1
LVPWd (mm)	0.8 ± 0.1	0.8 ± 0.1	0.8 ± 0.1	0.8 ± 0.1	0.8 ± 0	0.8 ± 0.1
LVPWs (mm)	1.2 ± 0.1	1.2 ± 0.1	1.1 0.1	1.2 ± 0.1	1.2 ± 0.1	1.2 ± 0.1
LV % FS	36.2 ± 6.3	31.4 ± 3	27 ± 2.3	38.4 ± 2.9	38.3 ± 1.5	35.9 ± 3.9
LVM (mg)	110.4 ± 15.9	110.6 ± 18.4	117.0 ± 20.1	99.6 ± 10.2	106.0 ± 7.2	100.4 ± 24.1
LVM/BW (mg/g)	39.3 ± 6.0	36.4 ± 4.5	41.7 ± 4.3	30.0 ± 4.2	32.7 ± 4.1	27.8 ± 6.0

All data are shown as mean ± standard deviation (SD). BW, body weight; LVIDd, left ventricular inner diameter in diastole; LVIDs, left ventricular inner diameter in systole; IVSd, interventricular septal thickness in diastole; LVPWd, left ventricular posterior wall thickness in diastole; LV %FS, left ventricular fractional shortening; LVM, left ventricular mass; bpm, beats per minute.

To evaluate the response to mechanical pressure overload, 8-week-old cPKO and control male mice were subjected to mechanical pressure overload by transaortic constriction (TAC), whereafter cardiac morphology and function was analyzed by echocardiography 1, 2, and 4 weeks after the procedure (Table II and data not shown). cPKO and control mice showed the same hypertrophic response to TAC and histological did not show any differences between cPKO mice and controls (data not shown). Thus, we conclude that cPKO mice have normal cardiac morphology and function both at basal conditions and following mechanical pressure overload.

Table II: Echocardiographic analysis of 8-week-old male cPKO mice compared to controls before and 4 weeks after machanical pressure overload induced by TAC.

	Before TAC			4 weeks after TAC		
	Palld$^{fl/fl}$; *Cre*$^{+/-}$ (n = 8)	*WT*; *Cre*$^{+/-}$ (n = 10)	*Palld*$^{fl/fl}$; *Cre*$^{+/-}$ (n = 10)	*Palld*$^{fl/fl}$; *Cre*$^{+/-}$ (n = 4)	*WT*; *Cre*$^{+/-}$ (n = 7)	*Palld*$^{fl/fl}$; *Cre*$^{+/-}$ (n = 6)
Age (weeks)	6.8 ± 0.4	6.8 ± 0.5	6.3 ± 0.6	11.8 ± 0.4	12.0 ± 0.2	11.2 ± 0.5
Body weight (g)	23.5 ± 1.7	22.0 ± 1.2	20.6 ±3.2	27.5 ± 3.1	25.9 ± 1.5	26.2 ± 2.5
Heart rate (bpm)	596.3 ± 107.9	581.5 ± 55.7	591.8 ± 58.3	576.8 ± 22	573.3 ± 69.7	532.3 ± 38.8
LVIDd (mm)	3.3 ± 0.1	3.3 ± 0.2	3.1 ± 0.2	3.8 ±0.2	3.8 ± 0.3	3.7 ± 0.3
LVIDs (mm)	2.0 ± 0.2	1.9 ± 0.2	1.9 ± 0.2	2.5 ± 0.1	2.7 ± 0.3	2.6 ± 0.4
IVSd (mm)	0.7 ± 0	0.8 ± 0.1	0.7 ± 0	0.9 ± 0.1	1.0 ± 0.1	1.0 ± 0.1
LVPWd (mm)	0.8 ± 0.1	0.8 ± 0	0.7 ± 0.1	0.9 ± 0.1	1.0 ± 0.1	1.0 ± 0.1
LVPWs (mm)	1.2 ± 0.1	1.2 ± 0.1	1.1 ± 0.1	1.4 ± 0.1	1.4 ± 0.1	1.4 ± 0.1
LV % FS	40.0 ± 3.6	41.8 ± 3.3	38.8 ± 5.7	35.5 ± 2.8	32.5 ± 3.7	28.6 ± 5.7
LVM (mg)	81.7 ± 8.3	87.1 ± 7.4	72.6 ± 7.9	133.6 ± 22.3	152.8 ± 26.5	139.8 ± 23.1
LVM/BW (mg/g)	34.7 ± 1.8	39.6 ± 2.7	35.6 ± 4.1	48.6 ± 6.6	59.3 ± 10.8	53.6 ± 8.6

Data comparison performed before and after TAC. See the Table I for the description of abbreviations.

Ablation of PALLD in adult mice results in dilated cardiomyopathy and systolic dysfunction

To investigate the effect of PALLD knockout at adult age, PALLD floxed mice were crossed with α-MHC-MerCreMer transgenic mice (Sohal et al., 2001) to generate inducible PALLD specific knockout (cPKOi) mice, which were induced at 7 weeks of age by intraperitoneal injection of tamoxifen dissolved in sesame oil (25 mg/kg/day) for 5 days. Effective knockout in the heart was confirmed by qRT-PCR on RNA obtained from the left ventricle 8 weeks after

induction, revealing an about 80% knockdown of the most common isoforms (90-92 kDa, 140 kDa, and 200 kDa isoforms (Figure 4A). Consistently, Western blot analysis on isolated adult cardiomyocytes (CMCs) using the PALLD 622 antibody showed nearly complete knockout of the targeted isoforms (Figure 4B). The antibody also recognized a band of around 65 kDa present in both cPKOi mice and control mice, which may correspond to the C-terminal isoform not targeted by our targeting approach (Figure 2A).

To evaluate the effect of PALLD ablation at adult stage on cardiac morphology and function, echocardiography was performed on cPKOi and control male mice at basal conditions and 8 and 24 weeks after tamoxifen induction. As shown in Figure 4C, cPKOi mice exhibit progressive cardiac dilation and systolic dysfunction starting from 8 weeks after induction. No cardiac hypertrophy or increase in heart weight to body weight was observed. Thus, PALLD is important for the normal heart function and its ablation at adult age results in the development of dilated cardiomyopathy (DCM).

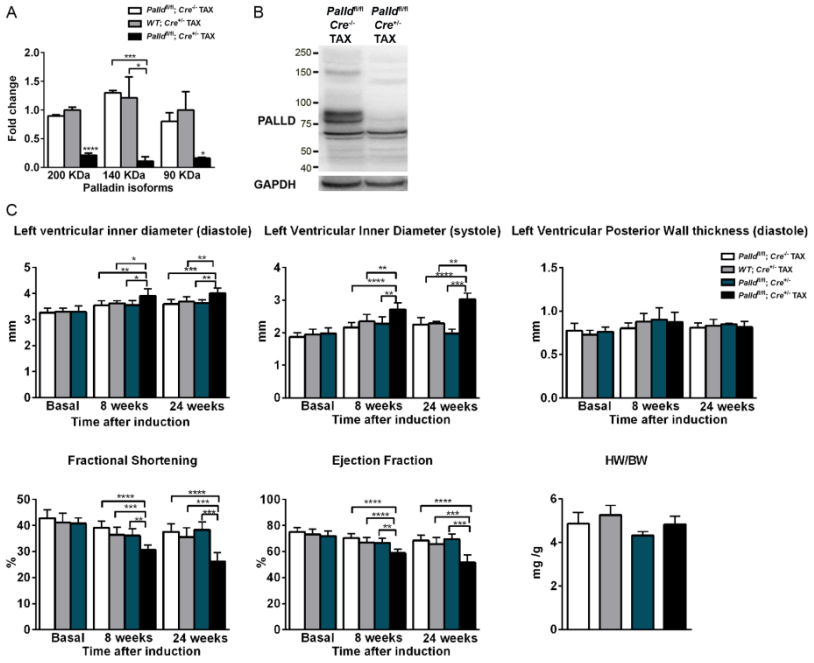

Figure 4: Induced knockout of PALLD in cPKOi mice results in DCM. A, qRT-PCR on left ventricular lysate of cPKOi and control mice 8 weeks after tamoxifen induction reveals an about 80% knockdown of 90, 140, and 200 kDa PALLD isoforms. n=3. **B**. Western blot analysis on adult cardiomyocytes isolated from cPKOi and WT mice 8 week after tamoxifen induction, showing nearly complete knockout of the 90, 140, and 200 kDa PALLD isoforms in adult CMCs..**C**, Echocardiographic analyses of cPKOi male mice compared to control mice at basal conditions and 8 and 24 weeks after tamoxifen induction. cPKOi mice develop progressive cardiac dilation and systolic dysfunction from 8 weeks after induction. All values are presented as mean ± SD. *P ≤ 0.05; **P ≤ 0.01; ***P ≤ 0.001; **** P ≤ 0.0001.

cPKOi mice exhibit reduced CMC contractility without differences in the kinetics of contraction.

Consistent with the reduced systolic function in cPKOi mice observed by echocardiography, a significantly reduction in contractility of left ventricular CMCs from cPKOi mice compared to control mice was found (Figure 5A). Furthermore, cPKOi CMCs showed a tendency to return to the relaxing state slower than control mice (Figure 5A).

cPKOi CMCs were also inclined to have reduced calcium transient amplitude compared to controls, while the rise and decay of intracellular Ca^{2+} were unaffected (Figure 5B). No significant differences were observed between cPKOi and control CMCs in the contractile response to forskolin stimulation (Church et al., 2000) (Figure 5C). Thus, the ablation of PALLD in cPKOi mice resulted in reduced CMC contractility compared to control mice without affecting the kinetics of contraction.

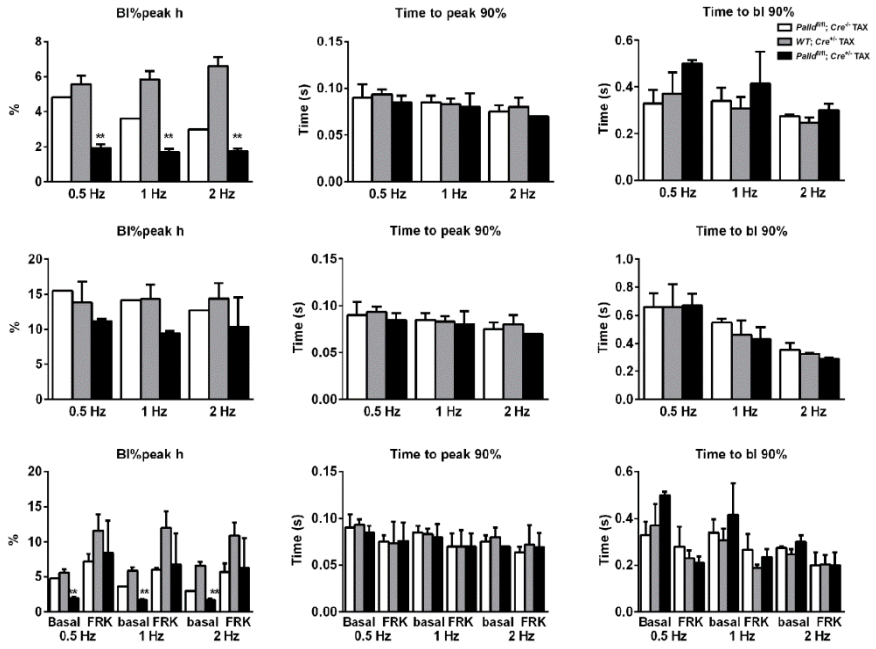

Figure 5: IonOptix analyses of ventricular CMC contractility and Ca^{2+} transients in cPKOi male mice compared to control mice 3 months after tamoxifen induction. A, Reduced CMC contractility in cPKOi mice compared to control mice. **B**, Analysis of Ca^{2+} transients using Fura-2/AM dye shows a trend towards reduced Ca^{2+} transient amplitude in cPKOi mice compared to control mice. **C**, Analysis of CMC contractility in the presence of 1 µM forskolin (FRK) shows no differences between cPKOi mice and control mice. Bl, base line. All values are shown as mean ± SD. **P ≤ 0.01.

Fibrosis and intercalated disc abnormalities in cPKOi mouse heart

Histological analyses on hearts from cPKOi male mice 6 months after tamoxifen induction showed no morphological abnormalities, while Picro Sirius red staining revealed severe interstitial fibrosis, which was not observed in control hearts (Figure 6). No apoptosis was observed by TUNEL staining (data not shown).

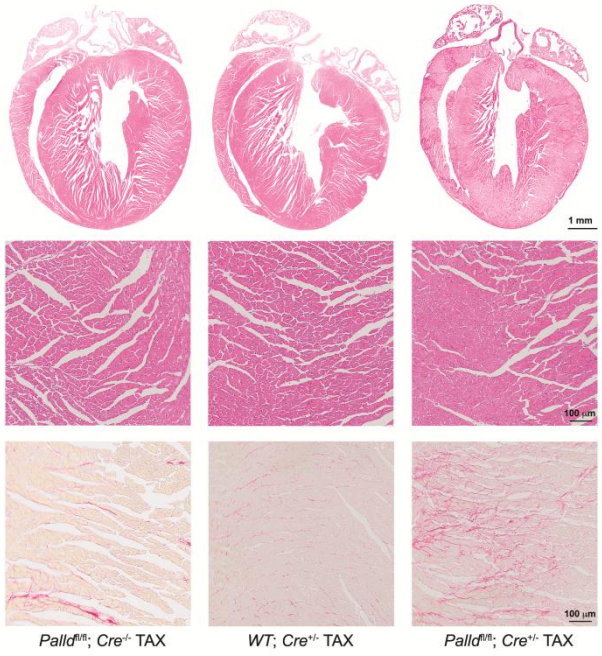

Figure 6: Histological analyses of hearts from cPKOi male mice compared to control mice 6 months after tamoxifen induction. H&E staining showed no morphological abnormalities in the heart of cPKOi mice compared to controls (top and middle), while the Picro Sirius Red staining showed the presence of interstitial fibrosis in cPKOi mice (bottom).

Electron microscopy analyses on papillary muscle from cPKOi and control male mice 6 months after tamoxifen induction revealed alterations of intercalated discs (ID) in cPKOi mice, which had a more

irregular and less electron dense appearance compared to those of control mice (Figure 7A), suggesting desmosomal abnormalities. Furthermore, Z-line streaming and irregularities was often observed in the vicinity of the altered IDs. In addition, while most sarcomeres had a normal organization, areas with misaligned and irregular Z-lines were observed (Figure 7B).

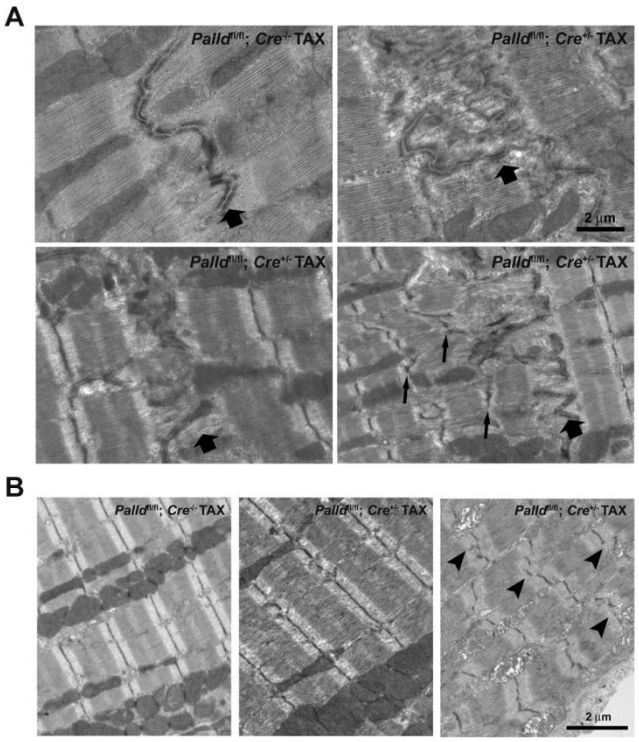

Figure 7: Transmission Electron microscopy analysis of papillary muscle from cPKOi male mice compared to control mice 6 months after tamoxifen induction. A, More irregular and less electron dense IDs observed in cPKOi mice compared to control mice (arrow). Z-line streaming and irregularities in the vicinity of the altered IDs in cPKOi (small arrows). **B**, cPKOi show mostly normal sarcomere organization, but areas with Z-line irregularities and misalignment are observed (arrowhead).

ERK1/2 activation in cPKOi mouse heart

To determine the pathways affected by the ablation of PALLD, western blot analysis was performed on left ventricular lysate from cPKOi and control mice 2 months after tamoxifen induction (Figure 9). Except for a slight upregulation of PALLD's homologue MYPN, no changes in the levels of PALLD associated proteins and other sarcomeric proteins were found. Western blot analyses for the activation of various cardiac signaling pathways, revealed a strong activation of extracellular signal-regulated protein kinase 1/2 (ERK1/2), while phosphorylation levels of the immediate upstream regulator of ERK, MEK1/2 were unchanged. Also, the Akt and p38 MAPK pathways were unaffected.

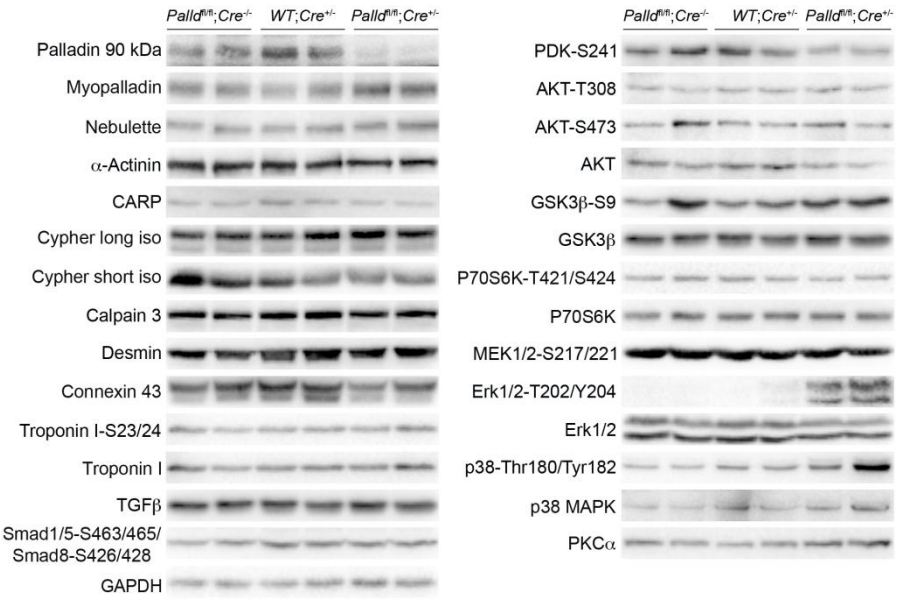

Figure 8: Western blot analysis on left ventricular lysate from cPKOi mice compared to control mice 2 months after tamoxifen induction. GAPDH was used as loading control. The blots are representative of at least three different experiments.

Upregulation of markers of pathological cardiac remodeling in cPKOi mouse heart

To determine the effect of PALLD knockdown in adult mice on cardiac gene expression, qRT-PCR was performed on left ventricular RNA from cPKOi and control male mice 6 months after tamoxifen induction (Table III) for various genes involved in cardiac remodeling, fibrosis, apoptosis, and inflammation. This revealed the upregulation of the cardiac stress responsive genes *natriuretic peptide B (nppb/bnp)*, *beta-cardiac myosin heavy chain (myh7)*, and *cardiac ankyrin repeat protein (ankrd1/carp)* (Figure 9, Table III). Furthermore, the antia-poptotic gene *B-cell CLL/Lynphoma 2 (bcl2)* was upregulated. On the other hand, no changes were found in the expression levels of other markers of cardiac remodeling, including *natriuretic peptide A* (*nppa/anf*), *alpha-cardiac myosin heavy chain* (*myh6*), *skeletal muscle alpha-actin* (*acta1*), and *cardiac muscle alpha-actin* (*actc1*). In addition, although our histological analyses showed severe interstitial fibrosis in cPKOi hearts, no significant changes were found in the expression levels of *collagen type I (col1a1), collagen type III (col3a1), connective tissue growth factor (ctgf), transforming growth factor beta 1 (tgfb1) and alpha-smooth muscle actin (α-SMA).* Also, consistent with the absence of apoptosis in cPKOi hearts, the apoptosis-related genes *bcl2-associated X-protein (bax) and tumor protein p53 (tp53)* were unaffected. Finally, no changes were found in genes encoding PALLD interacting genes and other sarcomeric proteins, including *nebulette (nebl), zasp*/*cypher*, *alp*, *desmin (des),* and *troponin C1 (Tnnc 1).* The upregulation of *nppb*, *myh7* and *carp* suggests cardiac remodeling and the presence of

chronic stress in the heart of cPKOi mice, consistent with an important role of PALLD for normal heart function.

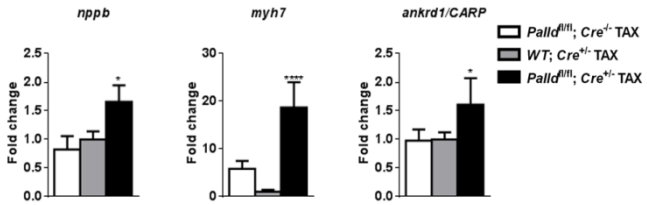

Figure 9: qRT-PCR analysis on left ventricular RNA from cPKOi mice compared to control mice 6 months after tamoxifen induction. cPKOi mice show upregulation of the cardiac stress markers *nppb*, *myh7*, and *ankrd1*.

Table III: qRT-PCR analysis on left ventricle from cPKOi mice compared to controls 6 months after

Gene	*Palld*$^{fl/fl}$; *Cre*$^{-/-}$ TAX (n = 5)	*WT*; *Cre*$^{+/+}$ TAX (n = 5)	*Palld*$^{fl/fl}$; *Cre*$^{+/-}$ TAX (n = 5)	P value *Palld*$^{fl/fl}$; *Cre*$^{-/-}$ TAX vs *Palld*$^{fl/fl}$; *Cre*$^{+/-}$ TAX	P value *WT*; *Cre*$^{+/+}$ TAX vs *Palld*$^{fl/fl}$; *Cre*$^{+/-}$ TAX
Nppa	0.84 ± 0.43	1.00 ± 0.17	1.2 ± 0.40	0.4285	0.4077
Nppb	0.75 ± 0.10	1.00 ± 0.11	1.5 ± 0.37	**0.0258***	**0.0494***
Myh6	0.67 ± 0.12	1.00 ± 0.10	0.67 ± 0.12	0.9670	**0.0073****
Myh7	4.97 ± 2.09	1.00 ± 0.43	14.6 ± 6.94	**0.0250***	**0.0015****
Actc1	0.86 ± 0.11	1.00 ± 0.04	0.94 ± 0.21	0.6435	0.6026
Acta1	0.35 ± 0.26	1.00 ± 0.48	0.48 ± 0.17	0.3506	**0.0370***
Col1a1	0.77 ± 0.14	1.00 ± 0.05	1.11 ± 0.41	0.2085	0.5672
Col3a1	0.88 ± 0.10	1.00 ± 0.14	0.94 ± 0.40	0.7625	0.7856
Ctgf	0.97 ± 0.42	1.00 ± 0.21	1.42 ± 0.32	0.1077	0.1237
Acta2	0.82 ± 0.19	1.00 ± 0.22	0.58 ± 0.17	0.2160	0.0729
Tgfb1	0.78 ± 0.10	1.00 ± 0.18	0.94 ± 0.14	0.1580	0.6061
Bcl2	0.79 ± 0.15	1.00 ± 0.14	1.3 ± 0.18	**0.0172***	**0.0533***
Bax	0.84 ± 0.16	1.00 ± 0.08	1.07± 0.27	0.2608	0.6442
Tp53	0.77 ± 0.05	1.00 ± 0.15	1.00 ± 0.24	0.1450	0.9980
Srf	0.94 ± 0.11	1.00 ± 0.06	1.12 ± 0.22	0.4629	0.1991
Mlk1	0.85 ± 0.07	1.00 ± 0.05	0.96 ± 0.15	0.3376	0.6250
Egr1	0.50 ± 0.04	1.00 ± 0.21	1.64 ± 0.82	0.1106	0.1508
Alp	1.18 ± 0.17	1.00 ± 0.20	1.44 ± 0.23	0.2685	0.0743
Zasp	0.97± 0.42	1.00 ± 0.29	1.82 ± 0.45	0.1475	0.0768
Des	0.94 ± 0.06	1.00 ± 0.06	0.92 ± 0.09	0.8028	0.2667
Nebl	0.86 ± 0.14	1.00 ± 0.22	0.87 ± 0.22	0.9260	0.4244
Tnnc1	1.07 ± 0.05	1.00 ± 0.06	1.05 ± 0.18	0.8094	0.6592
Ankrd1	1.00 ± 0.07	1.00 ± 0.11	1.58 ± 0.46	0.0908	**0.0512***
Atp2a2	0.94 ± 0.15	1.00 ± 0.11	0.85 ± 0.13	0.1878	0.6062

All values are presented as mean ± SD. *P ≤ 0.05; **P ≤ 0.01;

Discussion

PALLD regulates the MRTF-A/SRF signaling pathway in a dose dependent manner

PALLD is an immunoglobulin-C2-containing protein highly conserved among vertebrates, which plays a key role in actin cytoskeleton organization (Goicoechea et al., 2006; Goicoechea et al., 2008; Mykkänen et al., 2001; Otey et al., 2009a; Otey et al., 2005b; Parast and Otey, 2000). PALLD not only binds to several proteins involved in the regulation of actin dynamics, but directly binds to F-actin through its Ig3 domain and is able also to bundle actin filaments and promote actin polymerization (Beck et al., 2013; Dixon et al., 2008). In addition, PALLD binds through its C-terminal to MRTF-A, a transcriptional cofactor that in response to changes in the G-actin/F-actin ratio translates to the nucleus where it binds and activates SRF (Parmacek, 2007). In SMCs, PALLD was found to regulate gene expression by both directly and indirectly activating SMC promoter activity through the SRF pathway (Jin et al., 2010). Here we found that PALLD can activate the MRTF-A/SRF pathway also in muscle cells. In particular, we demonstrated that PALLD promotes SRF activity and increases MRTF-A activation of SRF in a dose dependent manner. In particular, while actin inhibited the MRTF-A-mediated activation of SRF, cotransfection with PALLD completely counteracted this effect, suggesting that PALLD activates SRF signaling though promotion of actin polymerization, resulting in translocation of MRTF-A to the nucleus where it activates SRF. It remains to be determined whether PALLD can also affect the shuttling

of MRTF-A between the cytoplasm and the nucleus through its direct binding to MRTF-A. Our results show that, also in striated muscle, PALLD plays a central role in the modulation of actin dynamics and regulation of the MRTF-A/SRF pathway. Further investigations are needed to determine the precise mechanism by which PALLD modulates this pathway.

Constitutive cardiac specific ablation of PALLD does not affect the normal heart function, whereas inducible cardiac ablation of PALLD at adult stage induces dilated cardiomyopathy

PALLD KO mice have previously been reported to be embryonic lethal due to neural tube closure defects (Luo et al., 2005), thus precluding the analysis of the role of PALLD in the heart. Therefore, to determine the role of PALLD in the heart *in vivo*, we floxed *palld* exon 15, allowing us to generate constitutive (cPKO) and inducible (cPKOi) cardiac specific PALLD knockout mice for the most common PALLD isoforms (90-92 kDa, 140 kDa, 200 kDa). Surprisingly, cPKO mice exhibited no cardiac phenotype either at basal levels or in response to TAC. On the other hand, cPKOi mice induced at adult stage developed cardiac dilation and systolic dysfunction within 8 weeks after induction. This was consistent with reduced CMC contractility, suggesting a direct role of palladin in regulating cardiac contractile function. In addition, cardiac interstitial fibrosis and ultrastructural abnormalities were observed. In particular, ICDs in cPKOi mice were disorganized and more convoluted compared to those of control mice. In addition, areas with irregular and misaligned Z-lines were observed, in particular, in the vicinity of

abnormal ICDs. The ICD is made up of three major cell junctions: the fascia adherens junction, where actin filaments are anchored and connect the sarcomere to the cell membrane; desmosomes, which anchor the cell membrane to the intermediate filament network; and gap junctions, which permits the passage of ions between cells, allowing the action potential to spread between cells (reviewed in Sheikh et al., 2009). PALLD binds directly to α-actinin and ALP, which are associated with the fascia adherens junction (Pashmforoush et al., 2001), suggesting that ablation of PALLD may destabilize the structure of the fascia adherens junction and induce alterations in the structure of the ID. However, more studies are required to determine this. At the molecular level, the cardiac changes in cPKOi mice were associated with upregulation of markers of pathological cardiac remodeling and stress (*nppb*, *myh7*, and *ankrd1/carp*) and strongly increased ERK1/2 phosphorylation. The activation of ERK, and thus the activation of MAPK signaling, could be a keystone in the development of DCM. In fact, the activation of ERK1/2 occurs prior to the development of fibrosis and severe cardiac dysfunction, indicating that it is a primary pathogenic response as a direct result of the PALLD ablation. Since MAPK signaling is induced in response to a multitude of external stimuli (Muslin, 2008), further investigation is required to determine why ERK1/2 is activated in cPKOi mice and which of its downstream targets are affected. Moreover, it remains to be determined whether altered SRF signaling may play a role in the cardiac phenotype.

The absence of a cardiac phenotype in cPKO mice is surprising based on the rather severe phenotype of cPKOi induced at adult stage.

To rule out the possibility that the phenotype of cPKOi mice may be due to the toxic effect of tamoxifen, we injected cPKO with tamoxifen at 7 weeks of age and, subsequently, evaluated cardiac function by echocardiography (data not shown). However, this did not induce any cardiac phenotype in cPKO mice, suggesting that early ablation of PALLD allows for the activation of compensatory mechanisms. A possible candidate is MYPN, which is highly similar in structure to the largest 200 kDa PALLD isoform predominantly expressed in striated muscle. Another possibility is that the recently discovered smaller PALLD isoforms, whose expression profile, tissue localization, and functions are still unknown (Wang and Moser, 2008), may compensate for the absence of the major PALLD isoforms. However, this remains to be determined.

All together our data demonstrates an important role of PALLD for normal heart function, suggesting PALLD as a potential CM gene. More studies are needed to determine the precise mechanisms connecting the ablation of PALLD to the development of dilated cardiomyopathy.

Acknowledgement

The authors thank Alessandra Rodano` for the maintenance and genotyping of mice.

Funding

This work was supported by grants from the Telethon Foundation, Italy (GGP12282 to M.L.B.) and the Italian Ministry of Education, Universities and Research (PRIN 2010-2011 no. 2010R8JK2X_006 to

M.L.B.).

References

Abel, E.D., H.C. Kaulbach, R. Tian, J.C. Hopkins, J. Duffy, T. Doetschman, T. Minnemann, M.E. Boers, E. Hadro, C. Oberste-Berghaus, W. Quist, B.B. Lowell, J.S. Ingwall, and B.B. Kahn. 1999. Cardiac hypertrophy with preserved contractile function after selective deletion of GLUT4 from the heart. *J Clin Invest*. 104:1703-1714.

Bagnall, R.D., L. Yeates, and C. Semsarian. 2010. Analysis of the Z-disc genes PDLIM3 and MYPN in Patients with Hypertrophic Cardiomyopathy. *International journal of cardiology*. 145:601-602.

Beck, M.R., R.D. Dixon, S.M. Goicoechea, G.S. Murphy, J.G. Brungardt, M.T. Beam, P. Srinath, J. Patel, J. Mohiuddin, and C.A. Otey. 2013. Structure and function of palladin's actin binding domain. *Journal of molecular biology*. 425:3325-3337.

Boncompagni, S., A.E. Rossi, M. Micaroni, G.V. Beznoussenko, R.S. Polishchuk, R.T. Dirksen, and F. Protasi. 2009a. Mitochondria are linked to calcium stores in striated muscle by developmentally regulated tethering structures. *Molecular biology of the cell*. 20:1058-1067.

Boncompagni, S., A.E. Rossi, M. Micaroni, S.L. Hamilton, R.T. Dirksen, C. Franzini-Armstrong, and F. Protasi. 2009b. Characterization and temporal development of cores in a mouse model of malignant hyperthermia. *Proceedings of the National Academy of Sciences*. 106:21996-22001.

Church, D., M. Rebsamen, D. Morabito, V. van Der Bent, M. Vallotton, and U. Lang. 2000. Role of cell contractions in cAMP-induced cardiomyocyte atrial natriuretic peptide release. *American Journal of Physiology-Heart and Circulatory Physiology*. 278:H117-H125.

Dixon, R.D., D.K. Arneman, A.S. Rachlin, N.R. Sundaresan, M.J. Costello, S.L. Campbell, and C.A. Otey. 2008. Palladin is an actin cross-linking protein that uses immunoglobulin-like domains to bind filamentous actin. *Journal of Biological Chemistry*. 283:6222-6231.

Duboscq-Bidot, L., P. Xu, P. Charron, N. Neyroud, G. Dilanian, A. Millaire, V. Bors, M. Komajda, and E. Villard. 2008. Mutations in the Z-band protein myopalladin gene and idiopathic dilated cardiomyopathy. *Cardiovascular research*. 77:118-125.

Endlich, N., E. Schordan, C.D. Cohen, M. Kretzler, B. Lewko, T. Welsch, W. Kriz, C.A. Otey, and K. Endlich. 2009. Palladin is a dynamic actin-associated protein in podocytes. *Kidney international*. 75:214-226.

Goicoechea, S., D. Arneman, A. Disanza, R. Garcia-Mata, G. Scita, and C.A. Otey. 2006. Palladin binds to Eps8 and enhances the formation of dorsal ruffles and podosomes in vascular smooth muscle cells. *Journal of cell science*. 119:3316-3324.

Goicoechea, S., B. Bednarski, R. Garcia-Mata, H. Prentice-Dunn, H. Kim, and C. Otey. 2009. Palladin contributes to invasive motility in human breast cancer cells. *Oncogene*. 28:587-598.

Goicoechea, S.M., D. Arneman, and C.A. Otey. 2008. The role of palladin in actin organization and cell motility. *European journal of cell biology*. 87:517-525.

Goicoechea, S.M., B. Bednarski, C. Stack, D.W. Cowan, K. Volmar, L. Thorne, E. Cukierman, A.K. Rustgi, T. Brentnall, and R.F. Hwang. 2010. Isoform-specific upregulation of palladin in human and murine pancreas tumors.

Jin, L. 2011. The actin associated protein palladin in smooth muscle and in the development of diseases of the cardiovasculature and in cancer. *Journal of muscle research and cell motility*. 32:7-17.

Jin, L., Q. Gan, B.J. Zieba, S.M. Goicoechea, G.K. Owens, C.A. Otey, and A.V. Somlyo. 2010. The actin associated protein palladin is important for the early smooth muscle cell differentiation. *PloS one*. 5:e12823.

KANKI, H., H. SUZUKI, and S. ITOHARA. 2006. High-efficiency CAG-FLPe deleter mice in C57BL/6J background. *Experimental animals*. 55:137-141.

Luo, H., X. Liu, F. Wang, Q. Huang, S. Shen, L. Wang, G. Xu, X. Sun, H. Kong, and M. Gu. 2005. Disruption of palladin results in neural tube closure defects in mice. *Molecular and Cellular Neuroscience*. 29:507-515.

Meyer, T., V. Ruppert, S. Ackermann, A. Richter, A. Perrot, S.R. Sperling, M.G. Posch, B. Maisch, and S. Pankuweit. 2013. Novel mutations in the sarcomeric protein myopalladin in patients with dilated cardiomyopathy. *European Journal of Human Genetics*. 21:294-300.

Miller, M.K., M.-L. Bang, C.C. Witt, D. Labeit, C. Trombitas, K. Watanabe, H. Granzier, A.S. McElhinny, C.C. Gregorio, and S. Labeit. 2003. The muscle ankyrin repeat proteins: CARP, ankrd2/Arpp and DARP as a family of titin filament-based stress response molecules. *Journal of molecular biology*. 333:951-964.

Muslin, A. 2008. MAPK signalling in cardiovascular health and disease: molecular mechanisms and therapeutic targets. *Clinical Science*. 115:203-218.

Mykkänen, O.-M., M. Grönholm, M. Rönty, M. Lalowski, P. Salmikangas, H. Suila, and O. Carpén. 2001. Characterization of human palladin, a microfilament-associated protein. *Molecular biology of the cell*. 12:3060-3073.

Otey, C.A., R. Dixon, C. Stack, and S.M. Goicoechea. 2009a. Cytoplasmic Ig-domain proteins: cytoskeletal regulators with a role in human disease. *Cell motility and the cytoskeleton*. 66:618.

Otey, C.A., R. Dixon, C. Stack, and S.M. Goicoechea. 2009b. Cytoplasmic Ig-domain proteins: cytoskeletal regulators with a role in human disease. *Cell Motil Cytoskeleton*. 66:618-634.

Otey, C.A., A. Rachlin, M. Moza, D. Arneman, and O. Carpen. 2005a. The palladin/myotilin/myopalladin family of actin-associated scaffolds. *Int Rev Cytol*. 246:31-58.

Otey, C.A., A. Rachlin, M. Moza, D. Arneman, and O. Carpen. 2005b. The Palladin/Myotilin/Myopalladin Family of Actin-Associated Scaffolds. *International review of cytology*. 246:31-58.

Parast, M.M., and C.A. Otey. 2000. Characterization of palladin, a novel protein localized to stress fibers and cell adhesions. *The Journal of cell biology*. 150:643-656.

Parmacek, M.S. 2007. Myocardin-Related Transcription Factors Critical Coactivators Regulating Cardiovascular Development and Adaptation. *Circulation research*. 100:633-644.

Pashmforoush, M., P. Pomiès, K.L. Peterson, S. Kubalak, J. Ross, A. Hefti, U. Aebi, M.C. Beckerle, and K.R. Chien. 2001. Adult mice deficient in actinin–associated LIM-domain protein reveal a developmental pathway for right ventricular cardiomyopathy. *Nature medicine*. 7:591-597.

Pogue-Geile, K.L., R. Chen, M.P. Bronner, T. Crnogorac-Jurcevic, K.W. Moyes, S. Dowen, C.A. Otey, D.A. Crispin, R.D. George, and D.C. Whitcomb. 2006. Palladin mutation causes familial pancreatic cancer and suggests a new cancer mechanism. *PLoS Med*. 3:e516.

Purevjav, E., T. Arimura, S. Augustin, A.-C. Huby, K. Takagi, S. Nunoda, D.L. Kearney, M.D. Taylor, F. Terasaki, and J.M. Bos. 2012. Molecular basis for clinical heterogeneity in inherited cardiomyopathies due to myopalladin mutations. *Human molecular genetics*. 21:2039-2053.

Ren, J., and L.E. Wold. 2001. Measurement of cardiac mechanical function in isolated ventricular myocytes from rats and mice by computerized video-based imaging. *Biological procedures online*. 3:43-53.

Sheikh, F., R.S. Ross, and J. Chen. 2009. Cell-cell connection to cardiac disease. *Trends in cardiovascular medicine*. 19:182-190.

Sohal, D.S., M. Nghiem, M.A. Crackower, S.A. Witt, T.R. Kimball, K.M. Tymitz, J.M. Penninger, and J.D. Molkentin. 2001. Temporally regulated and tissue-specific gene manipulations in the adult and embryonic heart using a tamoxifen-inducible Cre protein. *Circ Res*. 89:20-25.

Tanaka, N., N. Dalton, L. Mao, H.A. Rockman, K.L. Peterson, K.R. Gottshall, J.J. Hunter, K.R. Chien, and J. Ross. 1996. Transthoracic echocardiography in models of cardiac disease in the mouse. *Circulation*. 94:1109-1117.

von Nandelstadh, P., M. Ismail, C. Gardin, H. Suila, I. Zara, A. Belgrano, G. Valle, O. Carpen, and G. Faulkner. 2009. A class III PDZ binding motif in the myotilin and FATZ families binds enigma family proteins: a common link for Z-disc myopathies. *Mol Cell Biol*. 29:822-834.

Wang, H.V., and M. Moser. 2008. Comparative expression analysis of the murine palladin isoforms. *Developmental Dynamics*. 237:3342-3351.

Yamamoto, D.L., C. Vitiello, J. Zhang, D.S. Gokhin, A. Castaldi, G. Coulis, F. Piaser, M.C. Filomena, P.J. Eggenhuizen, and P. Kunderfranco. 2013. The nebulin SH3 domain is dispensable for normal skeletal muscle structure but is required for effective active load bearing in mouse. *Journal of cell science*. 126:5477-5489.

Zhou, Q., P.-H. Chu, C. Huang, C.-F. Cheng, M.E. Martone, G. Knoll, G.D. Shelton, S. Evans, and J. Chen. 2001. Ablation of Cypher, a PDZ-LIM domain Z-line protein, causes a severe form of congenital myopathy. *The Journal of cell biology*. 155:605-612.

Chapter 4

Conclusion

The Z-disc is a multiprotein complex that demarcates the lateral borders of the sarcomere. In addition to its structural function, the Z-disc plays a crucial role in efficient force transmission, mechanosensation, mechanotransduction, and generation of intracellular signaling. Its crucial role is highlighted by the fact that mutations in many genes encoding Z-disc proteins have been identified in patients with HCM, DCM, and RCM. In particular, 4 missense mutations in the *nebulette* gene have been demonstrated to be causative for DCM, and mutations in the gene encoding MYPN, a homologue of PALLD, have recently been identified in patients with DCM HCM, and RCM, suggesting that also PALLD may play a role as a CM gene. The aim of my PhD thesis project was to study the functional role on nebulette and PALLD in the heart.

Analysis of nebulette in the heart *in vivo* through the study of nebulette knockout mice demonstrated that nebulette is essential for the stabilization and integrity of the Z-line, although its ablation has no functional consequences. This suggests that nebulette missense mutations responsible of DCM have dominant gain-of-function effects.

To determine the role of PALLD in the heart *in vivo*, we generated constitutive and inducible cardiac specific PALLD knockout mice. While constitutive knockout of PALLD did not result in any cardiac phenotype either under basal conditions or following mechanical pressure overload, knockout of PALLD in adult mice

resulted in cardiac dilation and systolic dysfunction associated with fibrosis, ERK activation, and upregulation of markers of cardiac remodeling. The absent phenotype of constitutive PALLD knockout mice suggests that compensatory mechanisms can counteract the effect of PALLD ablation.

A better understanding of the mechanisms leading from *nebulette* gene mutations or PALLD ablation to DCM, is needed to develop targeted therapeutic strategies for DCM, which are not currently available.